Inaugural dissertation

for

obtaining the doctoral degree

of the

Combined Faculty of Mathematics, Engineering and Natural Sciences

of the

Ruprecht - Karls - University

Heidelberg

Presented by: Karam Khorani

M.Sc. of Science/Biochemistry

Born in: Baghdad/Iraq

Oral examination: 04/10/2023

Unraveling Druggable Key Nodes in Gene Regulatory and Signaling Networks by Integrative Analysis of Multi-omics Data from Head and Neck Cancer

Referees1: Prof. Dr. Dr. Georg Stöcklin

Referees2: Prof. Dr. Jochen Heß

To my wife (Sandra)

To my sisters (Aseel, Wasan, Dina)

"If learning the truth is the scientist's goal,
Then he must make himself the enemy to all that he reads"

Al-Hasan Ibn Al-Haytham (ALHAZEN)
965-1040 (Baghdad)

Summary

In summary, I conducted an integrative analysis of multi-omics data to highlight the most relevant alterations associated with cancer cells' plasticity depending on two different modes of action:

- The intrinsic modulation of cancer cells' plasticity in TME by unraveling the inverse regulation of SOX2- and SOX9-related gene networks in HNSCC and other tumor entities. Firstly, differentially expressed genes (DEG) related to SOX2 and SOX9 transcription were identified in TCGA-HNSC, which enables the clustering of patients into groups with distinct clinical features and survival. Secondly, a prognostic risk model was established by LASSO Cox regression based on expression patterns of DEGs in TCGA-HNSC (training cohort) and was confirmed in independent HNSCC validation cohorts as well as other cancer cohorts from TCGA. Moreover, differences in the mutational landscape among risk groups of TCGA-HNSC demonstrated enrichment of truncating NSD1 mutations for the low-risk group and elucidated DNA methylation as a modulator of SOX2 expression. Additionally, GSVA revealed differences in several oncogenic pathways among risk groups, including upregulation of gene sets related to oncogenic KRAS signaling for the high-risk group. Finally, in silico drug screen analysis revealed numerous compounds targeting EGFR signaling with significantly lower efficacy for cancer cell lines with a higher risk phenotype, but also indicated potential vulnerabilities.
- Cancer cell-extrinsic mechanisms and modulators of plasticity and the role of neuroglial activation as an emerging new component of TME that modulates cancer cell plasticity.

A SC-related 43-gene set was elucidated as an accurate surrogate for the presence of peripheral nerves across solid tumor entities. This model is characterized by higher oncogenic pathway activities such as TGF-β signaling in SC^{high} with an immunosuppressive phenotype and higher PI3K-AKT-MTOR pathway and cell cycle pathway activity in SC^{low} with an immune active phenotype and more sensitivity to

topoisomerase agents as potential treatment vulnerabilities. Finally, the impact of PI3K pathway activity on TME abundance of peripheral neurons is context-dependent and dominated by the *TP53* status.

Zusammenfassung

Zusammenfassend habe ich eine integrative Analyse von Multiomics-Daten durchgeführt, um die wichtigsten Veränderungen hervorzuheben, die mit der Plastizität von Krebszellen in Abhängigkeit von zwei verschiedenen Wirkmechanismen verbunden sind:

- Die intrinsische Modulation der Plastizität von Krebszellen in der Tumormikroumgebung durch die Entschlüsselung der inversen Regulation von SOX2- und SOX9-abhängigen Gensignaturen beim HNSCC und anderen Tumorentitäten. Erstens wurden in TCGA-HNSC differenziell exprimierte Genen (DEGs) identifiziert, die mit der SOX2- und SOX9-Transkription zusammenhängen, was die Einteilung von Patienten in Gruppen mit unterschiedlichen klinischen Merkmalen und Überlebensraten ermöglicht. Zweitens wurde ein prognostisches Risikomodell durch LASSO-Cox-Regression auf der Grundlage von Expressionsmustern der SOX2/SOX9-abhängigen DEGs für TCGA-HNSC (Trainingskohorte) erstellt und in unabhängigen HNSCC-Validierungskohorten sowie in anderen soliden Tumorkohorten aus TCGA bestätigt. Darüber hinaus zeigten die Unterschiede in der Mutationslandschaft zwischen den Risikogruppen bei TCGA-HNSC eine Anreicherung von trunkierenden NSD1-Mutationen in der Niedrigrisikogruppe und klärten die DNA-Methylierung als Modulator der SOX2-Expression auf. Darüber hinaus zeigte die GSVA-Unterschiede in mehreren onkogenen Signalwegen zwischen den Risikogruppen, einschließlich einer Hochregulierung von Gensätzen, die mit der onkogenen KRAS-Signalübertragung in der Hochrisikogruppe zusammenhängen. Schließlich ergab eine in-silico Analyse zahlreiche Medikamente, die auf den EGFR-Signalweg abzielen und bei Krebszelllinien mit einem höheren Risikophänotyp eine deutlich geringere Wirksamkeit aufweisen, aber auch auf potenzielle Schwachstellen hinweisen.

- Externe Mechanismen und Modulatoren sowie die Rolle der neuroglialen Aktivierung als neue Komponente der Tumormikroumgebung, die die Plastizität von Krebszellen beeinflussen.

Eine Signatur von 43 Genen mit Bezug zu SCs wurde als genaues Surrogat für das Vorhandensein von peripheren Nerven in soliden Tumorentitäten identifiziert. SC^{high} Tumore zeichneten sich durch eine höhere Aktivität onkogene Signalwege, wie z. B. TGF-β, und einen immunsuppressiven Phänotyp aus, während SC^{low} Tumoren durch eine höhere Aktivität des PI3K-AKT-MTOR-Signalwegs, Zellzyklus-Signalwege und einen immunaktiven Phänotyp charakterisiert sind sowie eine höhere Empfindlichkeit gegenüber Inhibitoren der DNA-Topoisomerasen als potenzielle Behandlungsschwachstellen aufweisen. Schließlich ist die Auswirkung der Aktivität des PI3K-Stoffwechsels auf die Tumormikroumgebung der peripheren Neuronen kontextabhängig und wird durch den TP53-Status dominiert.

List of Abbreviations:

HNSCC: Head and Neck Squamous Cell Carcinoma

HNC: Head and Neck Cancer

SCC: Squamous Cell Carcinoma

SOX: Sry-Related HMG Box

TP53: Tumor Protin 53

TGF-β: Transforming Growth Factor Beta

PI3k: Phosphoinositid-3-Kinase

miRNA: Micro-RNA

SCs: Schwann Cells

PNI: Perineural Invasion

TCGA: The Cancer Genome Atlas Program

CNA: Copy Number Alteration

LUSC: Lung Squamous Cells Carcinoma

LUAD: Lung Adenocarcinoma

PAAD: Pancreatic Adenocarcinoma

GBM: Glioblastoma

CESC: Cervical Squamous Cell Carcinoma and Endocervical Adenocarcinoma

ESCA: Esophageal Squamous Cells Carcinoma

PRAD: Prostate Adenocarcinoma

BRCA: Breast Invasive Carcinoma

CCLE: Cancer Cell Line Encyclopedia

FFPE: Formalin-Fixed Paraffin-Embedded Tissues

CNI: Cancer Neuron Interaction

IHC: Immunohistochemistry Staining

MSigDB: Molecular signature database

GOF: Gain-of-Function

EGFR: Epidermal Growth Factor Receptor

IARC: International Agency for Research on Cancer

OPSCC: Oropharyngeal Squamous Cells Carcinoma

OS: Overall survival

DSS: Disease-Specific Survival

PFS: Progression-Free Survival

GSVA: Gene Set Variation Analysis

TSNA: Tobacco-Specific Nitrosamines

PAH: Polycyclic Aromatic Hydrocarbons

HPV16: Human Papilloma Virus-16

NK: Natural Killer Cells

TAMs: Tumor-Associated Macrophages

MDSCs: Myeloid-Derived Suppressor Cells

DCs: Dendritic Cells

CC: Cancer Cells

CAFs: Cancer-Associated Fibroblasts

Treg: T- Regulatory Cells

MMPs: Matrix Metalloproteinases

ECM: Extracelluar Matrix

IFN-γ: Interferon-Gamma

LASSO: Least Absolute Shrinkage and Selection Operator

GEO: Gene Expression Omnibus

ANOVA: Analysis of Variance

DEG: Differentially Expressed Gene

RB: Retinoblastoma Protein

CRT: chemoradiotherapy

RT: Radiotherapy

CT: Chemotherapy

ICI: Immune Checkpoint Inhibitors

NPC: neural progenitor cells

TRKs: Tyrosine Receptor Kinases

Table of Contents

List of Figures

List of Tables and Supplements

1. Introduction

1.1. The Development and Causes of Cancer

Cancer is a disease of altered signaling and metabolism, causing uncontrolled division and survival of transformed cells. A host of molecules, factors, and conditions have been nominated as underlying causes for the initiation and progression of the disease [1]. The fundamental abnormality resulting in the development of cancer is the continual unregulated proliferation of cancer cells [2]. There are more than a hundred distinct types of cancer, which can differ substantially in their behavior and response to treatment [2]. The development of cancer and the fundamental feature of cancer is based on tumor clonality, the development of tumors from single cells that begin to proliferate abnormally. Cancer arises through the accumulation of genetic and epigenetic changes in genes whose encoded proteins act in a variety of signaling pathways [3, 4]. At the cellular level, the development of cancer is demonstrated as a process with multistep entailing mutation and selection for cells with progressively increasing capacity for proliferation, survival, invasion, and metastasis [2]. The initial step in the process is tumor inception, as a result of a genetic alteration leading to the abnormal proliferation of a single cell. The cell proliferation then conducts to the outgrowth of a population of clonally derived tumor cells. Tumor progression continues as additional mutations occur within cells of the tumor population. Tumors are classified based on the type of cell from which they arise. Most cancers fall into one of three main groups: carcinomas, sarcomas, and leukemias or lymphomas. Carcinomas, which include approximately 90% of human cancers, are malignancies of epithelial cells [2].

1.2. Head and Neck Squamous Cell Carcinoma (HNSCC)

Head and neck cancer (HNC) is the term given to a variety of malignant tumors that develop in the oral cavity, larynx, and pharynx, and are predominantly squamous cell carcinomas (SCCs) [4]. HNSCCs arise in the mucosal linings of the upper aerodigestive tract (Figure 1.1) and are unexpectedly heterogeneous in nature. HNSCCs remain the sixth leading cause of cancer-related morbidity and mortality, with 600,000

new cases diagnosed yearly [4].

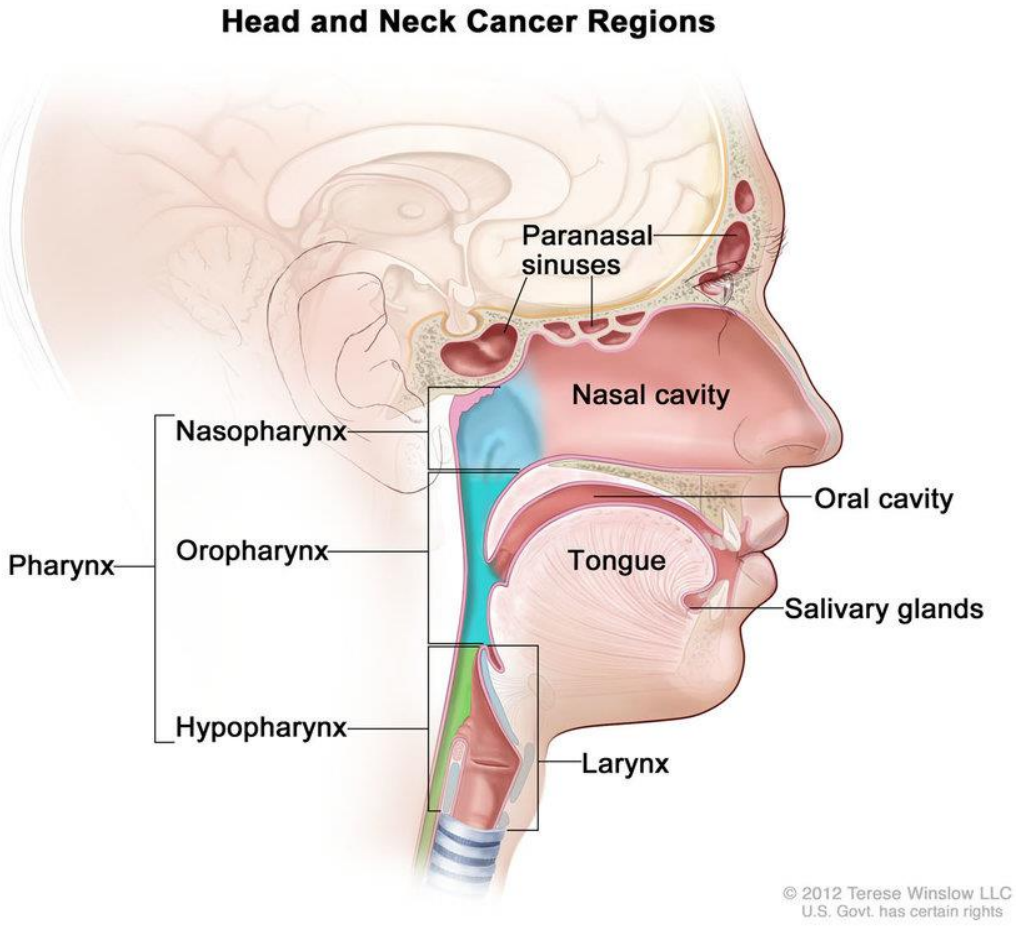

Figure 1.1: Anatomical structure and regions of the head and neck.

The head and neck region is composed of paranasal sinuses, nasal cavity, oral cavity, larynx, and pharynx (Including the nasopharynx, oropharynx, and hypopharynx). Credit: Terese Winslow LLC 2012.

1.3. Epidemiology and Risk Factors of HNSCCs

HNSCC is a heterogeneous disease and the main risk factors are tobacco smoking and alcohol consumption, and infection with high-risk types of human papillomavirus (HPV), in particular HPV16, [4]. The risk for HNSCC in smokers is approximately ten times higher than that of never smokers, and 70-80% of new HNSCC diagnoses are correlated with tobacco and alcohol use [5]. Smoking is more strongly

associated with laryngeal cancer and alcohol consumption with pharynx and oral cavity cancers. A combination of smoking and alcohol consumption causes a synergistic effect on the risk to develop HNSCC [6]. Although the mechanisms for alcohol-associated carcinogenesis are not fully understood, IARC listed both alcoholic beverages and acetaldehyde, its major metabolite, as human carcinogens in 2012 [7, 8]. Previous studies have demonstrated several carcinogenic effects of ethanol and acetaldehyde in humans. First, acetaldehyde disrupts DNA synthesis and repair and binds to proteins, resulting in structural and functional alterations [8-11], which includes enzymes involved in DNA repair and methylation, as well as glutathione, an important anti-oxidative peptide [8-11]. Second, acetaldehyde binds to DNA forming stable DNA adducts [8, 9, 11-14]. Third, ethanol is oxidized to acetaldehyde by microbes in the oral cavity [8, 15, 16]. The second main risk factor is tobacco consumption. Since the Surgeon General's report in 1964, there has been a tremendous effort to study the carcinogenic effects of tobacco products. These research efforts have led to significant advances in understanding the constituents of tobacco products. To date, over 70 known carcinogens have been described in cigarette smoke [5, 17]. Of the many toxic and carcinogenic substances resulting from tobacco exposure, tobacco-specific nitrosamines (TSNA) and polycyclic aromatic hydrocarbons (PAH) have been most heavily studied with regard to exposure and carcinogenicity [17] [5]. The third risk factor is infection with the oncogenic type of HPV. Nearly all adults in western counties have contact with oncogenic HPV during adolescence. In cervical cancer, the majority of cervical lesions typical oncogenic HPV types 16, 18, 31, and 45 are found [18]. The most frequently detected HPV type at the time of SCC diagnosis is HPV16 [19]. HPV16 plays a pathogenic role in a subset of HNSCC —mostly cancers of the oropharynx—with distinct epidemiological, clinical, and molecular characteristics compared with HPV16-negative counterparts [20]. Many recent studies have demonstrated that HPV16-positive OPSCCs are associated with improved prognosis [21]. Furthermore, these tumors display a higher sensitivity to treatment agents like chemotherapy and radiotherapy [21].

1.4. The Molecular Mechanisms of HPV-16 associated Carcinogenesis

The natural history of HPV16-induced head and neck tumors remains elusive. In contrast to cervical carcinomas, developing via dysplastic precursor lesions over a long period is well illustrated [22]. HPV16 is the most prevalent high-risk type in oropharyngeal cancers [21]. The HPV-DNA is more frequently found unintegrated in the cancers of the oropharynx compared to those that arise in the cervix and may include novel HPV-human DNA hybrids episomes [21, 23]. The HPV-associated carcinogenesis is mainly driven by two viral early genes (*E6* and *E7*, often referred to as HPV oncogenes), the physiological function of which is to trigger cell-cycle entry in the basal layer of the epithelium and thus permit viral genome replication [18, 21]. During HPV-associated carcinogenesis, p53 is marked for proteolytic degradation by E6 activity and thus inactivated. E7 binds to the retinoblastoma protein (RB) that triggers the cell cycle and releases the transcription factor E2F. This increases the transcription of genes that are relevant for cell proliferation [18, 21]. Nevertheless, HPV16-positive HNSCC with or without integrated viral genome also displayed different patterns of both human and viral gene expression and epigenetic regulations such as DNA methylation [21, 24]. These events imply that there may be an alternative mechanism of HPV viral oncogenesis that does not depend on E6/E7 expression or viral integration but may be driven by episomal E2/E4/E5 expression [25]. A study focused on the characterization of HPV and host genome interactions in primary HNSCC suggested that at least two-thirds of patients with high expression of E6 and E7 by RNA quantification have detectable integration sites in the genome [24]. Collectively, the accurate nature of the integration is the subject of an ongoing investigation.

1.5. The Genetic and Epigenetic Regulations in HPV- Positive and Negative HNSCCs

Several publications have reported the mutational landscape of HPV16-positive versus HPV16-negative HNSCC [26-28]. Across much of the genome, the copy number alterations from HPV16-positive and HPV16-negative tumors are mostly identical, and shared amplifications are 1q, 3q, 5p, 8q, and others.

Largely included deletions are 3p, 5q, 11q, and others [26-28]. In solid tumors, TP53 is the gene most frequently affected by mutations [26]. In a comparative study, whole exome analyses were performed in 15 types of solid tumors, 11 of them revealed TP53 as the most frequently mutated gene, in the other entities it ranked second twice and third once (preceded by KRAS or BRAF and NRAF) [18, 29]. In HNSCC, the mutation rate of TP53 is in the upper third of solid tumors with about 40%. Besides TP53, mutations of CDKN2A and RB1 (RB, retinoblastoma-associated protein) are often observed in HPV-negative HNSCC, however, they are missing in HPV16-associated OSCC [26, 30]. The Cancer Genome Atlas (TCGA) represents the most comprehensive integrative genomic analysis profiling 528 HNSCCs to provide a global landscape of somatic genomic alterations. The HPV-associated tumors are dominated by helical domain mutations of the oncogene PIK3CA, novel alterations involving loss of TRAF3, and amplification of the cell cycle gene E2F1. Smoking-related HNSCCs showed near-universal loss-of-function TP53 mutations and CDKN2A inactivation with frequent copy number alterations such as the amplification of 3q26/28 and 11q13/22. A subgroup of oral cavity tumors that have a favorable clinical outcome demonstrated infrequent copy number alterations in conjunction with activating mutations of HRAS or PIK3CA, coupled with inactivating mutations of CASP8, NOTCH1, and TP53. Other distinct subgroups contained loss-of-function alterations of the chromatin modifier NSD1, WNT pathway genes AJUBA and FAT1, and activation of oxidative stress factor NFE2L2, mainly in laryngeal tumors [27]. The TCGA reveals a limited number of pathways targeted by frequent genome alterations. Among receptor tyrosine kinases, EGFR/ERBB2 or FGFR1/3 alterations are the most frequent. Among downstream targets of the receptor tyrosine kinase (RTK)/RAS/phosphatidylinositol-3-OH kinase (PI3K) pathway, PIK3CA dominates with occasional HRAS and PTEN alterations. Further downstream, nearly every tumor has an alteration of genes governing the cell cycle. The tumor suppressors TP53 and CDKN2A, oncogenes CCND1 and MYC, are most often altered in HPV-negative tumors, whereas viral genes E6, E7, and E2F1 predominate in HPV-positive cases [27, 30-32]. In an integrative study based on proteogenomic characterization of

108 HPV-negative HNSCCs, a systematic catalog of HNSCC-associated proteins and phosphosites was identified that prioritizes copy number drivers and highlights an oncogenic role for RNA processing genes. Moreover, a systematic framework was provided to inform HNSCC biology and treatment by applying multi-omic analysis identifying three molecular subtypes with high potential for treatment with CDK inhibitors, anti-EGFR antibody therapy, and immunotherapy [33].

Besides the genetic aberrations, the epigenetic modifications of nucleic acids play a major role in the characterization of different tumor types [18, 27, 34]. The most important types are methylation of the DNA and modification of histones. The methylation of DNA is reversible, and its function is to use static information of the nucleic acid sequence in a variable manner. Different methylation patterns were well addressed in the context of tumor viruses including HPV [27, 35, 36].

1.6. The Mechanism of Treatment Failure in HNSCCs

In recent years, advances in drug therapy for HNSCCs have progressed rapidly. Treatment is generally multimodal, consisting of surgery followed by chemoradiotherapy (CRT) for oral cavity cancers and definitive CRT for pharynx and larynx cancers [4, 37]. In addition to cytotoxic anti-cancer agents such as platinum-based drugs (cisplatin and carboplatin) and taxane-based drugs (docetaxel and paclitaxel), the EGFR monoclonal antibody cetuximab is generally used in combination with radiation in HPV-negative HNSCCs where comorbidities prevent the use of cytotoxic chemotherapy [4, 37]. The FDA approved the immune checkpoint inhibitors (ICI) such as anti-programmed cell death-1 (PD-1) antibodies pembrolizumab and nivolumab for the treatment of recurrent or metastatic HNSCC and pembrolizumab as the primary treatment for the unresectable disease [4, 37].

1.6.1. Surgery and Radiotherapy

Treatment for HNSCC is usually selected based on the primary tumor subsite, TNM staging, and predicted functional outcomes following different treatment modalities. In general, early-stage (I or II) HNSCC is treated with local therapy, taking advantage of the ability of surgical removal or radiation to

offer a curative modality [38, 39]. The treatment failure in HNSCCs after surgical resection is based on a residual undetectable microscopic disease that causes aggressive invasive tumor growth in a local environment or disseminates by the lymph or blood vessel as dormant metastasis [40] [41]. Although radiation eradicates a large fraction of tumor cells, selected groups of tumor cells (clonogens) are able to survive and repopulate irradiated areas [42]. In the event of treatment failure after single modality radiation or surgery, retrieving with the alternative modality offers a high chance of cure [43, 44].

1.6.2. Chemotherapy

Clonal selection and enrichment of drug-resistant cancer cells are the most common drivers of treatment failure, and the identification of underlying molecular principles of tumor heterogeneity remains a major challenge [45].

The standard chemotherapy regimens for stage III or IV patients are cisplatin, 5-fluorouracil (5-FU), and docetaxel/paclitaxel with a response rate of 20% to 40% [40, 46-48]. A combined strategy of docetaxel, cisplatin, and 5-FU (TPF) treatment in a total of 358 unresectable HNSCC patients showed significantly improved progression-free (11.0 months in TPF and 8.2 months in PF) and OS (18.8 months in TPF and 14.5 months in PF) [49]. So, tumors with more advanced tumor or nodal stage, postoperative radiation, or chemoradiation, guided by pathological risk factors, reduce the risk of recurrence and improve survival [50, 51]. There are four main mechanisms that HNSCC cells acquire to avoid cell death following cisplatin, 5-FU [52, 53], and paclitaxel/docetaxel treatments [54-56], including DNA/RNA damage repair, drug efflux, apoptosis inhibition, and (EGFR)/focal adhesion kinase (FAK)/nuclear factor (NF)-κB activation [57]. The corresponding strategies to those four mechanisms can be translated into developing innovative cancer therapeutics to overcome chemotherapy resistance in HNSCC patients.

1.6.3. Targeted Therapy

In 2008, cetuximab was approved as the first molecular-targeted drug for HNSCCs, and it has come to be used in combination with RT and/or CT [58, 59]. The targeted therapy Cetuximab demonstrates that an

improved understanding of the molecular pathways underlying HNSCC will output valuable new treatment protocols. Cetuximab, a humanized mouse anti-EGFR IgG1 monoclonal antibody, improves locoregional control and overall survival in combination with radiotherapy in locally advanced tumors [58, 60]. In HNSCC, candidate sequencing studies have shown that EGFR is overexpressed most commonly through gene amplification and increased copy number [61], rather than activating mutations or truncation mutants such as EGFRvIII. Based on the limited dependence of HNSCC on EGFR signaling, inhibitors of EGFR have had variable success [40].

1.6.4. Immune Therapy

Cancer immune surveillance is considered to be an important host protection process to inhibit carcinogenesis and maintain cellular homeostasis. In the interaction of host and tumor cells, three essential phases have been proposed: elimination, equilibrium, and escape [62]. During tumor progression, even though an adaptive immune response can be induced by antigen-specific T cells, immune selection produces tumor cell variants that lose major histocompatibility complex class I and II antigens and decreases amounts of tumor antigens in the equilibrium phase. Moreover, tumor-derived soluble factors facilitate the escape from an immune attack and allow progression and metastasis. [62]. The release of negative regulators of immune activation (immune checkpoints) that limit antitumor responses has resulted in unprecedented rates of long-lasting tumor responses in patients with a variety of cancers. This can be achieved by antibodies blocking the cytotoxic T lymphocyte-associated protein 4 (CTLA-4) or the programmed cell death 1 (PD-1) pathway, either alone or in combination [63]. Therefore, ICI have emerged as a frontline treatment for multiple malignancies, enabling immunotherapy to join the ranks of surgery, chemotherapy, radiation, and targeted therapy for cancer treatment [64].

In 2016, anti-PD-1 monoclonal antibodies (Pembrolizumab and Nivolumab) have been approved by the FDA for RM-HNSCC treatment, which open a window for a historically 50% recurrence rate patient

population, despite aggressive multi-modality treatment [65]. Recently, ICI with anti-PD-1 antibodies have demonstrated groundbreaking improvements in clinical response in multiple human cancers, including HNSCC [66-68]. Patients with recurrent metastatic HNSCC (R/M HNSCC) may be cured by salvage resection, re-irradiation [69], or metastasectomy [70]. The remaining patients are considered for systemic therapy. First-line treatment should include ICI such as pembrolizumab, an IgG4 humanized antibody to PD1, in patients with PDL1-expressing tumors unless there is a contraindication to immunotherapy because of an underlying autoimmune disorder. A phase III trial compared pembrolizumab monotherapy or the combination of pembrolizumab with a platinating agent and 5-FU with the same chemotherapy combined with cetuximab. Pembrolizumab plus platinum and 5-FU is an appropriate first-line treatment for R/M HNSCC and pembrolizumab monotherapy is an appropriate first-line treatment for PD-L1-positive R/MHNSCC [71]. Immunotherapy resistance is associated with an impaired function of the immune system [72-74]. The anti-tumor immune response is an extremely complex multi-stage process depending on many factors. Based on the presence or absence of the immune system in the TME, there are three immunophenotypes of tumors: (1) “Hot” tumors, which are strongly infiltrated by T lymphocytes and many inflammatory signals are presented; (2) “cold” tumors, which are scanted of any immune cells infiltration nor inflammatory signs; (3) tumors with an immune exclusion, where immune cells are at the periphery or within the stromal tissue [72-74]. In contrast to the two other groups the group of patients with “Hot” tumors usually demonstrate a better prognosis [72-74].

1.7. Mechanisms Regulating Lineage Plasticity in Cancer

Lineage plasticity is the ability of cells to transform from one cell type to another and is an important part of tissue repair and maintenance of homeostasis. Cellular plasticity can be utilized in cancer when the molecular checkpoints controlling the process are compromised leading to emerging treatment resistance and disease recurrence [75]. So, cancer cell plasticity is a fundamental process in the

generation of tumor heterogeneity [76]. Various tumor cell-intrinsic and extrinsic factors have been demonstrated to be involved in regulating lineage plasticity. [45].

1.7.1. Intrinsic Factors in Modulation of Cancer Cell Plasticity

The mechanism of the tumor cell-intrinsic lineage plasticity depends on genetic factors including the loss of tumor suppressors and gain of oncogenes and the overexpression of several transcription factors, eventually resulting in the enabling of cellular reprogramming. The loss of tumor suppressor genes such as RB1, PTEN, and TP53 has been linked with the acquisition of lineage plasticity in multiple cancers [45]. In addition, altered expression of epigenetic modulators and microenvironmental components also play an important role in facilitating the switching of cellular identity in response to various stressors [75]. Since the discovery of the four reprogramming factors (Oct4, Sox2, Klf4, and c-Myc) by Takahashi and Yamanaka, many other transcription factors have also been highlighted that are linked to lineage reprogramming in development [75]. Many studies suggested Oct4, a homeodomain transcription factor, as a modulator of reprogramming and as cancer progression. It is considered a cancer stem cell marker for multiple cancers including head and neck, breast and liver [75, 77-79]. The SOX family members are upregulated in breast cancer and are involved in promoting tumor progression, invasion, metastasis, and chemoresistance [80]. In particular, SOX9 was identified as an important regulator of luminal to basal plasticity in basal-like breast cancer [80]. Resistance of cancer cell types with specific traits facilitating tumor evolution and treatment resistance could be achieved by transcriptional plasticity [81].

1.7.2. Extrinsic Factors in Modulation of Cancer Cell Plasticity

In addition to genetic and epigenetic mechanisms, cell-extrinsic factors such as inflammation, microenvironment, and therapeutic stress can induce cellular plasticity [81]. Different components in the tumor microenvironment (TME) such as fibroblasts, macrophages, endothelial cells, and infiltrating immune cells can conspire with the tumor cells to promote tumor cell plasticity [82, 83]. Furthermore,

stromal cells, components of the extracellular matrix (ECM) can also modulate cellular plasticity [84]. The matrix stiffness can promote the epithelial-mesenchymal transition (EMT) and stemness in different tumor entities [81]. Moreover, inflammation and therapeutic stress can induce cellular plasticity [85]. Chronic inflammation has long been identified as a hallmark of cancer [85]. and is an important player in tumor progression and metastasis [75] (e.g., Inflammatory cytokines, proinflammatory cytokines, and inflammation-associated myeloid cells are the three key inflammatory axes associated with stemness and EMT in breast cancer plasticity and malignancy [86, 87].

1.8. EMT As a Main Feature of Lineage Plasticity

EMT: a reversible change in molecular, morphological, and functional traits of epithelial cells to more mesenchymal phenotype during the metastatic cascade and/or in the emergence of drug resistance [88, 89]. The process of EMT was first identified in embryonic development in higher chordates, where the primary epithelial cells form mesenchymal tissue through a cell-state transition [90, 91]. EMT is a fundamental cell biological process during wound healing, and also pathological conditions such as fibrosis and cancer [92]. It involves a reduction in epithelial traits such as cell–cell adhesion and apicobasal polarity and a concomitant gain of mesenchymal traits such as increased invasion and migration. Importantly, EMT is viewed as a fulcrum of cellular plasticity in carcinomas [93]. EMT is influenced by different pathways which include transforming growth factor β (TGFβ), Wnt–β-catenin, bone morphogenetic protein (BMP), Notch, Hedgehog, and receptor tyrosine kinases [94]. With the discovery of many intermediate states between canonical epithelial and mesenchymal states, EMT is being rechristened as EMP (epithelial-mesenchymal plasticity) [94].

1.9. SOX Transcription Factors as Intrinsic Modulator in Cancer Cell Plasticity

Several recent studies provided compelling experimental evidence for the critical role of SOX (Sry-related HMG Box) transcription factors in mediating cancer cell plasticity [75]. The sex-determining region on the Y chromosome-related high mobility group box (SOX) transcription factor family contains

more than 20 members in vertebrates, which are classified into eight groups, denoted SoxA to SoxH [95]. The SOX protein family regulates self-renewal, fate specification, and differentiation of embryonic and adult stem/progenitor cells during development and to maintain tissue homeostasis [96, 97]. Several SOX proteins serve as prognostic biomarkers and potential therapeutic drug targets, but further investigations are required to understand the complexity and context dependency of their cancer-related functions [98]. In addition to the pivotal role in maintaining the stemness of cells, aberrant expression or function of SOX proteins is a common feature in numerous human cancers such as breast cancer, prostate cancer, renal cell carcinoma, thyroid cancer, brain tumors, gastrointestinal and lung tumors and has been attributed to cancer progression, modulation of the TME, and metastasis [98]. Regarding the involvement of SOX family members in tumorigenesis, SOX2 is the most thoroughly investigated transcription factor. In healthy organisms, it plays a role in stem cell regulation during embryogenesis, as well as during adult tissue regeneration [98, 99]. Together with Oct4 and Nanog, Sox2 regulates pluripotency and the self-renewal of stem cells, affecting promoters of a high number of other genes [100, 101]. It also has an influence on proliferation and apoptosis, as well as on the migration and adhesion of cells [102].

In human SCC, including lung (LUSC), esophageal (ESCA), and HNSCC recurrent gain on chromosome 3q26 encompassing the gene locus for the transcription factor SOX2 is a frequent event [103, 104].

A study demonstrated SOX2 promotes plasticity and antiandrogen resistance in TP53 and RB1-deficient prostate cancer using in *vitro* and in *vivo* human prostate cancer models [105]. In LUSC, SOX2 amplification and it's corresponding up-regulation were also frequent events but were linked to the indicators of favorable prognosis [103]. In line with previous studies, SOX2-positive cancer cells exhibited epithelial characteristics, while loss of SOX2 expression led to increased mesenchymal properties [106]. An association between SOX2 silencing and an EMT-like phenotype is also evident in lung cancer, and experimental data support a critical role of SOX2-mediated cellular plasticity in

tolerance against EGFR inhibition and metastatic dissemination [107]. Additionally, SOX9 was identified as a crucial regulator of luminal to basal reprogramming in basal-like breast cancer [80]. In lung cancer, an epigenetic switch between SOX2 and SOX9 allows phenotypic and oncogenic plasticity, enabling the cells to alter between proliferative and invasive states [108]. In the context of therapy-induced cancer cell plasticity, a recent study demonstrated that cisplatin resistance and drug-induced adaptation are acquired by loss of SOX2 and a concomitant gain of SOX9 expression in OSCC [106]. SOX2 is expressed in highly proliferative but minimally invasive lung cancer cells and again, phenotypic and oncogenic plasticity are acquired by a switch between differentiation programs controlled by either SOX2 or SOX9 [108]. Taken together, SOX2 and SOX9 have been identified as key regulators in determining cancer cell plasticity, drug resistance, and metastatic progression in several cancers.

1.10. The Components of The Tumor Microenvironment

Cancer research and treatment have switched from a cancer-centric model to a TME-centric one, highlighting the crucial role of TME in cancer biology [109]. Accumulating evidence shows that cellular and acellular components in TME are able to reprogram tumor initiation, growth, invasion, metastasis, and response to therapies [109, 110]. While several cellular and molecular mechanisms have been presented to affect cancer progression, the identity and role of all TME components remain elusive [111]. The main components of TME are stromal cells, vasculature, immune cells, and a milieu of signaling molecules within an ECM. Other components of the TME are cancer-associated fibroblasts (CAFs), adipocytes, and pericytes [111]. Many studies have demonstrated different hallmarks of TME play a crucial role in plasticity [112]. TME can be classified into six specialized microenvironments, namely, hypoxic niche, immune microenvironment, metabolism microenvironment, acidic niche, innervated niche, and mechanical microenvironment [109]. Hypoxia is able to reprogram cancer biology in various aspects, including cancer progression, stemness, and dormancy, as well as redox adaptation, intercellular communication, and therapeutic resistance [112]. Metabolic reprogramming is a common

event in cancer and often shows elevated glucose, lipid, glutamine, and amino acids metabolism, lactate accumulation, and ROS addiction [109, 113, 114]. Moreover, the mechanical regulation of the TME (stiffness of ECM) is another recently investigated specialized microenvironment [112]. Its formation depends mainly on intracellular components (vimentin, actin, and neurofilaments), extracellular components (collagen and fibrin), intercellular signaling (integrin), and stromal cells (fibroblasts) [115]. CAFs secrete matrix metalloproteinases (MMPs) including MMP2, MMP3, and MMP9, or activate yes-associated protein to promote ECM degradation and remodeling, EMT, and cancer-stem-cell stemness [116, 117]. Despite the heterogeneity of TME, similar biological roles are observed across multiple cancers related to metabolic support, angiogenesis, metastasis, chemoresistance, and immune regulation [116, 117].

1.11. Peripheral Nerves as Emerging Component Of TME

The neuro-glial activation is a recently identified hallmark of growing cancers [14]. Moreover, the innervated niche is an emerging specialized microenvironment focusing on the neural regulation of TME [109]. Mounting evidence indicates that the nervous system plays a central role in cancer pathogenesis. In turn, cancers and cancer therapies can alter the nervous system's form and function [118]. The close association between neurology and cancer science has been newly expanded. Accordingly, Monje and other scientists have suggested a novel field called "cancer neuroscience" to better study how the nervous system communicates with cancer. The main focus is electrochemical interactions, paracrine interactions, systemic neural-cancer interactions, and cancer-therapy effects on the nervous system [109] [118].

1.12. Perineural Invasion and Its Clinical relevance In the Context of CNI

As early in the 1900s nerve fibers were observed in several cancers [119, 120] among them HNSCC [121]. The main focus of the research was primarily on perineural invasion (PNI), which is described as a

tumor invasion of the existing locoregional nerves, leading to metastasis and reciprocal tumor and nerve growth [122]. Solid tumors disseminate in three well-known ways: direct invasion of surrounding tissue, lymphatic spread, and haematogenic spread. However, a fourth route of cancer spread is that of dissemination along nerves [123]. PNI is a common pathologic finding in SCCs, the most common type of HNSCCs that shows a high density of nerves and usually is associated with poor prognosis [124-126]. Molecular, cellular, and metabolic mechanisms are involved in PNI, which is characterized by a conservative symbiotic relationship between cancer cells and nerve cells [124, 127]. Substances secreted by nerve cells can induce cancer cells invasion, and cancer cells can promote the axonal growth of nerve cells. Due to the potential role of axonal growth in PNI, neurotrophins are considered possible molecular mediators leading to PNI [124].

1.13. Innervated Niche: An Emerging Microenvironment Focusing on The Neural Regulation Of TME

Nerves are emerging regulators of cancer progression. Cancer cells induce the outgrowth of nerves in the TME through the release of neurotrophic factors, and in return nerves liberate neurotransmitters that activate cancer growth and dissemination [128]. Nerves are composed of a variety of cells including neurons and Schwann cells (SCs). SCs are a major component of the peripheral nerves and have been recently identified as cells that promote cancer spread [129]. Furthermore, the contribution of nerves to the pathogenesis of malignancies has been raised as an important component of the TME [130]. However, the origin of these nerves and the mechanism of their inception are still elusive and need to be generously addressed.

Over the past decade, several landmark studies have demonstrated a fundamental role of the nervous system in cancer initiation and progression, and that ablation of specific nerve types (parasympathetic, sympathetic, or sensory) revoke tumor growth in a tissue-specific manner [130].

Nerves in tumors can regulate various cellular and molecular processes, such as angiogenesis, lymphangiogenesis, immunity and inflammation, fibroblasts and the extracellular matrix, DNA repair, and oncogene activation. Furthermore, nerves have been shown to infiltrate the TME and actively stimulate CC growth and dissemination [128, 131, 132]. The neural regulation of immune responses has been identified as an emerging field in cancer biology [133]. Both sympathetic and parasympathetic nerve fibers have been reported in different studies modulating immune response e.g. vagus nerve was suggested to be involved in regulating immune responses in the TME [131, 134, 135]. The nerves bundle along blood vessels and are able to provide a critical set of signals that help tumors to redevelop a vascular network, which ensures nutrition and communication during cancer proliferation and progression [130]. In the context of the effect of nerves on the intrinsic CC traits, nerves sustain tumor proliferation and induce resistance to apoptosis [136]. Most chemotherapies can trigger the p53-dependent apoptotic program of CC. Studies have demonstrated that the neurotransmitter catecholamine mediates chemotherapeutic resistance by activating β2-adrenergic receptor signaling of cervical cancer cells both in *vitro* and in *vivo* [136]. While evidently activated by non-mutational epigenetic reprogramming and, in some cases, genome instability and mutation, the increasing breadth of co-opted neuronal regulatory circuits in CC proposed that this concept warrants being a focal point as a significant hallmark-enabling feature that is conducive to multiple tumor phenotypes [137]. So, the high density of nerves in various modes of action has been reported in multiple human malignancies, including cancers of HNSCC, prostate, colon, rectum, breast, pancreas, stomach, lung, and skin [130, 138, 139].

The peripheral nervous fibers (autonomic and sensorial) are attracted by the TME via axonogenesis which is the outgrowth of nerves in the TME [128, 137]. Axonogenesis is driven by the secretion of neurotrophic factors (NTF) by CC and takes place from peripheral nerves in the surrounding tissues that emerge from the CNS and associated neural ganglia. In return, nerve endings in the TME, which can be

of adrenergic, cholinergic, or sensory origin, release neurotransmitters (NT) that stimulate corresponding receptors in stromal cells, immune cells, and cancer stem cells, resulting in the regulation of cancer growth and metastasis [128]. The tumor-derived factors recruit neural progenitor cells (NPC) to promote intratumor neurogenesis [140]. Neurogenesis (increased number of neurons), and neural reprogramming process in TME, are biological phenomena and mechanisms to induce innervation and nerve growth [141, 142]. Intratumor sympathetic fibers are associated with the early phases of cancer triggering an angiogenic switch via adrenergic signaling. In later phases, parasympathetic fibers contribute to stimulating cancer cells to invasion and metastasis [140]. Furthermore, cancer cells release chemical messengers, e.g., axon guidance molecules and nerve growth factor (NGF) to emphasize neo-neurogenesis and axonogenesis. In HNSCC, axon guidance molecules such as netrins, secreted by cancer cells act in synergy with neurotrophic growth factors to enhance axonogenesis therefore, there is a bidirectional crosstalk between tumors and nerves within TME and this plays an active role in the cancer process [143, 144]. In a landmark study, nerve fibers' impact on oral cancer tumor growth has been proven in several mouse models and their clinical relevance has been demonstrated in a retrospective analysis of samples from oral cancer patients [25]. The p53 tumor suppressor has been identified as an important regulator and its loss of function leads to adrenergic trans-differentiation of tumor-associated sensory nerves through loss of the microRNA miR-34a, thereby promoting tumor development and malignant progression [25]. So, it is conceivable that tumor innervation and co-opted neuronal signaling in cancer cells will prove to modulate additional hallmark capabilities and associated parameters, e.g., phenotypic plasticity [137, 145] (Figure. 1.2).

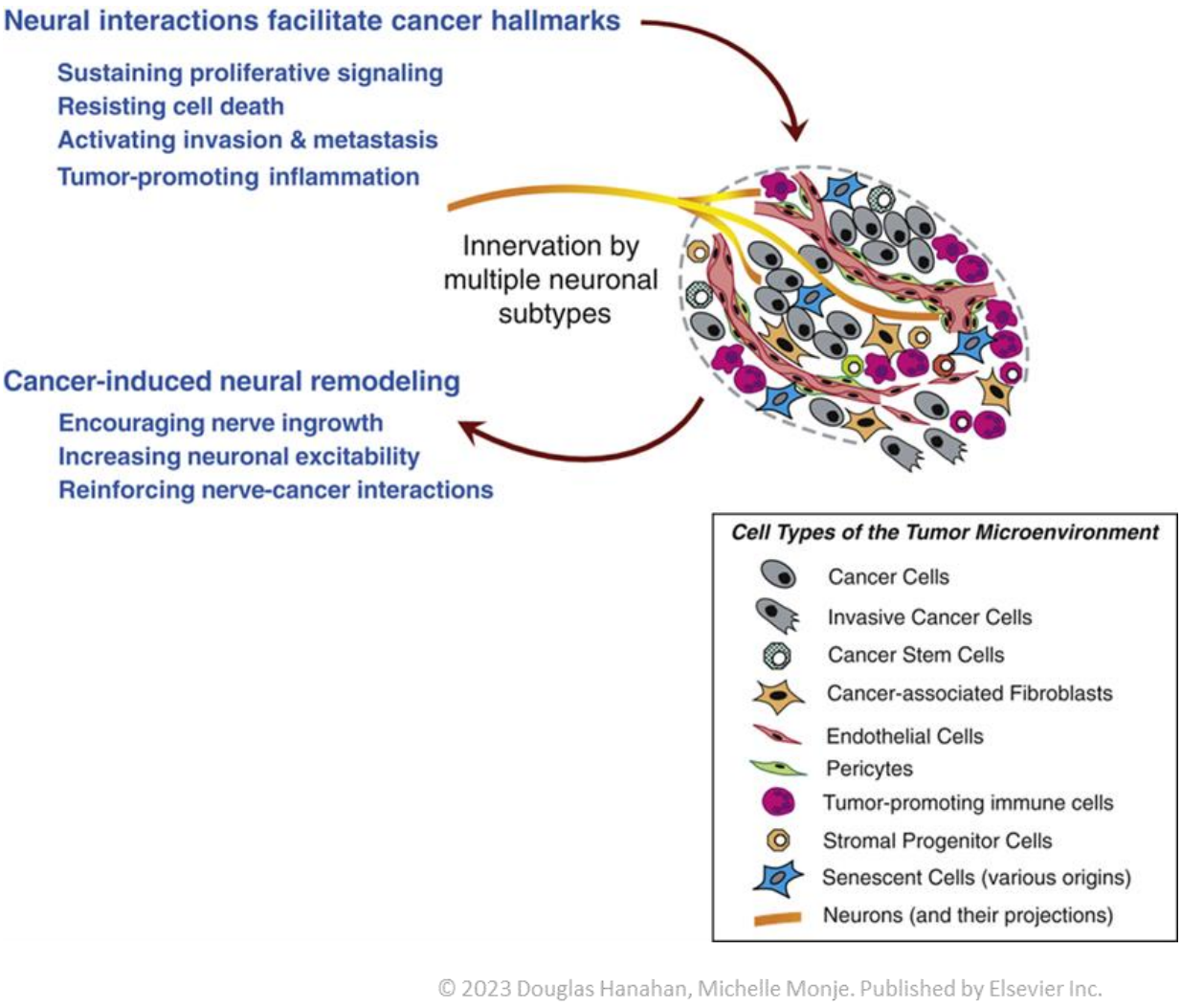

Figure 1.2: *Neurons and their axonal projections are implicated as a common, functionally enabling constituent of the heterotypic cellular TME.*

1.14. Schwann Cells as Surrogate Marker of Peripheral Nerves in Cancer

In addition to neurons, SCs as peripheral glial cells, a key component in neural repair and regeneration, and the most prevalent cell type in peripheral nerves might play a critical role in carcinogenesis [123]. In response to nerve damage caused by invading cancer cells, activated SCs begin to proliferate and migrate from nerves toward cancer cells [146, 147]. Studies have shown that SCs enable cancer progression by adopting a de-differentiated phenotype, similar to the SCs response to nerve trauma [129]. SCs interact with cancer cells and the

accompanying process of axonal sprouting at the premalignant phase provides the first access of cancer to nerves, which leads to neural dissemination at an early disease stage [146, 148]. Many Studies have demonstrated the role of SCs act as an active player of nerve dependence in cancer. In pancreatic and colon cancer, SCs colonize neoplastic sites before the onset of cancer invasion [147]. So, as its crucial role in attracting cancer cells to the perineural niche and enabling adhesion of cancer cells to the nerves [48, 148] (Figure. 1.3).

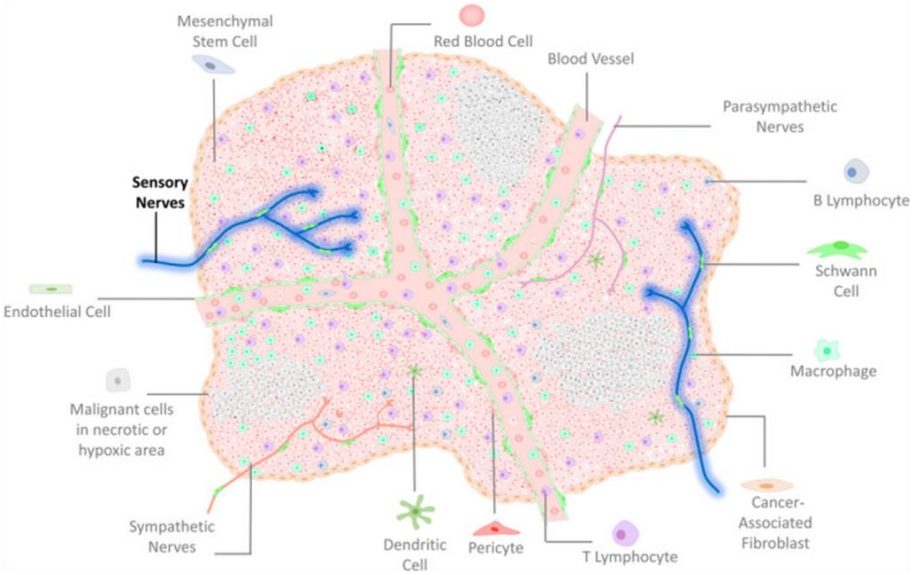

Figure. 1.3: *Schematic illustration showing the complexity of TME with its known components, outlining the newly discovered sensory nerves within the tumor.*

1.15. Aims of Study

Various tumor cell-intrinsic and extrinsic factors have been demonstrated to be involved in regulating lineage plasticity. The mechanism of the tumor cell-intrinsic lineage plasticity (e.g., mutational landscape, epigenetic regulation, signaling, and gene regulatory networks), while tumor cell-extrinsic lineage plasticity depends on (e.g., cellular and matrix components of TME).

So, in this study I aimed extensively to examine cancer cell plasticity in the pathogenesis and therapy of HNSCC and other tumors.

1.15.1. Focus on cancer cell-intrinsic mechanisms and modulators of plasticity in particular the role of SOX family members in cancer lineage plasticity, and more precisely the inverse regulation of SOX2- and SOX9-related gene networks in HNSCC and other tumor entities.

The clinical relevance of inverse SOX2-SOX9 expression for HNSCC and other tumor entities and the establishment of risk models to identify patients with primary HNSCC and other cancers at a higher risk for treatment failure, who might benefit from a therapy targeting SOX2/SOX9-related gene regulatory and signaling networks. In addition to the molecular and cellular characterization of the predicted risk models in HNSCC and other tumor entities.

1.15.2. Focus on cancer cell-extrinsic mechanisms and modulators of plasticity, particularly the role of molecular mechanisms contributing to the complex crosstalk between cancer cells, neurons, and their associated glial cells such as Schwann cells.

The clinical relevance of nerve fibers and associated cells such as Schwann cells for HNSCC and other tumor entities and the molecular characterization of cancer-nerve crosstalk in HNSCC and other tumor types. Finally, the establishment and analysis of pre-clinical models as a proof-of-concept for new therapeutic strategies.

2. Material and Methods

2.1. Key Resources

Details on all publicly available data, patient cohorts, online tools, software, and algorithms used in this thesis are listed in (Table. 1A-B). All data are anonymized and the TCGA ethics and policies were originally published by the National Cancer Institute. Patient cohorts used in this thesis are TCGA-HNSC consisting of 499 primary HNSC as a training cohort and validation cohorts for HNSCC (GSE117973, CPTAC-HNSC, GSE65858, and GSE39368), and for other tumor entities from TCGA such as CESC, ESCA, LUSC, LUAD, PAAD, PRAD, GBM, and BRCA. The CCLE data from the GDSC1-2 and PRISM screening projects as well as the Oncopredict scores. Information on the HPV16 status was accessed from Cao et al., with a cutoff of 100 counts for HPV16 positivity [149].

***Table 1.A**: Summary of data resources, online tools.*

Description	Data types	Source	Link	Accession Date
Cancer Cell Line Encyclopedia (CCLE)	Cell line information	depmap portal	https://depmap.org/portal/	2023-01-05
	Gene expression 20Q4	depmap portal	https://depmap.org/portal/	2023-01-05
	GDSC 1&2	depmap portal	https://depmap.org/portal/	2023-01-05
GSE117973	Gene expression	GEO: GSE117973	https://www.ncbi.nlm.nih.gov/geo/query/acc.cgi	2020-10-11
	Tumor Tissues	GEO: GSE117973	https://www.ncbi.nlm.nih.gov/geo/query/acc.cgi	2016-11-21
CPTAC-HNSC	Gene expression	GDC Portal	LinkedOmics: http://www.linkedomics.org	2023-01-03
	Copy number data	GDC Portal	LinkedOmics: http://www.linkedomics.org	2023-01-03
GSE65858	Gene expression	GEO: GSE65858	https://www.ncbi.nlm.nih.gov/geo/query/acc.cgi	2023-01-03
GSE39368	Gene expression	GEO: GSE39368	https://www.ncbi.nlm.nih.gov/geo/query/acc.cgi	2023-01-03
GSE143716	Gene expression	GEO:GSE143716	https://www.ncbi.nlm.nih.gov/geo/query/acc.cgi	2023-01-03
Molecular SignaturesDatabase (MSigDB)	Gene sets (version 7.2)	MSigDB	https://www.gsea-msigdb.org/gsea/msigdb/index.jsp	2020-10-07
	Immunhistochemical staining	This study		
Protein Atlas	GAP43 Abcam ab75810 rabbit	Human Protein Atlas	https://www.proteinatlas.org/	2021-08-05
Protein Atlas	UCHL1 Sigma HPA005993 rabbit	Human Protein Atlas	https://www.proteinatlas.org/	2021-08-05
Protein Atlas	S100B abcam ab52642 rabbit	Human Protein Atlas	https://www.proteinatlas.org/	2021-08-05
Protein Atlas	SNCA Sigma HPA005459 rabbit	Human Protein Atlas	https://www.proteinatlas.org/	2021-08-05
Protein Atlas	NCAM1 Invitrogen MA5-16446 mouse	Human Protein Atlas	https://www.proteinatlas.org/	2021-08-05
TCGA-HNSC	Clinical data	cBioPortal	https://www.cbioportal.org/	2020-08-17
		GDC portal	https://gdac.broadinstitute.org/	2020-08-17
	Gene expression	GDC portal	https://www.cbioportal.org/	2019-02-19
	Mutation data	cBioPortal	https://www.cbioportal.org/	2020-09-01
	Copy number data	cBioPortal	https://www.cbioportal.org/	2020-08-17
	Copy number data	Firehose Broad GDAC	https://gdac.broadinstitute.org/	2020-08-17
	miRNA counts	Firehose Broad GDAC	https://gdac.broadinstitute.org/	2022-08-17
TCGA-LUSC	Gene expression	(GDC) Data Portal	LinkedOmics: http://www.linkedomics.org	2020-08-17
	miRNA counts	Firehose Broad GDAC	https://gdac.broadinstitute.org/	2022-08-17
TCGA-CESC	Gene expression	(GDC) Data Portal	LinkedOmics: http://www.linkedomics.org	2020-08-17
	miRNA counts	Firehose Broad GDAC	https://gdac.broadinstitute.org/	2022-08-17
TCGA-ESCA	Gene expression	(GDC) Data Portal	LinkedOmics: http://www.linkedomics.org	2020-08-17
	miRNA counts	Firehose Broad GDAC	https://gdac.broadinstitute.org/	2022-08-17
TCGA-BRCA	Gene expression	(GDC) Data Portal	LinkedOmics: http://www.linkedomics.org	2020-08-17
	miRNA counts	Firehose Broad GDAC	https://gdac.broadinstitute.org/	2022-08-17
TCGA-LUAD	Gene expression	(GDC) Data Portal	LinkedOmics: http://www.linkedomics.org	2020-08-17
	miRNA counts	Firehose Broad GDAC	https://gdac.broadinstitute.org/	2022-08-17
TCGA-PAAD	Gene expression	(GDC) Data Portal	LinkedOmics: http://www.linkedomics.org	2020-08-17
	miRNA counts	Firehose Broad GDAC	https://gdac.broadinstitute.org/	2022-08-17
TCGA-PRAD	Gene expression	(GDC) Data Portal	LinkedOmics: http://www.linkedomics.org	2020-08-17
	miRNA counts	Firehose Broad GDAC	https://gdac.broadinstitute.org/	2022-08-17
Panglao DB (Schwann cells signature)	single cell RNA sequencing data	Panglao DB	https://panglaodb.se/index.html	2020-08-01
Schwann cells related gene sets (Rodents)	unbiased single-cell transcriptomic	[25]		2020-08-01
Anova Tukey HSD calculator	Independent multiple data treatments		https://astatsa.com › OneWay_Anova_with_TukeyHSD	2023-03-01
gProfiler	gene, protein, microarray probes		https://biit.cs.ut.ee/gprofiler/	2020-03-08
Harmonizome	gene, gene sets	Mayan lab	https://maayanlab.cloud/Harmonizome/	2020-07-01
Kassandra	deconvolution data (immune cells, stromal etc.)	Boston Gene	https://science.bostongene.com/kassandra/	2020-09-01
Cibersortx	deconvolution data (immune cells)	Alizadeh and Newman Lab	https://cibersortx.stanford.edu/	2020-09-01
xCell	deconvolution data (immune cells, stromal, etc.)	Butte lab and Aran lab	https://xcell.ucsf.edu/	2020-09-01

***Table 1.B:** Summary of software, and algorithms.*

Name	Version	Link	Reference
annotate	1.62.0	https://cran.r-project.org/	RRID:SCR_003005
AnnotationDbi	1.48.0	https://bioconductor.org/	RRID:SCR_006442
Biobase	2.46.0	https://cran.r-project.org/	RRID:SCR_003005
BiocGenerics	0.32.0	https://cran.r-project.org/	RRID:SCR_003005
broom	0.7.11	https://cran.r-project.org/	RRID:SCR_003005
CePa	0.7.0	https://cran.r-project.org/	RRID:SCR_003005
circlize	0.4.13	https://cran.r-project.org/	RRID:SCR_003005
clusterProfiler	3.12.0	https://cran.r-project.org/	[150]
ComplexHeatmap	2.0.0	https://cran.r-project.org/	[151]
CoNVaQ	0.1.0	https://exbio.wzw.tum.de/convaq/	[152]
dplyr	1.0.7	https://cran.r-project.org/	RRID:SCR_003005
edgeR	3.26.8	https://cran.r-project.org/	[153]
enrichplot	1.4.0	https://cran.r-project.org/	RRID:SCR_003005
eulerr	6.1.1	https://cran.r-project.org/	RRID:SCR_003005

forcats	0.5.1	https://cran.r-project.org/	RRID:SCR_003005
futile.logger	1.4.3	https://cran.r-project.org/	RRID:SCR_003005
GenVisR	1.16.1	https://cran.r-project.org/	RRID:SCR_003005
ggbreak	0.0.8	https://cran.r-project.org/	RRID:SCR_003005
ggplot2	3.3.5	https://cran.r-project.org/	RRID:SCR_003005
ggpubr	0.4.0	https://cran.r-project.org/	RRID:SCR_003005
ggrepel	0.9.1	https://cran.r-project.org/	RRID:SCR_003005
gmodels	2.18.1	https://cran.r-project.org/	RRID:SCR_003005
graph	1.62.0	https://cran.r-project.org/	RRID:SCR_003005
gridExtra	2.3	https://cran.r-project.org/	RRID:SCR_003005
GSEABase	1.46.0	https://cran.r-project.org/	[154]
GSVA	1.32.0	https://cran.r-project.org/	[155]
IGV	2.8.0	http://www.broadinstitute.org/igv	[156]
illuminaHumanv4.db	1.26.0	https://cran.r-project.org/	RRID:SCR_003005
IRanges	2.20.2	https://cran.r-project.org/	RRID:SCR_003005
jstable	1.0.7	https://cran.r-project.org/	RRID:SCR_003005
lattice	0.20-45	https://cran.r-project.org/	RRID:SCR_003005
limma	3.40.6	https://cran.r-project.org/	[157]
maftools	2.0.16	https://cran.r-project.org/	[157]
Matrix	1.3-4	https://cran.r-project.org/	RRID:SCR_003005
MVisAGe	0.2.1	https://cran.r-project.org/	RRID:SCR_003005
org.Hs.eg.db	3.8.2	https://bioconductor.org/	RRID:SCR_006442
prodlim	2019.11.13	https://cran.r-project.org/	RRID:SCR_003005
purrr	0.3.4	https://cran.r-project.org/	RRID:SCR_003005
QuPath	0.2.3	https://qupath.github.io/	[158]
R Version	3.6.1	https://www.r-project.org/	RRID:SCR_001905
RColorBrewer	1.1-2	https://cran.r-project.org/	RRID:SCR_003005
readr	2.1.1	https://cran.r-project.org/	RRID:SCR_003005
readxl	1.3.1	https://cran.r-project.org/	RRID:SCR_003005
rlist	0.4.6.2	https://cran.r-project.org/	RRID:SCR_003005
RStudio	1.2.1335	https://www.rstudio.com/	RRID:SCR_000432
S4Vectors	0.24.4	https://cran.r-project.org/	RRID:SCR_003005
stringr	1.4.0	https://cran.r-project.org/	RRID:SCR_003005
survey	4.1-1	https://cran.r-project.org/	RRID:SCR_003005
survminer	0.4.9	https://cran.r-project.org/	RRID:SCR_003005
tblhelpr	0.2.0	https://cran.r-project.org/	RRID:SCR_003005
tibble	3.1.6	https://cran.r-project.org/	RRID:SCR_003005
tidyr	1.1.4	https://cran.r-project.org/	RRID:SCR_003005
tidyverse	1.3.1	https://cran.r-project.org/	RRID:SCR_003005
vcd	1.4-9	https://cran.r-project.org/	RRID:SCR_003006
VennDiagram	1.7.1	https://cran.r-project.org/	RRID:SCR_003007
xgboost	1.5.0.2	https://cran.r-project.org/	RRID:SCR_003008
Oncopredict	0.1	https://cran.r-project.org/	[159]

XML	3.99-0.3	https://cran.r-project.org/	RRID:SCR_003009
corrplot	0.92	https://cran.r-project.org/	[160]
rstatix	0.7.2	https://cran.r-project.org/	rpkgs.datanovia.com/rstatix/
Hmisc	5.0-1	https://cran.r-project.org/	hbiostat.org/R/Hmisc/
hgu95a.db	3.16	https://bioconductor.org/packages/hgu95a.db/	[160]
crosstable	0.5.0	https://cran.r-project.org	https://github.com/DanChaltiel/crosstable/
Subio64	1.4	https://www.subioplatform.com	Subio Inc., Tokyo, Japan

2.2. Tissue Microarrays and Immunohistochemical Staining

Paraffin-embedded tissue specimens of primary HNSC from surgical resections of the GSE117973 cohort were provided by the tissue bank of the National Center for Tumor Diseases (NCT, Institute of Pathology, University Hospital Heidelberg, Heidelberg, Germany) and were analyzed according to protocols (ethic votes: S-206/2005 and S-232/2022), approved by the Ethics Committee of Heidelberg University, with written informed consent from all participants. The generation of tissue microarrays (TMAs), a summary of clinical and histopathological data, an assessment of HPV16 status, and IHC staining for SOX2 have been described elsewhere [161], [162].

IHC staining was performed according to Thierauf et al. [163] on formalin-fixed paraffin-embedded (FFPE) sections from a TMA with a polyclonal rabbit anti-SOX9 antibody (HPA001758, Sigma-Aldrich). Stained TMAs were scanned with the Nanozoomer HT Scan System (Hamamatsu Photonics), and the scoring procedure was performed using the NDP.view 2 software (Hamamatsu Photonics). The final immunoreactivity score (IRS, ranging from 1-16) was computed by multiplying a score for the amount of stained cancer cells (1 = no staining; 2 = 1-33%; 3 = 34-66%; 4 = 67-100%) and a score for staining intensity (1 = no staining; 2 = low; 3 = moderate; 4 = high).

For the IHC-staining with the anti-GAP43 antibody and five other established peripheral nerve and SCs marker proteins were selected (Anti-UCHL1, Anti-S100B, Anti-NCAM1, and Anti-SNCA). IHC-stained slides were scanned with the VENTANA DP 200 Slide Scanner (Roche, Mannheim, Germany), and

quantification of areas with GAP43-positive neurons was done by visual inspection of ten independent areas on digital images.

2.3. Differential Expressed Gene (DEGs) Analysis

Cases of the TCGA-HNSC cohort were ranked according to either SOX2 or SOX9 transcript levels (FPKM) and those with the lowest or highest expression were selected, respectively, according to quartiles (top and top 25%). Significantly DEGs (-1>log2FC<1 and adj. P<0.05) among groups with lowest versus highest SOX2 or SOX9 expression (n=125 each subgroup) were computed by either limma-voom or edgeR packages in R Studio (4.0.2). The common gene set (n=57) was identified by using Venn diagrams.

2.4. LASSO-Penalized Cox Regression Analysis

A LASSO-penalized Cox regression analysis was applied to prioritize the most relevant prognostic candidate genes using the glmnet package in RStudio (4.0.2). The prioritized 15-gene set was used to establish the regression risk model based on 5-years overall survival of TCGA-HNSC. The risk score was computed by the maxstat package in R studio (4.0.2). The analytical formula for risk assessment was based on following coefficients: EVPLL = -0.107583793, ADAMTS6 = -0.083781705, C12orf56 = -0.083235761, EXPH5 = -0.078477708, PDZD2 = -0.057412849, SERPINA11 = -0.029773486, TPRG1 = -0.029335434, EGR2 = -0.000104553, PLAU = 0.000159152, DCBLD1 = 0.0012265, TNFRSF12A = 0.002378353, ADTRP = 0.006139973, UGT1A7 = 0.010549492, CAMK2N1 = 0.016350322, RASL11A = 0.023046717.

2.5. Copy Number Alteration (CNA) Analysis

Segmented data for TCGA-HNSC were downloaded from the “Firehose Broad GDAC”. A value of segment bigger than 0.2 or less than -0.2 were defined as gain or loss, respectively. Group comparisons were done with differences in frequency of specific events at any chromosomal location tested for significance by a two-tailed Fisher’s exact probability test with an accepted P-value significance at a

defined percentage difference level using CoNVaQ. Summary plots were visualized with the IGV_2.4.19 software (Integrative Genomic Viewer_2.4.19).

2.6. Somatic Mutation Analysis

Mutation counts and candidate genes identified by MutSig 2.0 [164] for TCGA-HNSC were accessed from cBioPortal. Statistically significant differences between subgroups were determined by the chi-square test using R studio (4.0.2).

2.7. GSVA Analysis for Regulatory Networks and Oncogenic Pathway of MSigDB

Gene sets of the category Hallmark (H) of C6 from the Molecular Signatures Database (MSigDB) were used and enrichment scores were computed by gene set variation analysis (GSVA) package in R using Gaussian Kernel [155] that computes the distribution of enrichment scores of different gene sets based on TCGA-HNSC RNA-seq data counts. Statistical differences in GSVA scores among groups were analyzed by an independent two-sided t-test.

To integrate the selected SCs gene set in the computational analysis GSVA scores were computed for different gene sets, which are related to the peripheral nervous system (PNS) in particular SC based on RNA-seq data of the TCGA-HNSC, n=499 cohort. This model provided harmonized Schwann cell scores (SC score), which we stratified into three groups of SC score (low, moderate, and high). Furthermore, eleven gene sets were selected from MsigDB [165] and applied to the GSVA model with the same purpose of ranking the TCGA-HNSC. To compare the SC score with other published gene sets, three gene sets were selected from a study that provided an unbiased single-cell transcriptomic characterization of the non-diseased rodent PNS [25]. Lastly, I computed the GSVA scores for a SCs gene set provided by Panglao DB [166] that is based on single-cell data of mice and humans. The scores of the established gene sets were compared to the SC score using Spearman's correlation.

GSVA scores for gene sets with a statistical difference were visualized in a multicolored heatmap using the package Complexheatmap) in R studio (4.0.2).

2.8. Reverse Phase Protein Array (RPPA) Data Analysis

RPPA data were downloaded from cBioPortal. Statistical differences in RPPA data for selected candidate proteins between low-risk and high-risk tumors were analyzed by independent two-sided t-test.

2.9. DNA Methylation Analysis

DNA methylation data for TCGA-HNSC were accessed from The PanCancer-Atlas. The global mean beta value was computed based on beta values for the 15,000 genes with the highest variance across all samples, excluding genes of sex chromosomes. Beta values for individual probes annotated for SOX2 of TCGA-HNSC and TCGA-CESC were available from the maplab online tool.

2.10. In Silico Drug Screening Analysis

Gene expression data of HNSCC cell lines (n=45) from Lepikhova et al. were available under the GEO accession number GSE108062 and drug sensitivity data were obtained from the supplemental material. Normalized RNA-seq data (log2-transformed TPM values using a pseudo-count of 1, version 20Q3) of selected cancer cell lines from the Cancer Cell Line Encyclopedia (CCLE) were downloaded from the Dependency Map (DepMap) portal of the Broad Institute. Drug response data of the Sanger GDSC1 and GDSC2 drug screen and the PRISM Repurposing drug screen (version 19Q4) were obtained from the DepMap portal of the Broad Institute.

Statistical differences in drug responses for cancer cell lines were analyzed by Spearman´s correlation using the risk score as a continuous variable.

The Oncopredict scores [159] were computed using the R package (Oncopredict) for TCGA-HNSC based on the CCLE RNA-seq and the drug response IC50 of GDSC1-2.

Statistical differences for the SC score (high vs low) were computed by the Wilcoxon rank test.

2.11. Establishment of the Schwann Cell-Related Gene Set

The Harmonizome tool represents a collection of processed datasets gathered to serve and mine knowledge about genes and proteins from over 70 major online resources [167]. It provided 547

proteins co-occurring with the keyword “Schwann cell” in abstracts of biomedical publications from the “TISSUES Text-mining” Tissue Protein Expression Evidence Scores. The scores indicate the relative strength of the functional associations between genes/proteins and their attributes. Standardized values are related to empirical p values as abs (standardized values) = (-log10p-value) and they are only available for initially continuous data sets. Based on the cutoff $p<0.05$, n=43 genes were selected to build a SCs-related gene set.

2.12. Immune Phenotype Analysis

In order to infer the enrichment of immune cells in groups of TCGA-HNSCC patients deconvolution data for different cell types were downloaded from xCell (n=64), CibersortX (n=22), and Kassandra (n=22) to visualize the enrichment of these cells between SC score (high vs low) for TCGA-HNSCC, (n=330) and TCGA-CESC (n=222).

3. Results

3.1. Establishment of a Plasticity-Associated Risk Model Based on a SOX2- and SOX9-Related Gene Set in Head and Neck Squamous Cell Carcinoma

3.1.1. Inverse SOX2 And SOX9 Expression and Clinical Relevance in an OPSCC Cohort

IHC staining of tissue microarrays (TMAs) with tumor samples of an oropharyngeal SCC (OPSCC) cohort [162] revealed a heterogeneous SOX9 expression pattern ranging from low to prominent nuclear staining in cancer cells (Figure. 3.1A).

In total, an immune reactivity score (IRS, range 1-16) was computed for n=139 cases and demonstrated a statistically significant association between a $SOX9^{high}$ expression pattern (IRS>8) and HPV16-negative OPSCC (p<2.34E-04) or larger tumor size (p=1.2E-02) (Table S1).

Kaplan-Meier plots confirmed an unfavorable progression-free (PFS) and disease-specific survival (DSS) for OPSCC with $SOX9^{high}$ (5-years PFS 25.4% and 5-years DSS 33.6%) versus $SOX9^{low}$ expression (5-years PFS 56% and 5-years DSS 59.9%) (Fig. 3.1B).

However, $SOX9^{high}$ expression did not serve as an independent risk factor for unfavorable survival in a multivariate Cox regression model, which might be explained by the close association with the HPV16 status (data not shown). Comparison with IRS for SOX2, which were assessed for the same OPSCC cohort in a previous study [98] revealed an inverse SOX2 versus SOX9 expression pattern in almost 60% of cases for which data for both proteins were available (Table S2).

It is worth noting that the lowest frequency of HPV16-positive OPSCC was detected for the $SOX2^{low}$/$SOX9^{high}$ subgroup which had a significantly shorter PFS and DSS (5-years PFS 31.6% and 5-years DSS 44.7%) as compared to the $SOX2^{high}$/$SOX9^{low}$ subgroup (5-years PFS 57.7% and 5-years DSS 62.7%) in this OPSCC cohort (Fig. 3.1C).

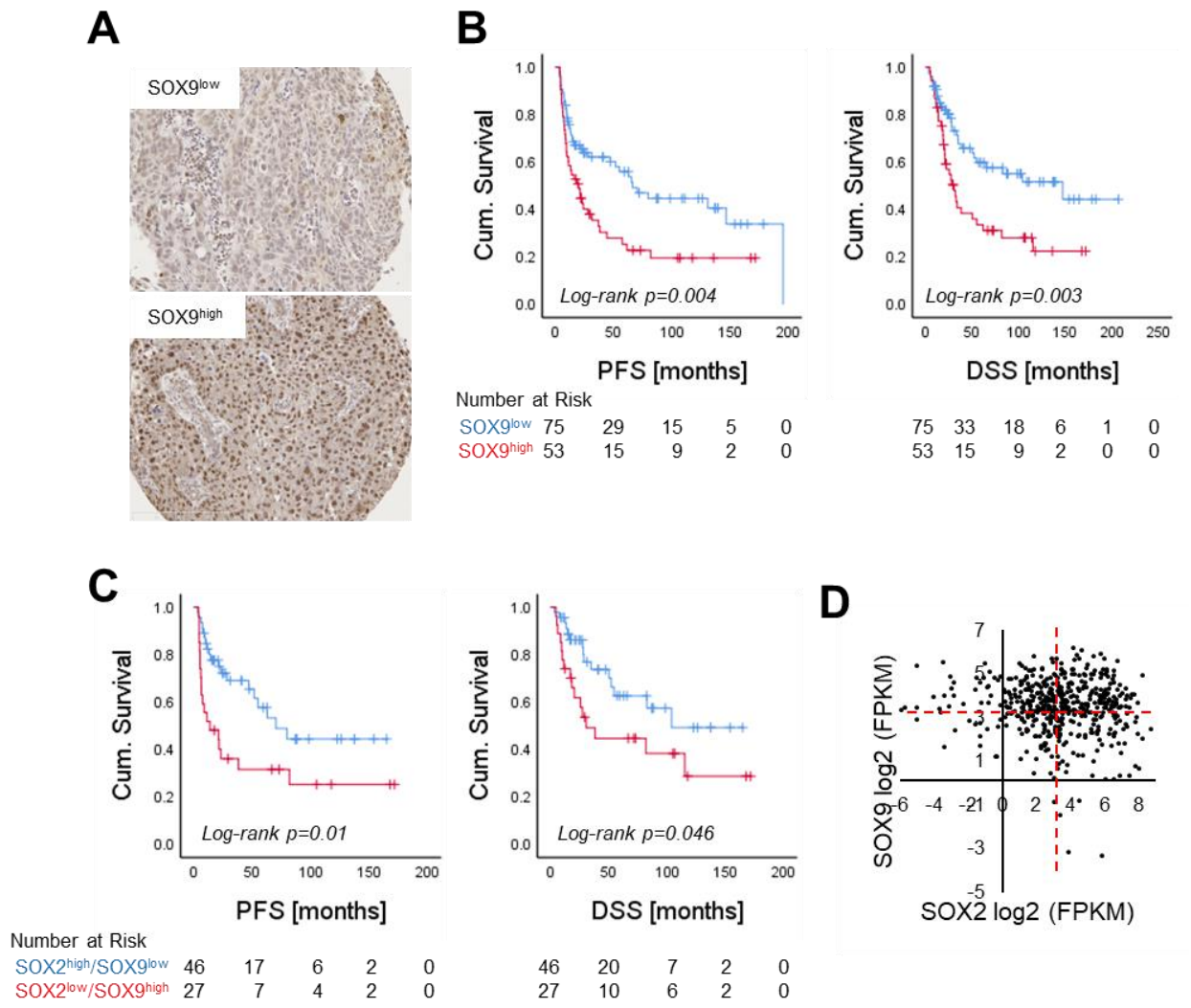

Figure 3.1: Clinical relevance of SOX2 and SOX9 protein expression in OPSCC. (A) *Representative pictures of an IHC staining with an anti-SOX9 antibody show heterogeneous nuclear staining (brown signal) in cancer cells of OPSCC samples. Histological staining with hematoxylin to visualize tissue architecture; scale bar = 200 µM. Kaplan-Meier plots illustrate significant differences in progression-free survival (PFS) or disease-specific survival (DSS) between groups with low or high SOX9 expression* ***(B)****, or between SOX2^{high}/SOX9^{low} and SOX2^{low}/SOX9^{high} subgroups* ***(C)****. **(D)** Dot plot summarizes the distribution of SOX2 and SOX9 transcript levels for cases of TCGA-HNSC. Red dashed lines indicate median levels of either SOX2 or SOX9 transcript levels, respectively. Data provided kindly from the thesis by Julia Schwärzler 2020. Regulation und Funktion der Transkriptionsfaktoren IRX4, SOX9 und SOX2 in der Pathogenese des HPV-assoziierten Plattenepithelkarzinoms im Kopf- und Halsbereich.*

3.1.2. SOX2 and SOX9-related DEGs in the TCGA-HNSC

SOX2 and SOX9 transcript levels were analyzed for samples of the TCGA-HNSC cohort, and an inverse expression was evident for almost 50% of cases (Fig. 3.1D). Samples were ranked according to either SOX2 or SOX9 transcript values and stratified into low or high expression based on the median to define $SOX2^{low}/SOX9^{low}$, $SOX2^{high}/SOX9^{low}$, $SOX2^{low}/SOX9^{high,}$ and $SOX2^{high}/SOX9^{high}$ subgroups for crosstab analysis. In line with the OPSCC cohort, the $SOX2^{high}/SOX9^{low}$ subgroup was enriched for HPV16-positive OPSCC, while almost all tumors of the $SOX2^{low}/SOX9^{high}$ subgroup were HPV16-negative (Table S3).
As the activity of both transcription factors critically depends on post-transcriptional regulation, protein modifications, and protein-protein interaction [97, 98], I assumed that a gene set related to inverse SOX2 and SOX9 expression more reliably reflects their impact on tumor cell plasticity than individual transcript or protein levels. Subgroups of the TCGA-HNSC cohort were defined based on quartiles of samples with the lowest or highest SOX2 or SOX9 transcript levels, respectively, to conduct differential gene expression analysis (Fig. 3.2A-B). Both approaches revealed a set of common differentially expressed genes (DEGs, n=57, Fig. 3.2C, Table S4), which were categorized into four groups related to SOX2 and SOX9 expression (Fig. 3.2D).

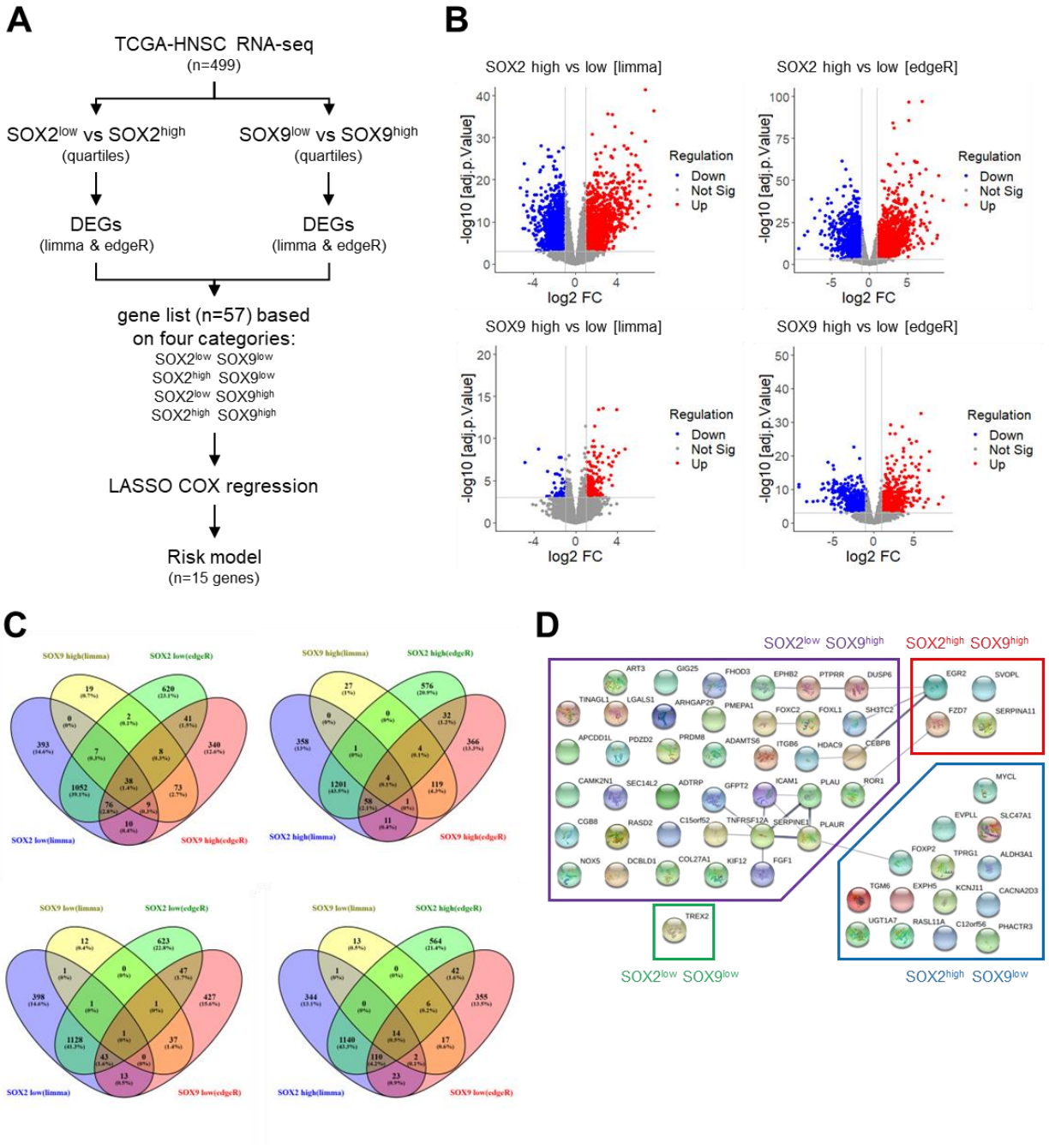

Figure 3.2: Identification of SOX2 and SOX9-related DEGs for TCGA-HNSC. ***(A)*** *Schematic summary of the study design.* ***(B)*** *Volcano plots illustrate significant DEGs (|log2FC|>1 and adj. p<0.05) for subgroups with high versus low SOX2 (upper graphs) or SOX9 (lower graphs) transcript levels by either limma voom (left graphs) or edgeR (right graphs).* ***(C)*** *Venn diagrams show common DEGs (n=57) for distinct combinations of SOX2 and SOX9 expression patterns.* ***(D)*** *Protein-protein interaction network of DEGs (n=57) based on STRING (https://string-db.org/).*

Hierarchical clustering based on transcript levels of these DEGs defined two main clusters (A and B), each with two sub-clusters (Fig. 3.3A). HPV16-positive OPSCC were significantly more frequent in cluster A comprising the $SOX2^{high}$ group and perineural invasion was significantly associated with the $SOX9^{high}$ group in cluster B (Table S5). Sub-cluster A2 was enriched for cases with $SOX2^{high}/SOX9^{low}$ and had a significantly more favorable prognosis considering DSS and OS as compared to sub-cluster B2 resembling the $SOX2^{low}/SOX9^{high}$ subgroup (Fig. 3.3B-C).

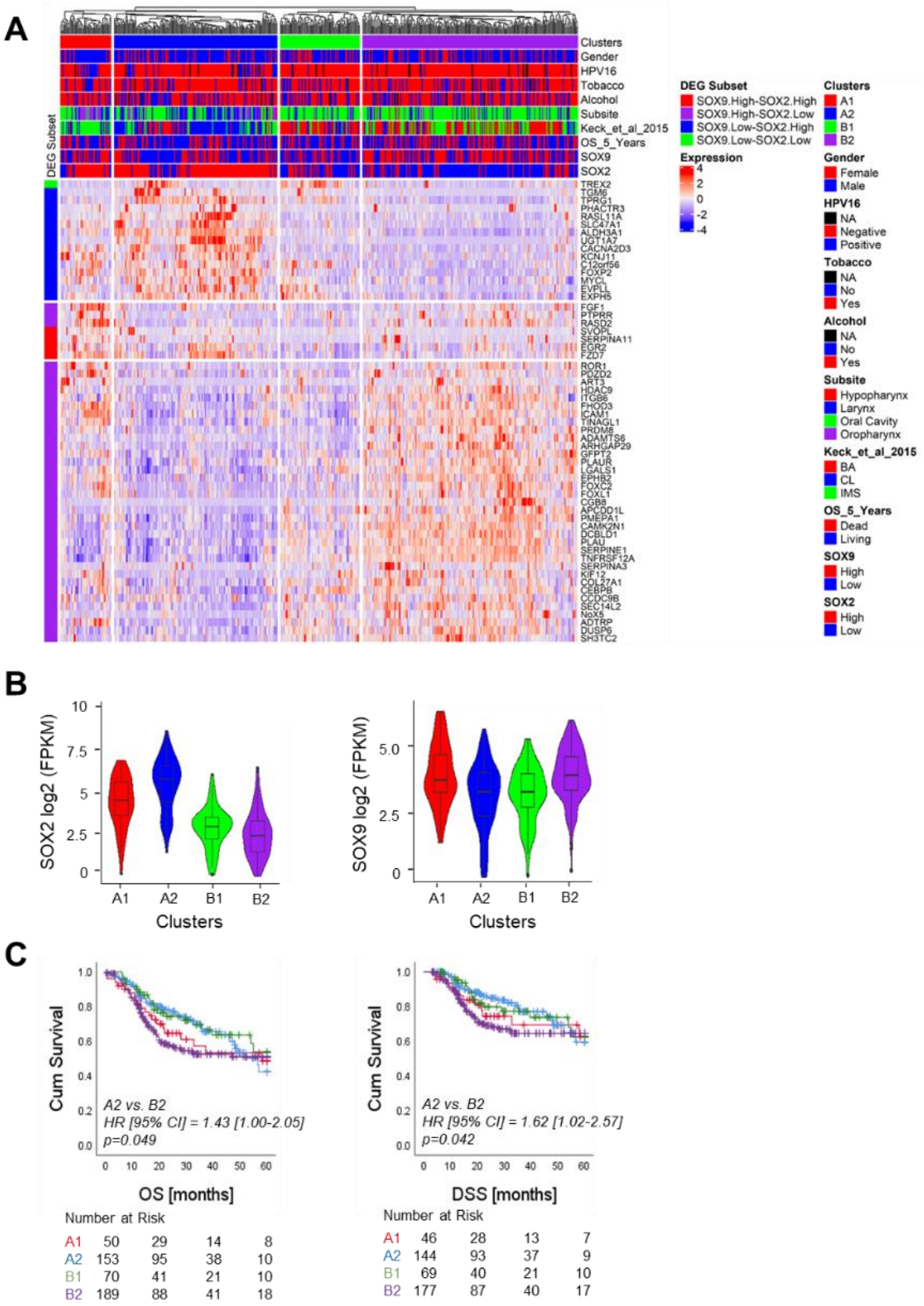

Figure 3.3: Identification of common DEGs related to SOX2 and SOX9 transcription in TCGA-HNSC. (A)

Heatmap illustrates an unsupervised hierarchical cluster analysis based on DEG transcript levels (n=57) for TCGA-HNSC. ***(B)*** *Violin plots illustrate variations of SOX2 (left graph) or SOX9 transcript levels (right graph) for sub-clusters.* ***(C)*** *Kaplan-Meier plots for five-years overall survival (left graph) or disease-specific survival (right graph) of sub-clusters. Numbers of patients at risk at the indicated time points are given below.*

3.1.3. Prognostic Risk Model Based on SOX2 And SOX9-Related DEGs

Next, a prognostic risk model for five-years OS was established applying LASSO Cox regression analysis based on SOX2 and SOX9-related DEGs (Fig. 3.4A-C).

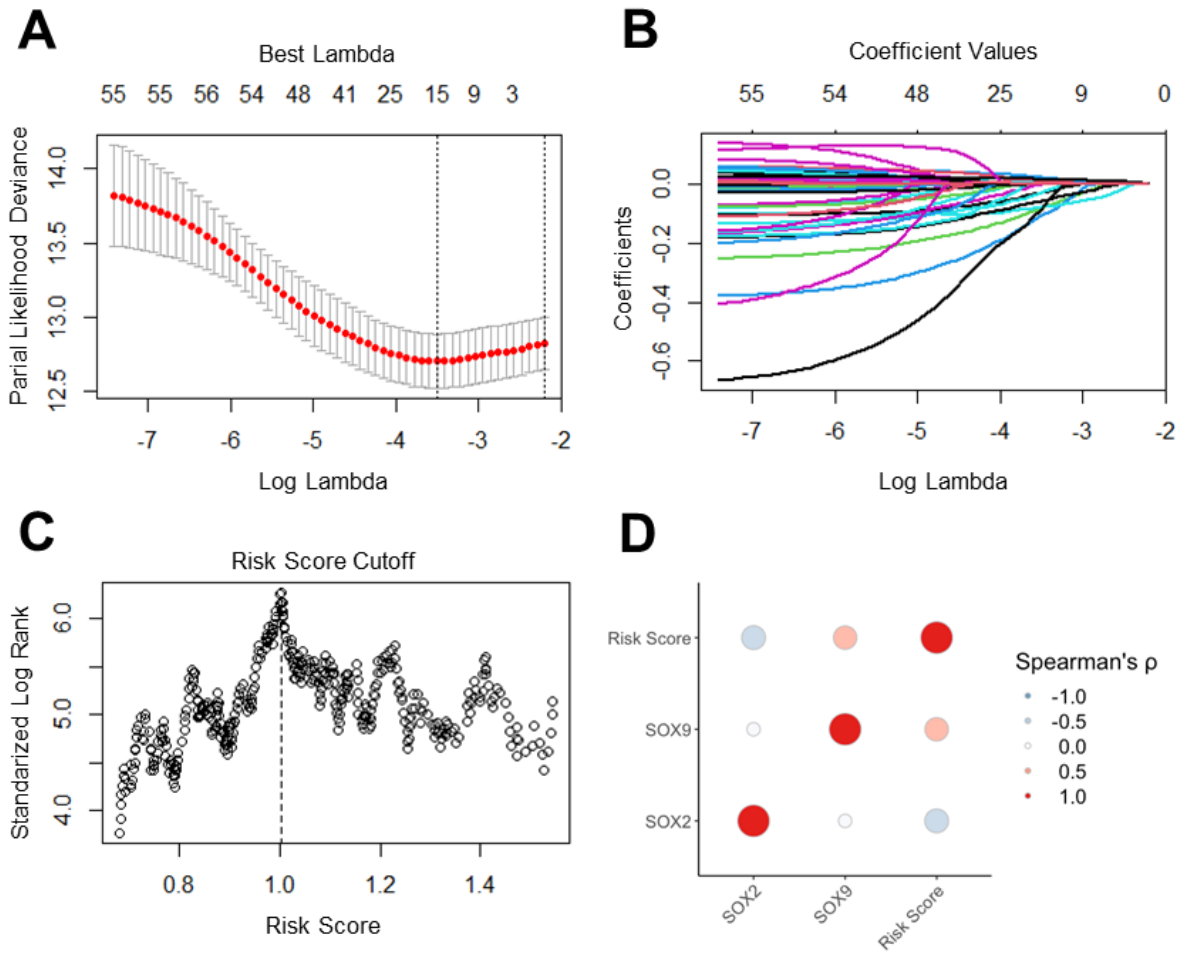

Figure 3.4: LASSO Cox regression analysis based on SOX2 and SOX9-related DEGs for TCGA-HNSC. *The prediction of a risk model was based on applying LASSO-penalized Cox regression models. Two vertical lines in* ***(A)*** *represent the lambda. best and lambda. min cutoffs for the selection of variables. The non-zero coefficient values of the risk model variables are illustrated in* ***(B)****. The coefficient values either negative (good prognosis) or positive (poor prognosis) were used to predict a risk score for individual cases. Patient stratification into high and low-risk groups was done by best risk score cutoff (****C****).* ***(D)*** *Dot*

plot illustrates inverse and positive correlations between SOX2 and SOX9 expression and the risk score for the TCGA-HNSC cohort.

The analysis revealed a 15-gene set separating the TCGA-HNSC cohort in low-risk and high-risk groups (Fig. 3.5A). As expected, the low-risk group had significantly higher SOX2 expression, while the high-risk group had significantly higher SOX9 expression and unfavorable survival (5-years DSS 53.5% and 5-years OS 37.3%) as compared to the low-risk group (5-years DSS 70.8% and 5-years OS 60.4%) (Fig. 3.4D, Fig. 3.5B-C).

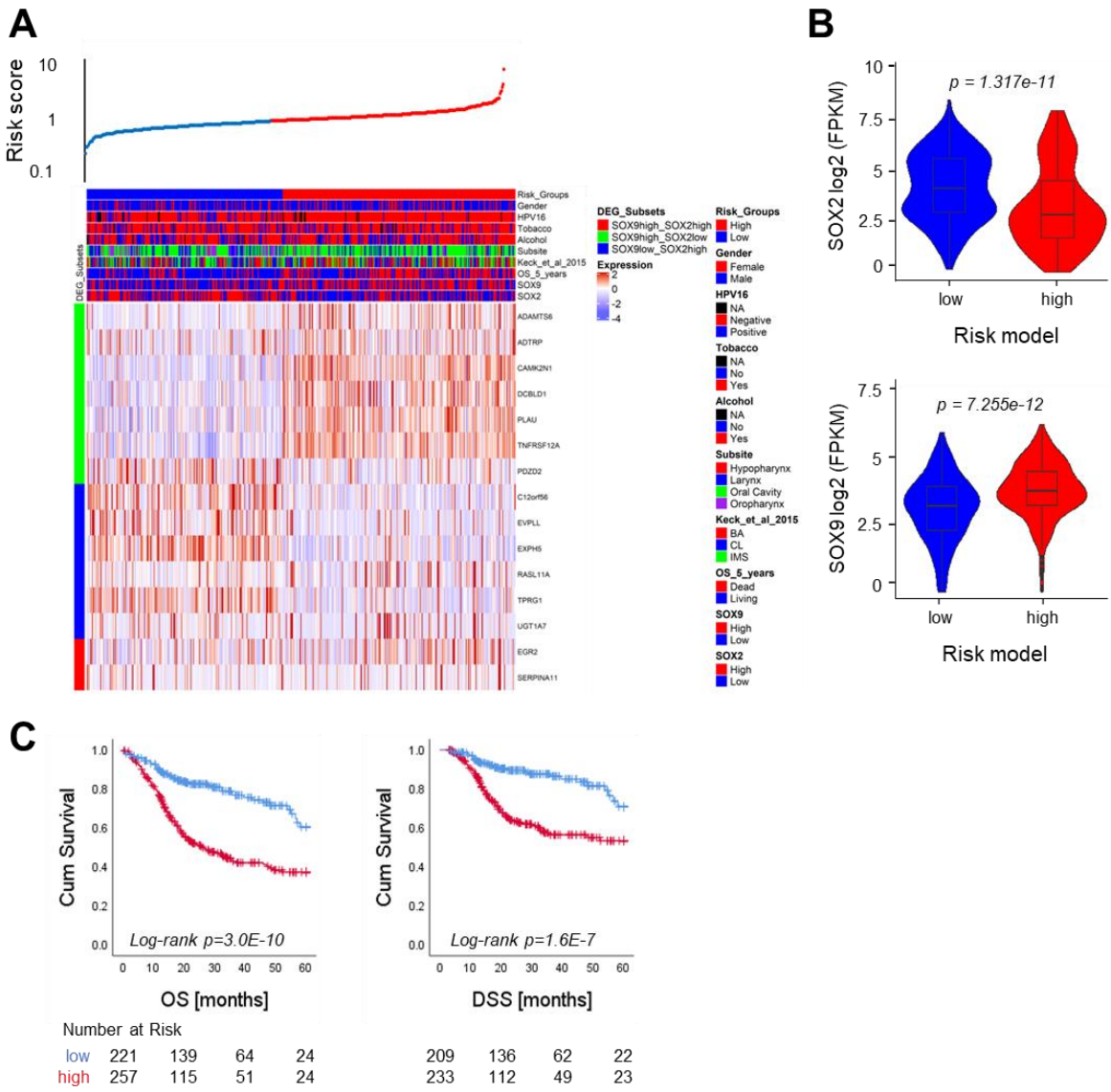

Figure 3.5: Establishment of a risk model for TCGA-HNSC. (A) *Heatmap illustrates transcript levels of the 15-gene set for TCGA-HNSC, with ranked columns according to the risk score.* ***(B)*** *Violin plots demonstrate significantly higher SOX2 transcript levels for the low-risk group (upper graph), and significantly higher SOX9 transcript levels for the high-risk group (lower graph).* ***(C)*** *Kaplan-Meier plots confirm unfavorable five-years overall survival (left graph) or disease-specific survival (right graph) for the high-risk (red line) as compared to the low-risk group (blue line). Numbers of patients at risk at the indicated time points are given below.*

Most HPV16-positive OPSCCs were part of the low-risk group, while the high-risk group was enriched for tumors with pathological lymph node metastasis, angiolymphatic and perineural invasion (Table S6). Subgroup analysis demonstrated a significant prognostic value of the risk model for almost all categories tested (Fig. 3.6A), and multivariate Cox regression models confirmed that the risk model served as an independent prognosticator for OS (HR: 2.344, p=1.0E-03) and DSS (HR: 2.590, p=2.5E-03) (Table S7). Subgroup analysis also indicated a superior performance of the risk model for HNSCC patients with a smoking history and HPV16-negative tumors whose treatment included radiotherapy (Fig. 3.6).

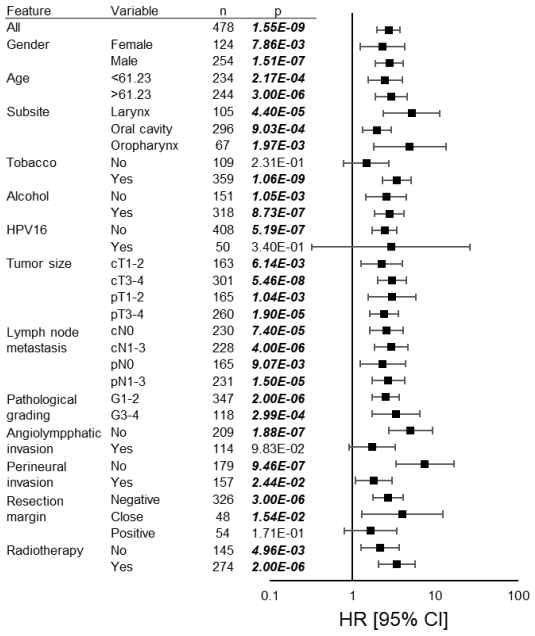

Figure 3.6: Uni- multivariate COX regression based on the predicted risk model.
Forrest plot summarizes hazard ratios (HR) and 95% confidence intervals (95% CI) for five-years overall survival of the indicated features and variables with the low-risk group as a reference in TCGA-HNSC.

This assumption was further supported by Kaplan-Meier plots for subgroups with or without radiotherapy considering five-years progression-free, disease-specific, or overall survival as clinical endpoints (Fig. 3.7A-C).

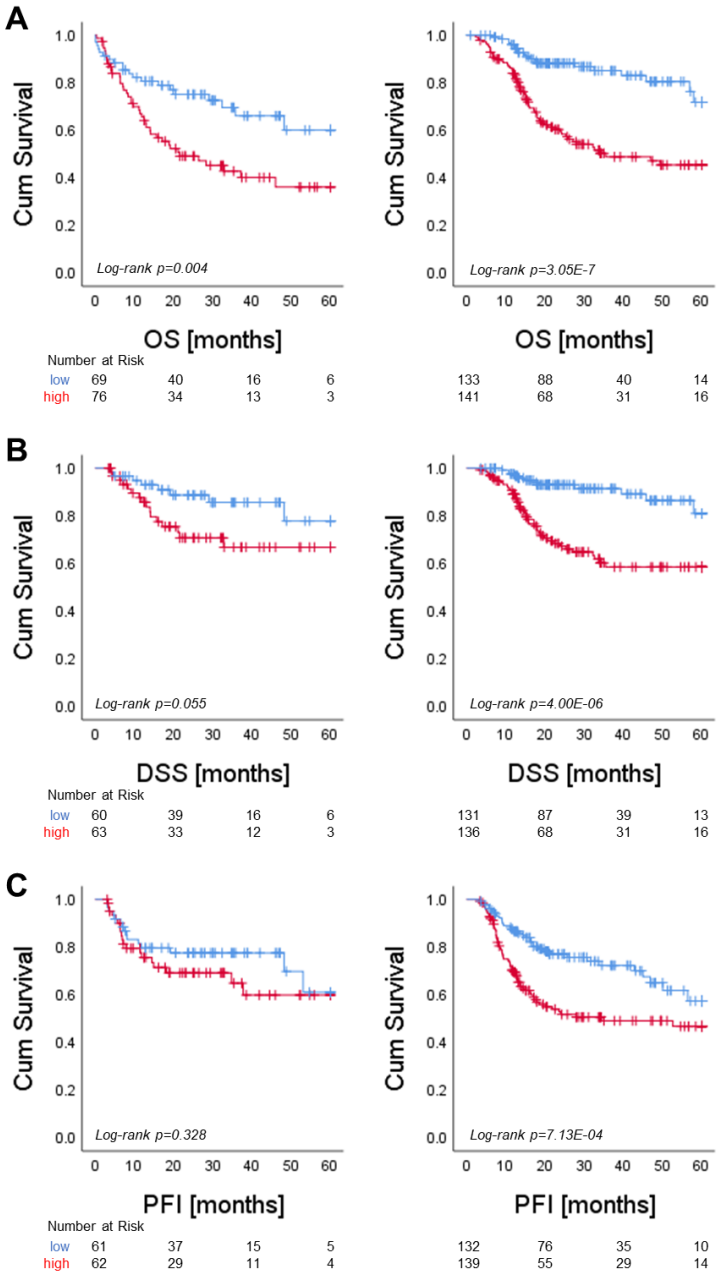

Figure 3.7: Survival analysis for patients with or without radiotherapy of TCGA-HNSC. *Kaplan-Meier plots for subgroups with (right panel) or without (left panel) radiotherapy show differences between low-*

*risk (blue line) and high-risk (red line) groups in five-years overall **(A)**, disease-specific **(B)**, and progression-free survival **(C)**. Numbers of patients at risk at the indicated time points are given below.*

3.1.4. Differences in the Mutational Landscape Among Risk Groups in TCGA-HNSC

An integrative analysis of multi-omics data was conducted to elucidate differences in the mutational landscape and the DNA methylome as potential drivers in the establishment and maintenance of inverse SOX2 and SOX9 regulation. Though no significant difference was evident in the global copy number alteration (CNA) fraction, we identified hot-spot regions with significant differences in copy number gain (11q21) or deletion (8p11-p23 and 16q21) among low-risk and high-risk groups (Fig. 3.8A-B). However, hot spot regions did neither overlap with candidate genes of the 15-gene set for the risk model nor with SOX2/SOX9-related DEGs (n=57).

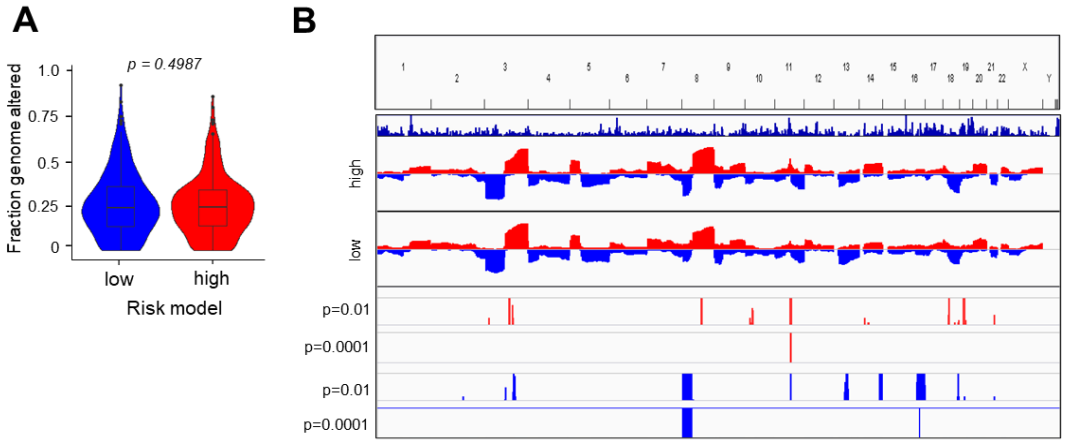

***Figure 3.8: CNV analysis based on risk model for TCGA-HNSC. (A)** Violin plot shows no significant difference among risk groups in the genome alteration fraction. **(B)** Frequency plots summarize copy number gains (red) and losses (blue), indicating hot spot regions with significant differences among risk groups.*

Moreover, no major difference in total somatic mutation counts was evident between low-risk and high-risk groups, but significant differences was identified in the mutation frequency for selected candidate genes, which are annotated as significantly mutated genes for TCGA-HNSC (Fig. 3.9-B). Most significant

differences were detected for *TP53* with higher mutation frequency for the high-risk group and *NSD1* with higher mutation frequency for the low-risk group (Fig. 3.9B).

While the difference in *TP53* somatic mutations was mainly attributed to the enrichment of HPV16-positive samples in the low-risk group, the higher relative frequency of *NSD1* mutations was also evident in HPV16-negative HNSCC (data not shown).

In the past, disruptive *NSD1* mutations in HNSCC were associated with favorable prognosis and a global DNA hypo-methylation [168-170]. Indeed, the low-risk group was particularly enriched for truncating *NSD1* mutations (Fig. 3.9C), accompanied by significantly lower beta values for global DNA methylation as compared to the high-risk group (Fig. 3.9D).

HNSCC with truncating *NSD1* mutations also exhibited a significantly lower beta mean level for SOX2 methylation and higher SOX2 transcript levels (Fig. 3.9E-F), indicating that differences in SOX2 and SOX9 transcript ratios depend at least in part on epigenetic regulation.

This assumption was further supported by prominent differences in DNA methylation of 14 probes in the region upstream of the SOX2 gene (TSS1500), which were closely related to the presence of *NSD1* mutations and SOX2 transcript levels (Fig. 3.9G-I). In contrast, no major differences were detected in DNA methylation of probes annotated for *SOX9* (data not shown).

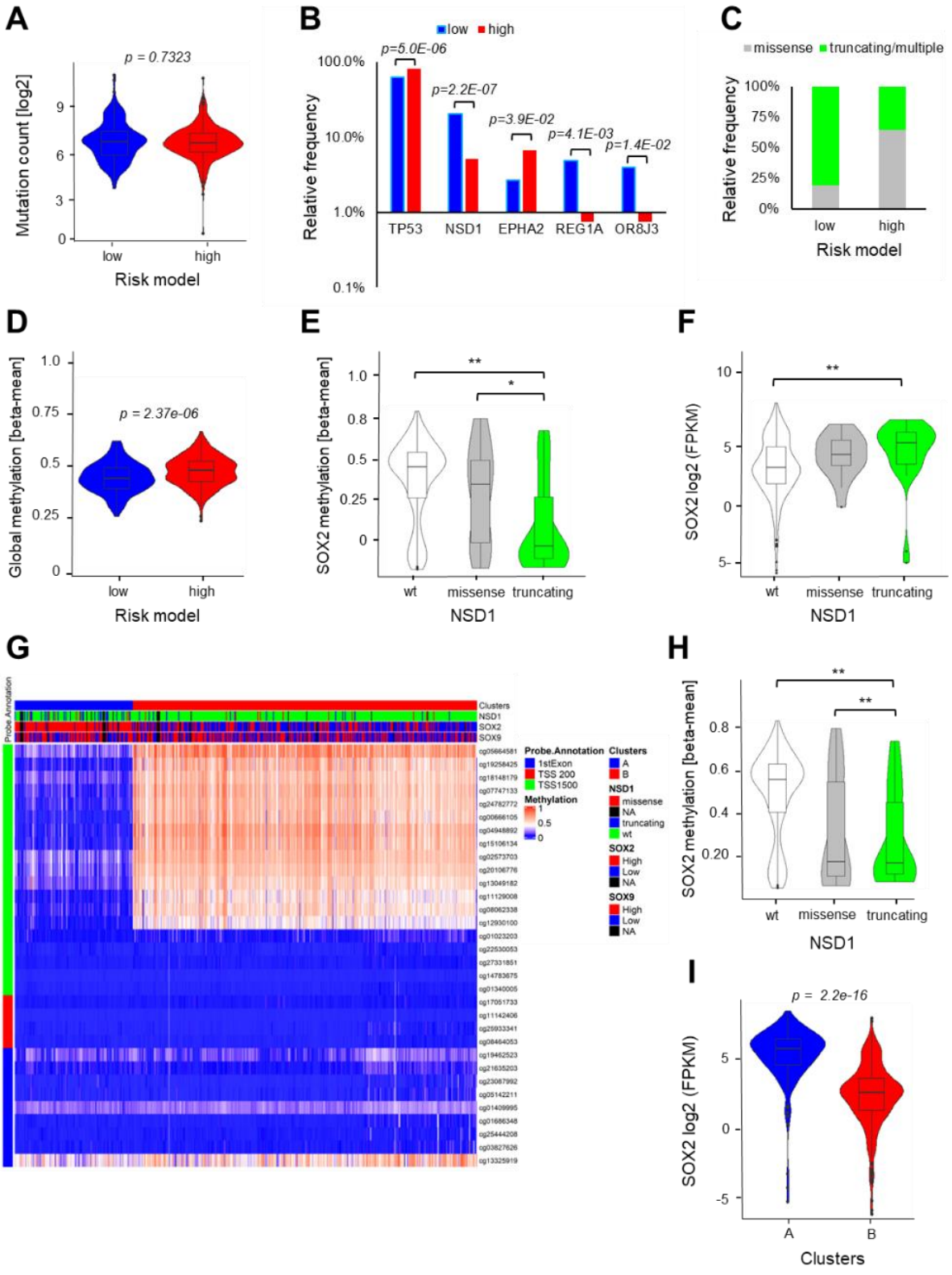

Figure 3.9: Differences in somatic mutations among risk groups and SOX2 regulation by DNA methylation. (A) *Violin plot demonstrates no significant difference in total mutation counts among risk*

*groups. Bar plots show significant differences among risk-groups in the relative frequency of patients with somatic mutations for indicated genes **(B),** and illustrate the relative frequency of patients with truncating NSD1 mutations for each risk group **(C)**. Violin plots demonstrate significant differences in beta mean values for global DNA methylation among risk groups **(D)**, in the beta mean values for DNA methylation of SOX2-annotated probes **(E)**, and SOX2 transcript levels **(F)** between cases with truncating, missense or no (wt) somatic NSD1 mutations. **(G)** Heatmap illustrates an unsupervised hierarchical cluster analysis for TCGA-HNSC based on DNA methylation levels of indicated SOX2-annotated probes, which are ranked according to their genomic position. Violin plots demonstrate significantly lower beta mean values for methylation of selected probes (n=14) in HNSCC with NSD1 mutations as compared to wildtype counterparts **(H)**, and significantly higher SOX2 transcript levels in cluster A with lower methylation of selected probes **(I)**. * p<0.05 and ** p<0.005.*

3.1.5. SOX2 Regulation and Expression of SOX2/SOX9-Related DEGs in the TCGA-CESC

Next, the SOX2 regulation and expression of SOX2/SOX9-related DEGs (n=57) in squamous cell carcinoma of TCGA-CESC were investigated, which exhibit the highest relative frequency of HPV16-related tumors and belong to the top four human cancers in TCGA among glioma, lung and head and neck cancers with highest median SOX2 transcript levels (data not shown). We observed a trend towards higher SOX2 expression in HPV16-positive cervical cancers as compared to their HPV16- negative counterparts (p=0.06), and hierarchical clustering with SOX2/SOX9-related DEGs revealed two subgroups resembling cluster A2 ($SOX2^{high}/SOX9^{low}$) and B2 ($SOX2^{low}/SOX9^{high}$) of the TCGA-HNSC cohort (Fig. 3.10A-B). Both subgroups exhibit inverse SOX2 and SOX9 transcript levels, and a statistically significant difference in OS with an unfavorable prognosis for the $SOX2^{low}SOX9^{high}$ subgroup (5-years OS 58.2%) as compared to the $SOX2^{high}SOX9^{low}$ subgroup (5-years OS 80.4%) (Fig.3.10C-D).

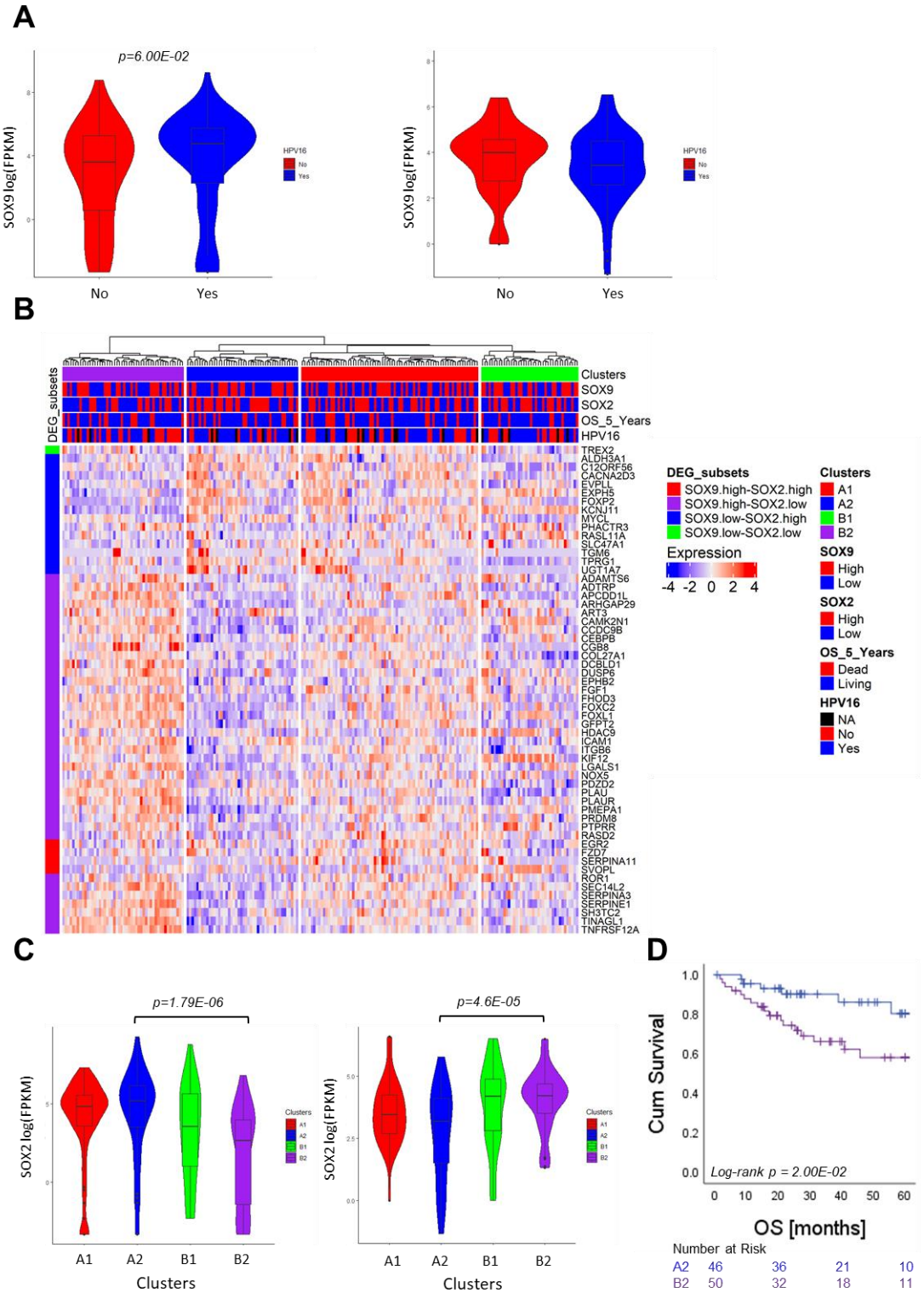

Figure 3.10: Expression of SOX2 and SOX9 and related 57-gene set for the TCGA-CESC cohort. (A) *Violin plots illustrate variation of SOX2 (left graph) or SOX9 transcript levels (right graph) for HPV16-negative or HPV16-positive cases of the TCGA-CESC cohort.* ***(B)*** *Heatmap illustrates an unsupervised hierarchical*

cluster analysis based on DEG transcript levels (n=57) for TCGA-CESC. ***(C)*** *Violin plots illustrate variation of SOX2 (left graph) or SOX9 transcript levels (right graph) for sub-clusters.* ***(D)*** *Kaplan-Meier plots for five-years overall survival of cases in clusters A1 versus A2. Numbers of patients at risk at the indicated time points are given below.*

Additionally, the DNA methylation pattern of probes annotated for SOX2 in TCGA-CESC was investigated and in line with TCGA-HNSC identified prominent differences in a subset of probes in the distal regulatory region of the SOX2 gene locus (Fig. 3.11A). As expected, SOX2 transcript levels were inversely correlated with DNA methylation of these probes, but the frequency of truncating *NSD1* mutations was rather low in this TCGA cohort (Fig. 3.11A-B), indicating the existence of other modes of action for the establishment and maintenance of SOX2 regulation by DNA methylation.

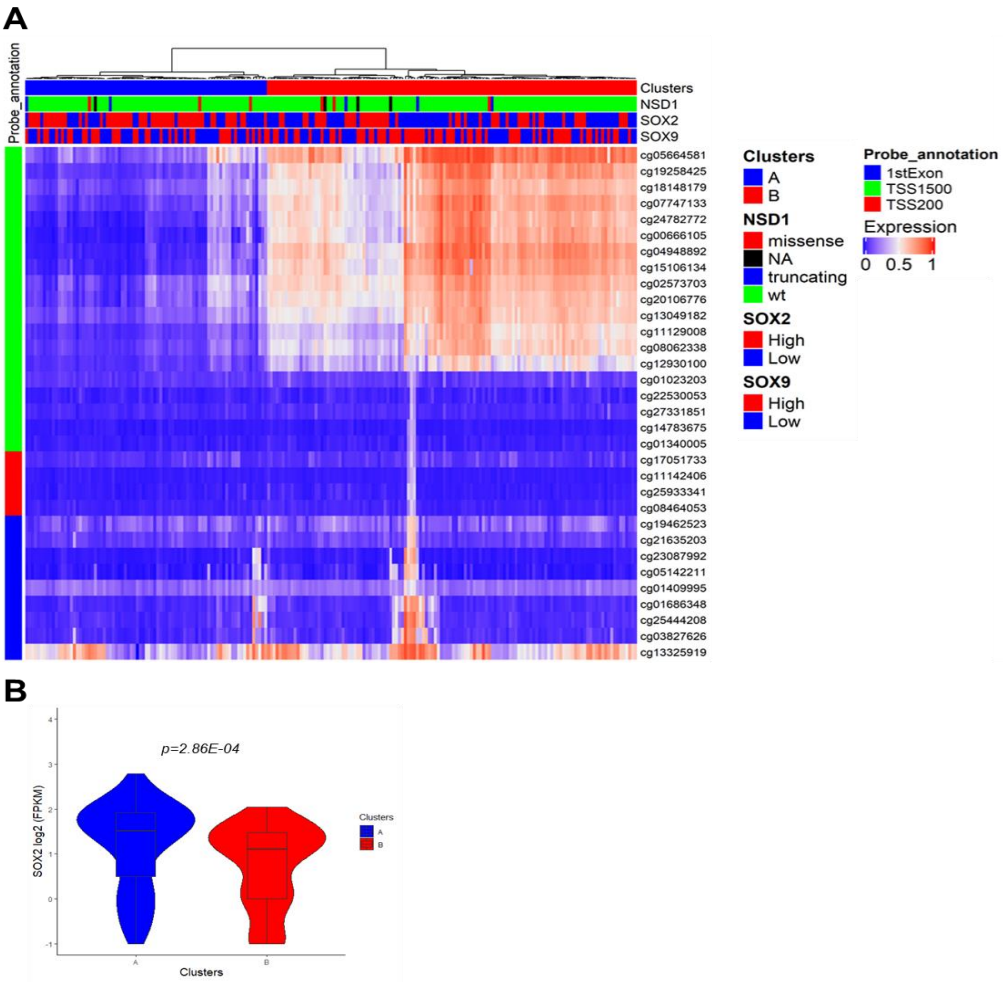

Figure 3.11: Regulation of SOX2 by DNA methylation for the TCGA-CESC cohort. (A) *Heatmap represents an unsupervised hierarchical cluster analysis for TCGA-CESC based on DNA methylation levels of indicated SOX2-annotated probes, which are ranked according to their genomic position.* ***(B)*** *Violin plot demonstrates significantly lower SOX2 expression of samples in cluster B as compared to cluster A with variable DNA methylation of selected probes (n=14) for the TCGA-CESC cohort.*

3.1.6. Upregulation Of Oncogenic KRAS Signaling in The High-Risk Group

Gene set variation analysis (GSVA) for hallmark and oncology gene sets in MSigDB was performed to identify differences in cellular processes or signaling networks among risk groups as potential drug targets for high-risk patients with a $SOX2^{low}SOX9^{high}$ phenotype. This analysis revealed significantly higher GSVA scores for several oncogenic gene sets, including those related to EMT, hypoxia, *CTNNB1,* and *LEF1*, in the high-risk as compared to the low-risk group (Fig. 3.12A, Table S8). In addition, multiple of the top-ranked gene sets indicated accelerated KRAS signaling for the high-risk group, which was supported by significantly higher KRAS (Fig. 3.12B) and RAF1 protein levels (Fig. 3.12C) and a highly significant difference in GSVA score for the Hallmark-KRAS-Signaling UP gene set among risk groups (Fig. 3.12B-D).

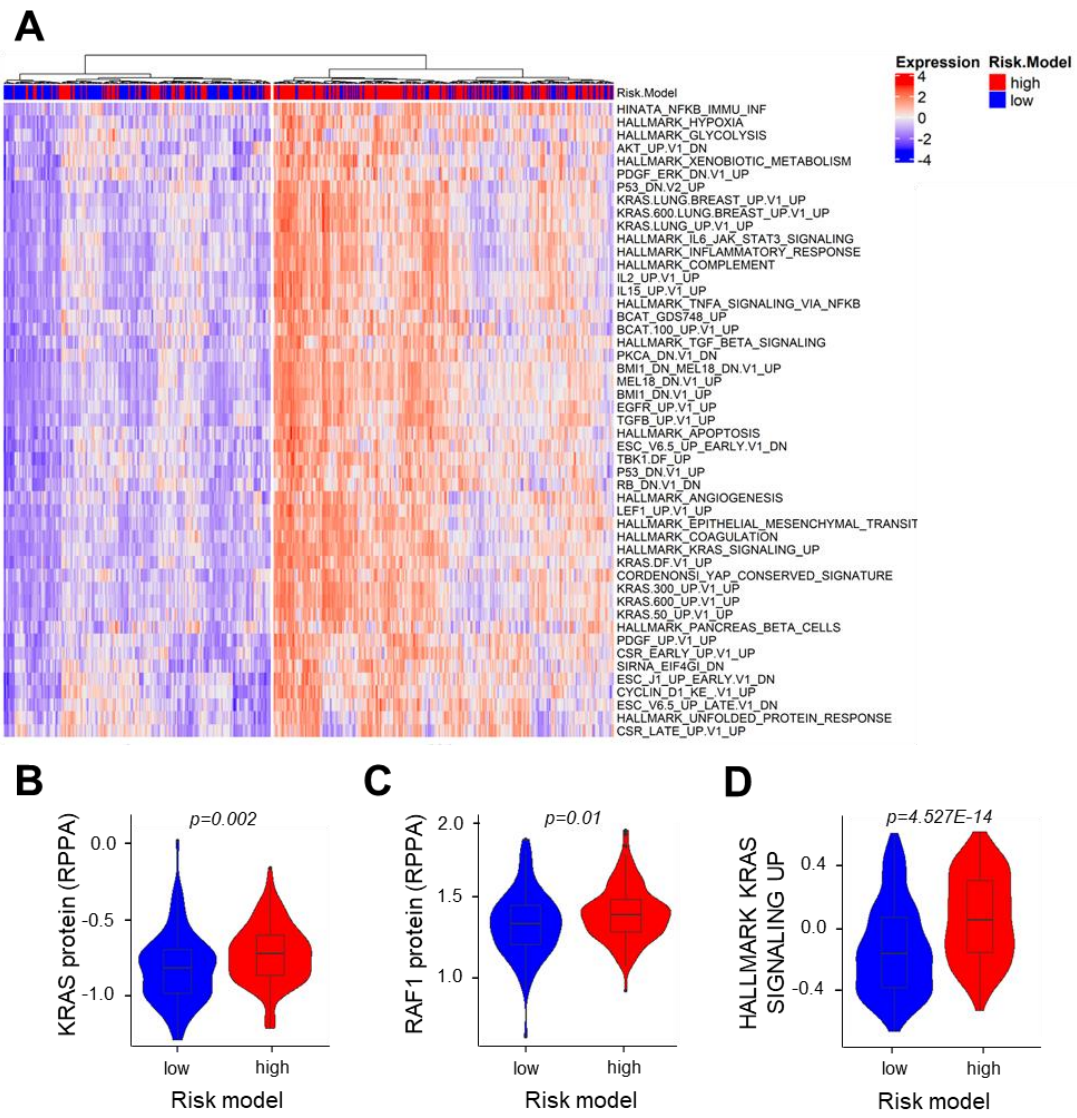

Figure 3.12: Differences in oncogenic gene sets among risk groups of TCGA-HNSCC patients. (A) *Heatmap shows an unsupervised hierarchical cluster analysis based on GSVA scores of top-ranked MSigDB gene sets (h-hallmark and c6-oncogenic signature) with significant differences among risk groups. Violin plots demonstrate significantly higher KRAS* ***(B)*** *and RAF1 protein levels* ***(C)*** *and higher GSVA scores for active KRAS signaling* ***(D)*** *for the high-risk as compared to the low-risk group.*

3.1.7. Validation of the Risk Model in Independent HNSCC Cohorts and Other Tumor Entities

The risk model was applied to transcriptome data of four independent HNSCC cohorts (GSE117973, GSE39368, GSE41613, GSE65858), which confirmed a highly significant difference in five-years OS among risk groups for the combined validation cohort applying Kaplan-Meier plots (5-years OS 31.2% for

the high-risk versus 61.1% for the low-risk group), univariate (HR: 2.582; p=3.0E-08), and multivariate Cox regression models (HR: 3.091; p=2.0E-08) adjusted for tobacco, HPV16, tumor size and lymph node metastasis (Fig. 3.13A, Table S9). Again, subgroup analysis demonstrated a good performance of the risk model for HPV16-negative HNSCC (data not shown), the high-risk group exhibited a $SOX2^{low}$ and $SOX9^{high}$ expression pattern (Fig. 3.13B), and GSVA scores indicated differences in KRAS signaling among risk groups (Fig. 3.13C).

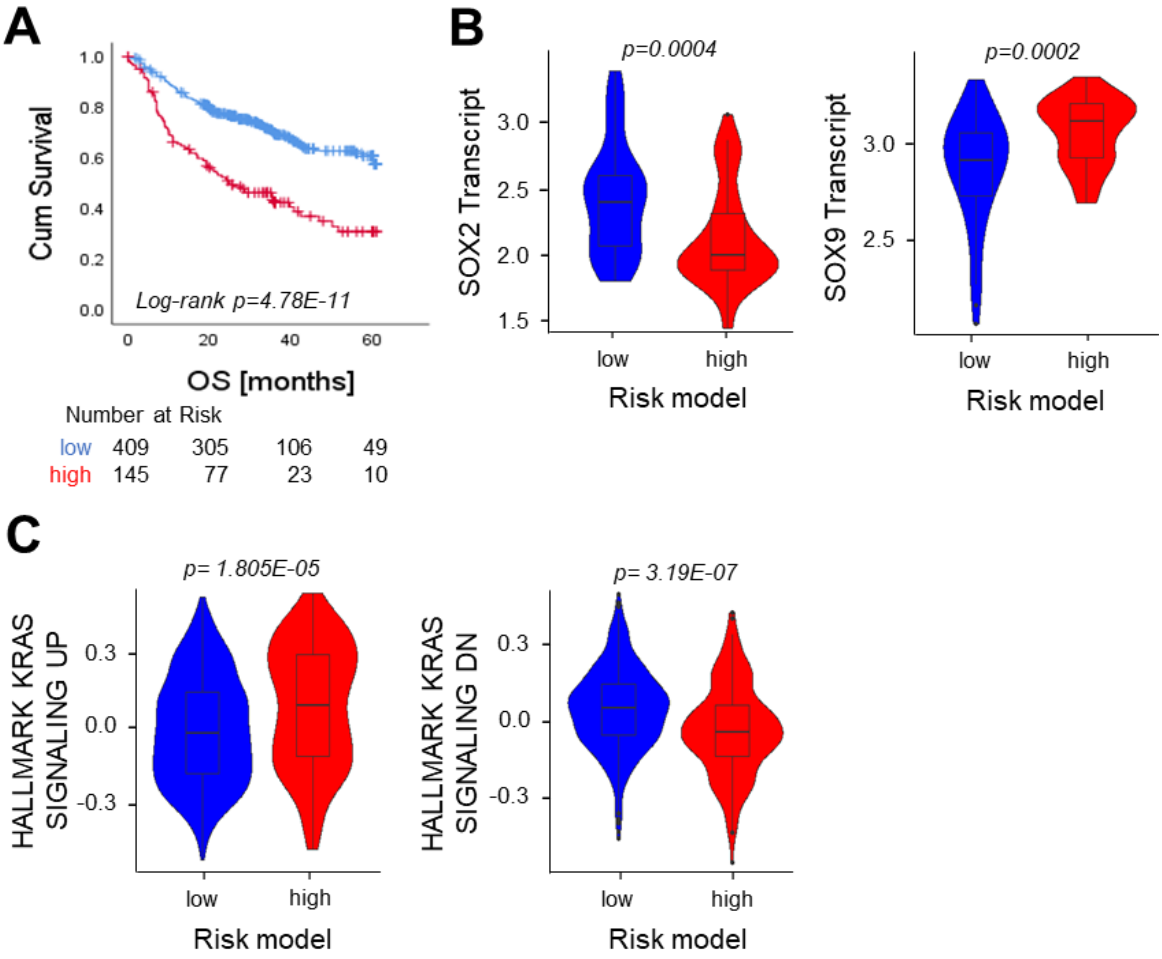

Figure 3.13: Differences in oncogenic gene sets among risk groups of independent HNSCCC cohorts. (A) *Kaplan-Meier plot shows significantly shorter five-years overall survival for the high-risk (red line) as compared to the low-risk group (blue line) of the combined HNSCC validation cohorts. Numbers of patients at risk at the indicated time points are given below.* ***(B)*** *Violin plots confirm lower SOX2 (left graph) and higher SOX9 transcript levels in the high-risk group (right graph) for an independent HNSCC cohort (GSE41613).* ***(C)*** *Violin plots show significantly higher GSVA scores for a KRAS upregulated gene*

set in the high-risk group (left graph), and for a KRAS downregulated gene set in the low-risk group (right graph).

Next, the question was addressed, whether the newly established risk model serves as a reliable and robust prognosticator for other human cancers beyond HNSCC. The risk model was applied on transcriptome data from other TCGA cohorts, and an unfavorable five-years OS was found for the high-risk as compared to the low-risk group for esophageal carcinoma (TCGA-ESCA) (Fig. 3.14A), adenocarcinoma of the lung (TCGA-LUAD) and pancreas (TCGA-PAAD), glioblastoma (TCGA-GBM), and the subgroup of invasive ductal breast carcinoma of TCGA-BRCA (data not shown). In addition, the risk model served as an independent risk factor for OS in TCGA-PAAD and TCGA-LUAD as assessed by multivariate Cox regression models (Table S10). High-risk tumors of TCGA-ESCA shared a $SOX2^{low}$ and $SOX9^{high}$ expression pattern, a higher GSVA score for a gene set related to active KRAS signaling, and a lower GSVA score for a gene set downregulated by active KRAS signaling (Fig. 3.14B-C).

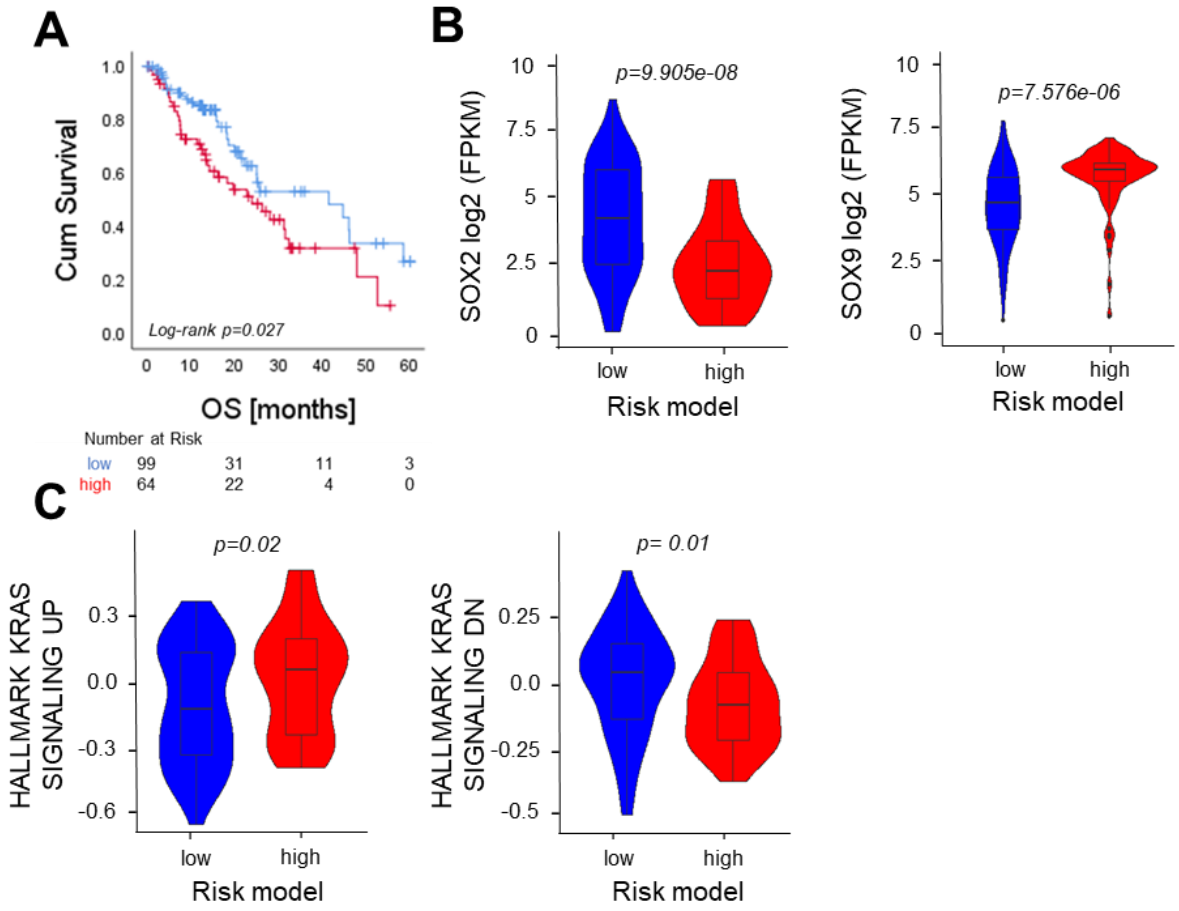

Figure 3.14: Prognostic value of the risk model for TCGA-ESCA. (A) *The Kaplan-Meier plot demonstrates significant differences in five-years overall survival for TCGA-ESCA stratified by the risk model. Numbers of patients at risk at the indicated time points are given below. Violin plots confirm lower SOX2 transcript levels (left graph) and higher SOX9 transcript levels in the high-risk group (right graph,* ***B****), and higher GSVA scores for a KRAS upregulated gene set (left graph) and lower GSVA scores for a KRAS downregulated gene set (right graph) in the high-risk-group (****C****). The statistically significant differences were measured using a two-sided t-test.*

3.1.8. The Drug Response of Cancer Cells Resembling a High-Risk Phenotype

Finally, an in-silico drug sensitivity analysis was conducted to identify potential vulnerabilities of high-risk tumors with a $SOX2^{low}SOX9^{high}$ phenotype and to investigate whether the newly established model could predict a higher risk of treatment failure for specific drug targets. We computed the risk score based on the expression pattern of the 15-gene set for 45 HNSCC cell lines for which transcriptome data and drug sensitivity scores (DSS) were available for FDA-approved compounds(n=220) [171]. The risk

score was positively correlated with SOX9 transcript levels, and an inverse correlation was evident for SOX2 expression and the risk score as well as SOX9 expression (Fig. 3.15A). This data indicated that molecular traits related to inverse SOX2 and SOX9 expression contributing to different risk phenotypes are at least in part cancer cell-intrinsic. Comparison of the risk score with the DSS, which indicates higher efficacy at a lower drug concentration revealed several drugs with either a significant positive or an inverse correlation (Fig. 3.15B; Table S11). HNSCC cell lines with a higher risk score shared a higher resistance towards Galiellalactone (STAT3 inhibitor), the alkylating compound Pipobroman and SB-743921 (kinesin spindle protein inhibitor) but are more sensitive for drugs targeting key components of oncogenic pathways, such as NTRK signaling (Lestaurtinib), Hedgehog signaling (Vismodegib) or RAS-RAF signaling (NVP-RAF265). One shortcoming of this approach was the limited amount of HNSCC cell lines for in silico analysis. Hence, we computed the risk score for cancer cell lines from head and neck, esophagus, lung, pancreas, breast, and brain cancers of the Cancer Cell Line Encyclopedia (CCLE) for which compound response data were available from two independent drug screens: Sanger GDSC1 and GDSC2 (n=293) [172] and PRISM Repurposing Screen (n=253) [173]. Again, the risk score was positively correlated with SOX9 transcript levels, and an inverse correlation was evident for SOX2 expression and the risk score as well as SOX9 expression for selected cancer cell lines in both screening sets (data not shown). Comparison of IC50 z-scores from both screening sets, which indicates drug efficacy at higher concentration, revealed several compounds with significant differences in response efficacy for selected cancer cell lines with higher versus lower risk scores (Table S12-13). Strikingly, cancer cell lines with a higher risk score were less sensitive in both drug screens to numerous compounds targeting EGFR signaling (Fig. 14C, Table S12-13), which might be due to a higher activity of pathways downstream of or related to RAS-RAF signaling in these cells.

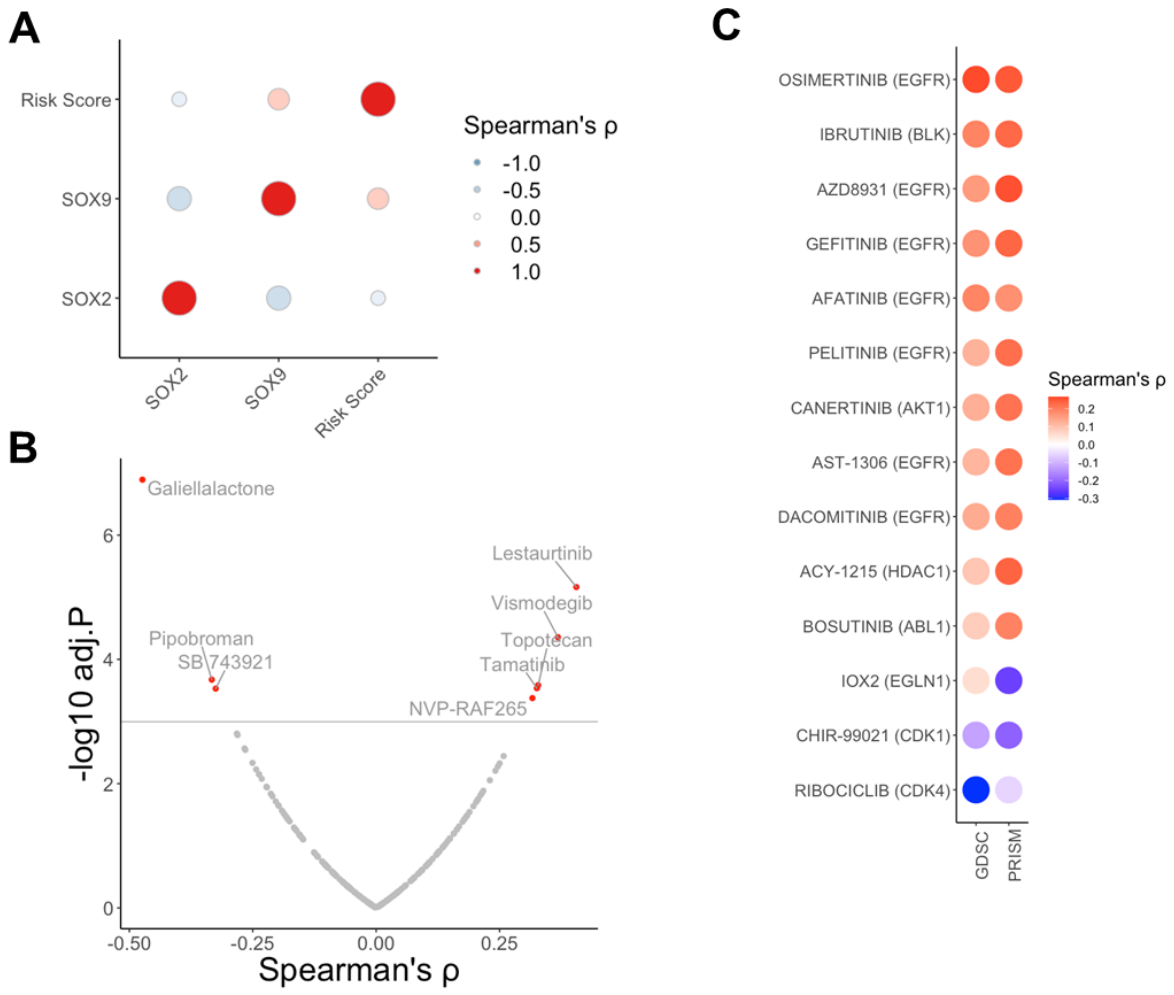

Figure 3.15: In silico drug response analysis for cancer cell lines of CCLE. (A) *Dot plot illustrates inverse and positive correlations between SOX2 and SOX9 expression and the risk score for HNSCC cell lines (n=45).* ***(B)*** *Volcano plot summarizes the result of the in-silico drug response analysis for HNSCC cell lines (n=45). Red dots indicate compounds with a statistically significant (p<0.05) positive or inverse correlation between the risk score and the drug sensitivity score.* ***(C)*** *Dot plot illustrates inverse and positive correlations between the risk score and drug response data (IC50 or log-fold change viability values) for selected compounds from the Sanger GDSC1-2 and the PRISM Repurposing screens based on cancer cell lines from head and neck, esophagus, lung, pancreas, breast and brain cancers of the Cancer Cell Line Encyclopedia (CCLE).*

3.2. Cancer-Neuron Interaction as A Potential Mode of Action for Cancer Cell Plasticity

The components of the TME play a crucial role in cancer cell plasticity, and neuro-glial activation is a recently identified hallmark of growing cancers [14]. The contribution of nerves to the pathogenesis of

malignancies has been raised as an important component of the TME [130]. However, the origin of these nerves and the mechanism of their inception are still elusive and need to be generously addressed. In line with the former results from cross-tabulation analysis of the patient's clusters based on the inverse correlation of SOX2 and SOX9 expression values the group with $SOX2^{high}$ was significantly enriched for HPV16 positive OPSCC and perineural invasion was significantly associated with the $SOX9^{high}$ group with unfavorable prognosis. So, in the following section, I aimed to investigate the role of nerve fibers and their associated cells such as SCs as a modulator of extrinsic mode of action in plasticity the clinical relevance of NF and associated cells for HNSCC and other tumors and to address the molecular characterization of the CNI in HNSCC and other tumor types. Finally, establish and analyze pre-clinical models as proof-of-concept for new therapeutic strategies.

3.2.1. Establishment of the Schwann Cell-related 43-gene Set as Surrogate Marker of Peripheral Nerves in Tumors

I assumed that the abundance of SCs serves as an accurate surrogate for the presence of peripheral nerves in a tumor and utilized the Harmonizome online tool [167] to establish an SC-related 43-gene set from 547 proteins co-occurring with the keyword Schwann cell in abstracts of biomedical publications from the TISSUES Text-mining Tissue Protein Expression Evidence Scores dataset (cut-off p-value<0.05) (Table S14).

GSVA scores were computed based on RNA-seq data from TCGA-HNSC for the SC-related 43-gene set, eleven gene sets of the MSigDB related to SCs or the peripheral nervous system, three gene signatures available for the unbiased single-cell transcriptomic characterization of the non-diseased rodent, and one SCs gene signature of Panglao DB curated from single-cell data of mice and humans. This analysis revealed a positive and significant correlation between the newly established SC-related 43-gene set and most other gene sets tested, except for one gene set: GO_PERIPHERAL_NERVOUS_SYSTEM_MAINTENANCE (Fig. 3.16A, Table S15).

The positive correlation was also confirmed with gene expression data from four independent HNSCC cohorts and other solid tumors from TCGA with similar risk factors and histopathological characteristics (LUSC, CESC, and ESCA) or with well-established cancer-neuron-interaction in TME (LUAD, BRCA, PAAD, PRAD) [174, 175] (Fig. 3.16A, data table not shown).

In order to further substantiate the predictive accuracy of the SC-related 43-gene set, the enrichment of immune and stromal cells was inferred by deconvolution of gene expression data utilizing xCell [176]. The comparison of these data with GSVA scores for the SC-related 43-gene set confirmed a positive and significant correlation with the enrichment of astrocyte-like cells and neurons for TCGA-HNSC and independent HNSCC cohorts (Fig. 3.16B, Table S16).

It is worth noting that a significant and inverse correlation was also observed for several immune cells, in particular T cells. Quantitative assessment of peripheral neurons adjacent to and within the tumor demonstrated an increase in the number of positive areas for HNSCC with a high GSVA score (SC^{high}, n=25) as compared to SC^{low} tumors (n=25, Fig. 3.16C-D).

In summary, the newly established SC score based on the SC-related 43-gene set provides an adequate tool to infer the abundance of peripheral nerves in the TME and to explore their mutual interaction with tumor cells during cancer development and therapy.

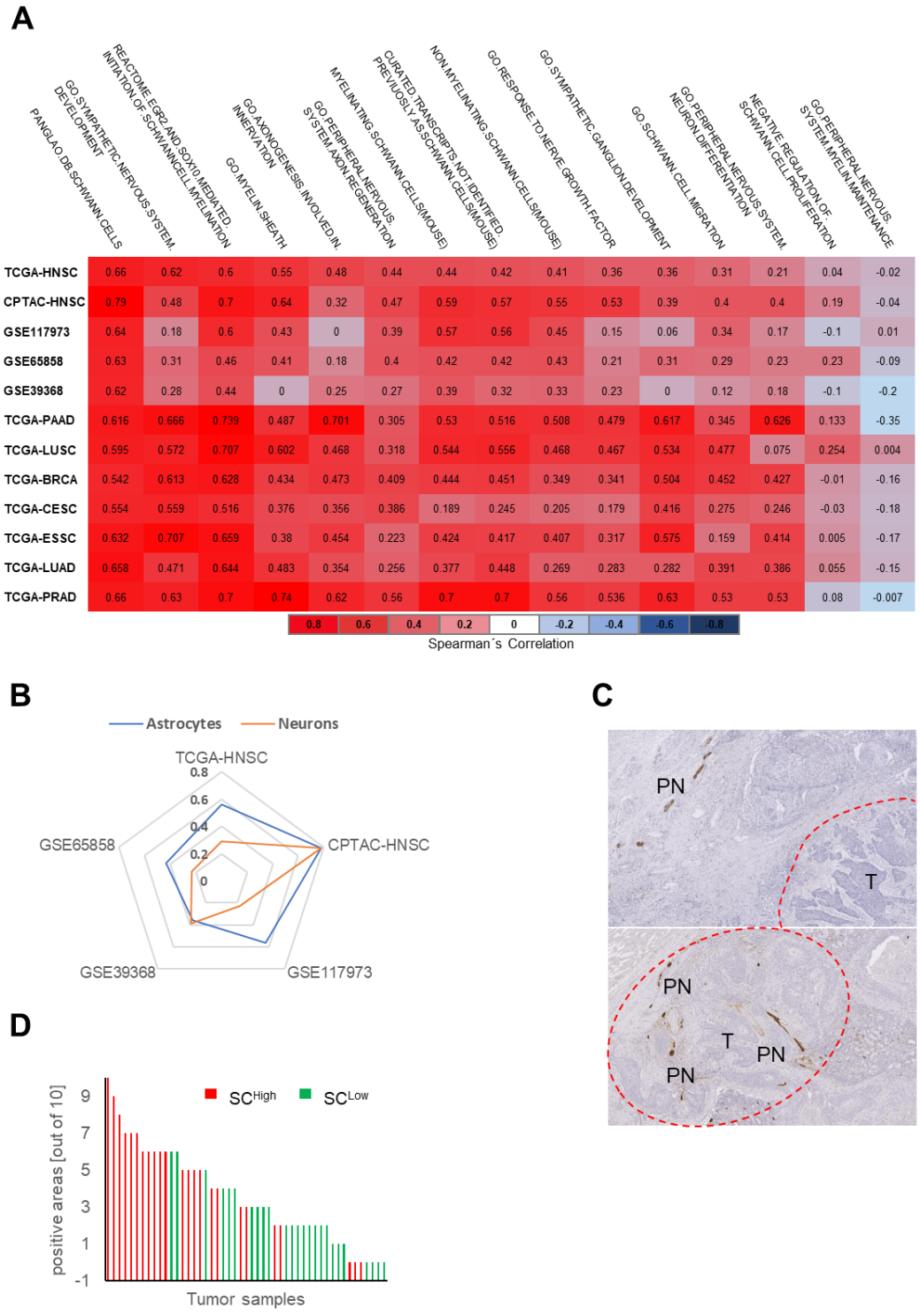

Figure 3.16: Correlation coefficient of SC score with other gene sets TCGA-HNSC and other Validation cohorts. (A) *Correlation coefficient matrix using Spearman's correlation for the SC score based on GSVA scores using the predicted gene set (n=43) with other peripheral nervous system-related gene sets (n=15) in TCGA-HNSCC and other independent HNSCC cohorts (CPTAC-HNSCC, GSE117973, GSE65858,*

GSE39368) as well as other tumor entities form TCGA (PAAD, LUSC, BRCA, LUAD, CESC, ESCA, PRAD). Positive correlations are indicated in red color) and negative correlations in blue color. ***(B)*** *Spider plot presenting the correlation coefficient for SC score with the scores of astrocytes (blue color) and neurons (orange color) from xCell deconvolution matrix in TCGA-HNSCC and four independent HNSCC cohorts.* ***(C)*** *Representative pictures of an IHC-staining with an anti-GAP43 antibody show positive staining (brown signal) in peripheral nerve fibers (PN) adjacent to and within the tumors (T) of FFPE tumor sections from GSE117973. Histological staining with hematoxylin to visualize tissue architecture; scale bar = 200 µM.* ***(D)*** *Bar plot presents the quantitative assessment of positive areas with peripheral neurons adjacent to and within the tumor and demonstrates an increase in the number for HNSCC with a high GSVA score SC^{high} (red, n=25) as compared to SC^{low} (green, n=25) tumors.*

3.2.2. Association of the SC-related 43-gene Set and Peripheral Nerves in the TME

As a further proof-of-concept for the accuracy of the SC-related 43-gene set to serve as a molecular surrogate for peripheral neuron abundance in the TME, we examined FFPE tumor sections from a HNSCC cohort (n=50) for which transcriptome data were available (GSE117973) by IHC staining with an anti-GAP43 antibody. GAP43 was selected as it is expressed in axons of peripheral neurons and SCs and showed the best specificity with almost no positive staining in tumor cells or stromal cells of the TME as compared to other established marker proteins (Fig. 3.17A-E).

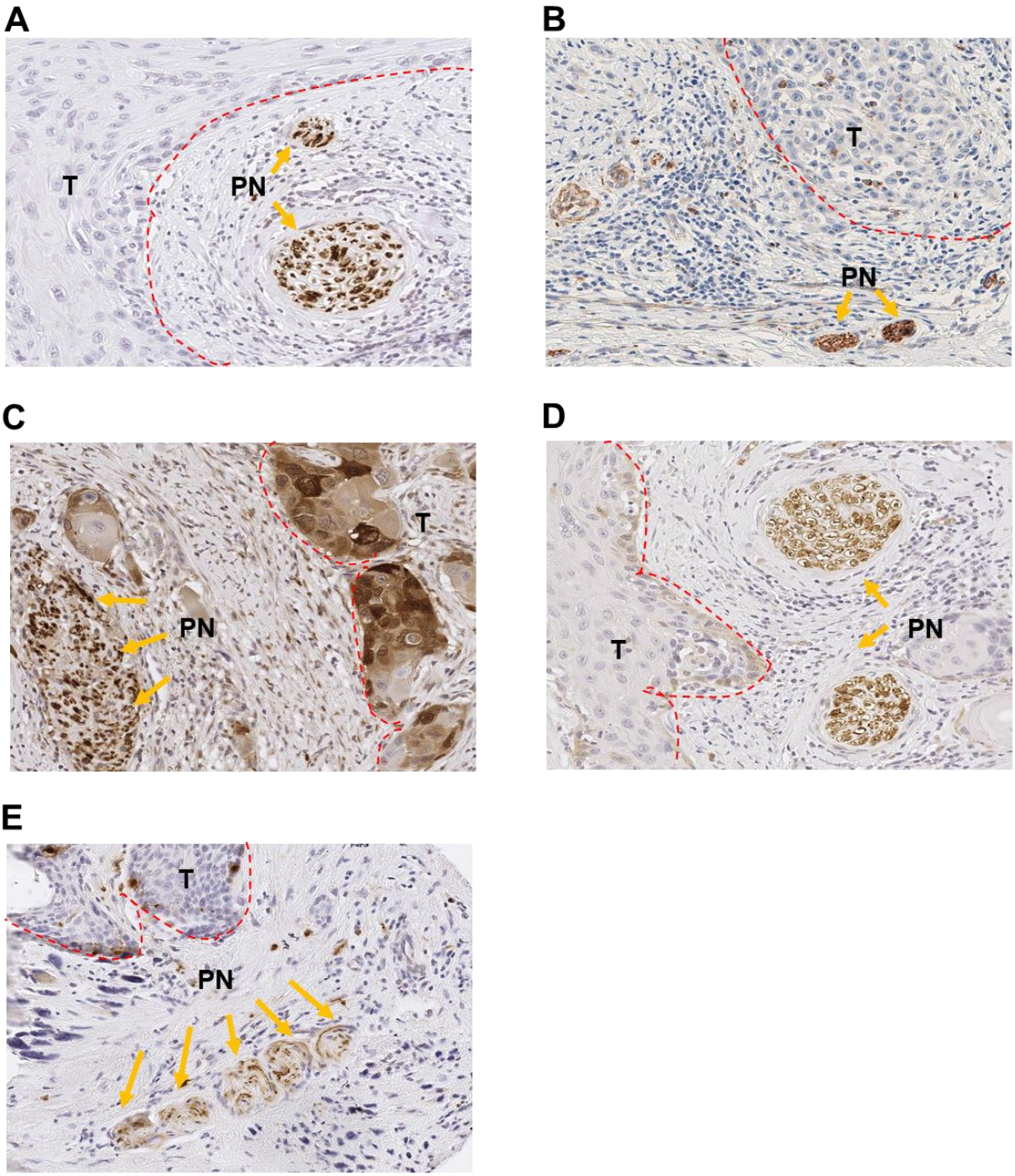

Figure 3.17: IHC-Staining of FFPE-Tumor-Tissue Sections with Schwann Cells and Peripheral Nerves Markers in GSE117973. *Representative pictures of an IHC-staining with FFPE tumor sections from GSE117973 and specific antibodies for protein markers of Schwann cells and peripheral nerves: anti-GAP43 (**A**), anti-NCAM1 (**B**), anti-UCHL1 (**C**), anti-SNCA (**D**), and anti-S100B (**E**). Pictures show heterogeneous positive staining (brown signal) in peripheral nerve fibers (PN), (orange arrow) adjacent to and within the tumor tissue (T), (red dotted line). Histological staining with hematoxylin to visualize tissue architecture; scale bar = 200 µM.*

3.2.3. Association of the SC score with Clinical Features and the Mutational Landscape

To explore potential differences in clinical and histopathological features across HNSCCs with distinct SC scores, tumors of the TCGA-HNSC cohort were ranked and classified into three groups: SC^{low} (lower quartile), $SC^{moderate}$, and SC^{high} (upper quartile). A cross-tabulation analysis demonstrated a highly significant enrichment of HPV16-positive OPSCC for the SC^{low} group which were almost absent in the SC^{high} group (p=2.33E-06), while SC^{high} tumors were enriched for perineural invasion (p=2.50E-04) (Table S17). Concerning the mutational landscape, SC^{high} tumors exhibited a significantly lower fraction of global genomic alterations as compared to HNSCC with low or moderate SC scores, with hot spot regions (p<0.0005) of copy number gains at chromosomes 3q and 9p and copy number losses at chromosomes 11q and 16q (Fig. 3.18A-B).

While no statistically significant difference was evident for the total count of somatic mutations between HNSCCs with low, moderate, or high SC scores (Fig. 3.18C), we identified several MutSig genes with significant differences in the relative frequency of somatic mutations (Fig. 3.18D, Table S18)**.** In line with a recent study [25], we observed a significant (p=0.0078) and gradual rise in the relative frequency of somatic *TP53* mutations with increasing SC scores, which was also evident for somatic *NOTCH1* mutations (p=0.0262, Fig. 3.18D).

In contrast, a significant and gradual decline in the relative somatic mutational frequency with increasing SC scores was evident for *AGTR1* (p=0.03), RSRC1 (p=0.02), and *PTEN* (p=0.002). The higher frequency of somatic mutations in *PTEN* in combination with *PIK3CA* copy number gain at chromosome 3q26 for SC^{low} as compared to SC^{high} HNSCC suggested an inverse association between PI3K pathway activity in cancer cells and peripheral nerve abundance in the TME potentially due to impaired tumor-related neurogenesis.

This assumption was further supported by a higher frequency of somatic mutations in *PTEN* in combination with copy number gain at chromosome 3q for SC^{low} as compared to SC^{high} tumors of CPTAC-HNSC (data not shown).

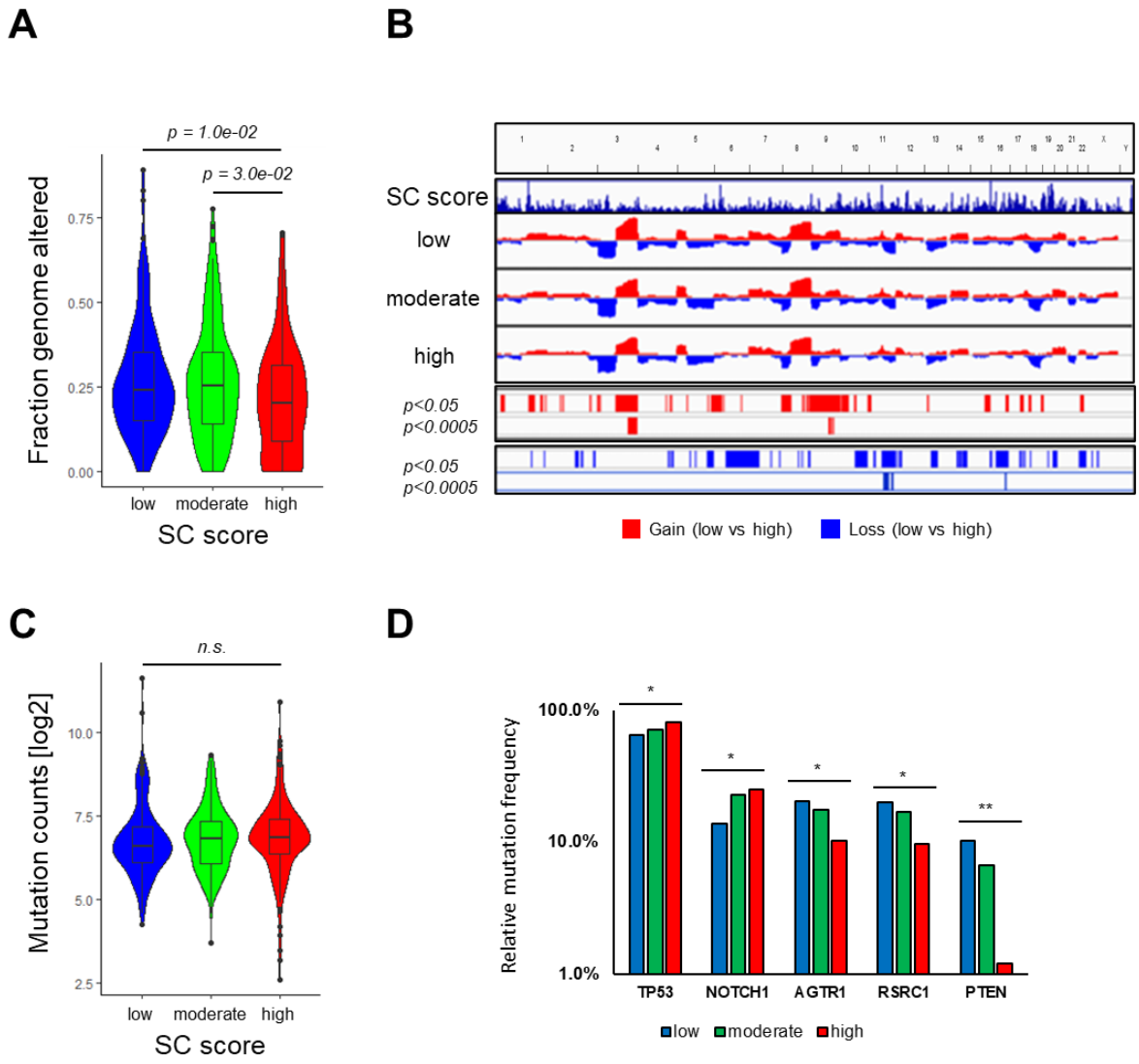

Figure 3.18: Differences in the mutational landscape for tumors with low, moderate, and high SC score for TCGA-HNSC. (A) *Violin plot shows statistically significant differences in the fraction genome altered for indicated in groups classified by the SC score (low, moderate, high).* ***(B)*** *Frequency plots summarize copy number gains (red) and losses (blue) and indicate hot spot regions with significant differences among groups with high or low SC score.* ***(C)*** *Violin plot shows no statistically significant difference in mutational counts between indicated groups classified by the SC score (low, moderate, high).* ***(D)*** *Bar plot illustrates Mutsig genes (TP53, NOTCH1, AGTR1, RSRC2, PTEN) with statistically significant differences in somatic mutation frequency among groups classified by the SC score (low, moderate, high). Statistical*

difference in the fraction genome altered and mutational counts for indicated in groups classified by the SC score was determined using ANOVA-Tukey HSD, while the significant differences in relative mutational frequency for the former groups were determined by Chi-square test (p<0.05 and ** p<0.005).*

3.2.4. Association of the SC score with Gene Regulatory Networks and Oncogenic Pathway Activity

To substantiate the potential role of PTEN-PI3K signaling and to identify other underlying molecular principles of the mutual cancer-neuron-interaction, GSVA scores for hallmark gene sets of the MSigDB (category H) [165] were computed based on RNA-seq data from TCGA-HNSC and significant differences between SC^{low} and SC^{high} tumors were identified using the limma package in R (Fig. 3.19A, Table S19). In line with differences in the mutational landscape, significantly higher GSVA scores were evident for the P53 pathway (p=4.8e-03), PI3K-AKT-MTOR (p=1.0e-02), and MTORC1 signaling (p= 7.03e-10) (Fig. 3.19A and B). Other gene sets with a higher GSVA score for SC^{low} HNSCC resemble processes of metabolism and cell cycle progression, such as *MYC* or *E2F* target genes, oxidative phosphorylation, DNA repair, and G2M checkpoint (Fig. 3.19A). In contrast, top-ranked gene sets with higher GSVA scores for SC^{high} HNSCC were related to well-established oncogenic processes and pathways, such as epithelial-mesenchymal transition, hedgehog and TGF-β signaling, KRAS, and angiogenesis (Fig. 3.19A and B). Significantly higher GSVA scores for PI3K-AKT-MTOR and MTORC1 signaling in SC^{low} tumors and TGF-β signaling and epithelial-mesenchymal transition in SC^{high} tumors were also evident in other solid tumors from TCGA, such as CESC and BRCA (Fig. 3.19C). Finally, a significantly higher TGF-β pathway activity for SC^{high} HNSCC was confirmed with PROGENy (Fig. 3.19D, Table S20) and could contribute to a suppressed TIME with reduced numbers of TILs (Table S16) or be related to a higher resistance to radio- and/or chemotherapy.

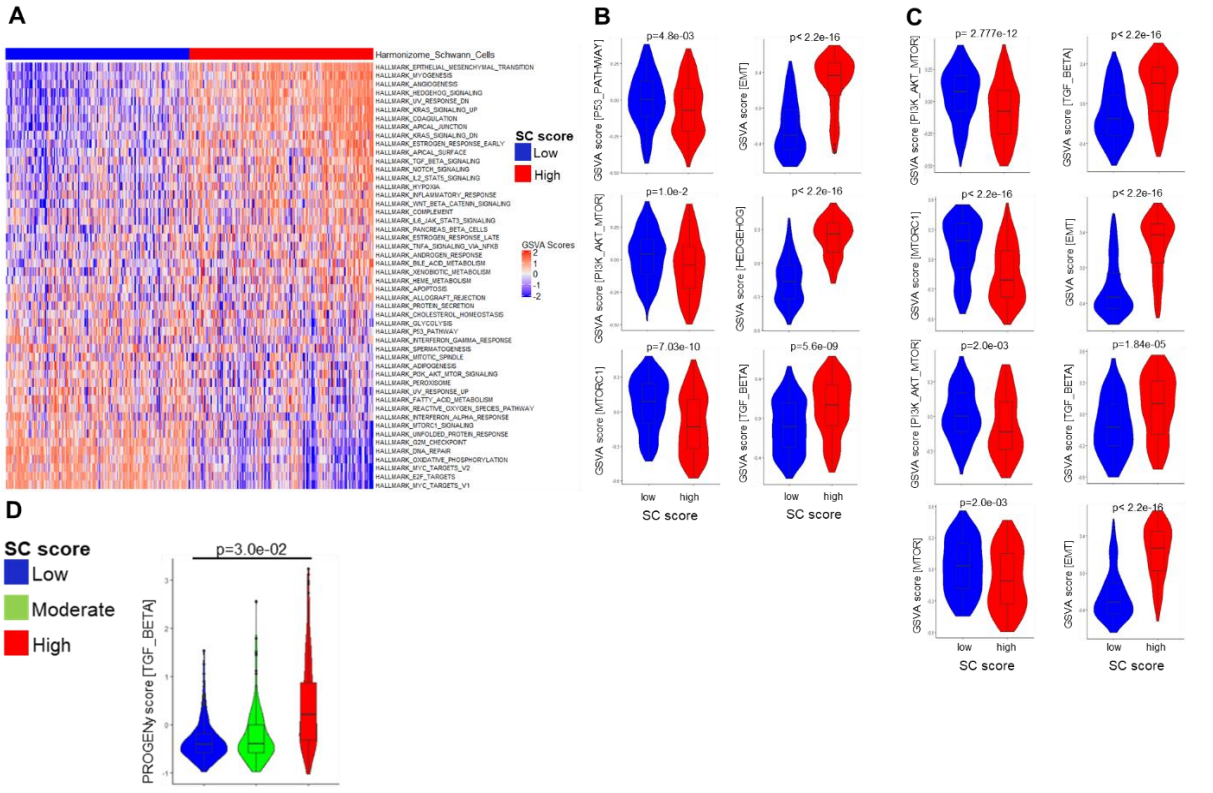

Figure 3.19: Differences in oncogenic gene sets among risk groups in TCGA-HNSC and other validation TCGA cohorts such as CESC and BRCA. (A) *Heatmap shows an unsupervised hierarchical cluster analysis based on GSVA scores of top-ranked MSigDB gene sets (h-hallmark) with significant differences among tumors with high or low SC score.* ***(B)*** *Violin plots demonstrate statistically significant differences between tumors with high or low SC scores for indicated gene sets in TCGA-HNSC,****(C)*** *and other tumors such as BRCA and CESC****. (D)*** *Violin plot demonstrates the significant differences between SC score groups (low, moderate, high) for TGF-β pathway score****.*** *The statistical significance was determined using ANOVA-Tukey HSD****.***

3.2.5. Context-Dependent Impact of PI3K Pathway Activity

To further explore the impact of PI3K pathway activity on the abundance of SCs as surrogate for peripheral nerves in the TME in the context of somatic *TP53* mutations, tumors of the TCGA-HNSC cohort were stratified into four groups: tumors without somatic *TP53, PTEN*, or *PIK3CA* mutations or *PIK3CA* amplification (TP53^{wt}/PTEN-PIK3CA^{wt}), tumors with somatic *TP53* mutations but without somatic *PTEN* or *PIK3CA* mutations or *PIK3CA* amplification (TP53^{mut}/PTEN-PIK3CA^{wt}), tumors without somatic *TP53* mutation but with somatic *PTEN* or *PIK3CA* mutations or *PIK3CA* amplification (TP53^{wt}/PTEN-

PIK3CA^{mut}), or tumors with somatic *TP53* mutations and with somatic *PTEN* or *PIK3CA* mutations or *PIK3CA* amplification (TP53^{mut}/PTEN-PIK3CA^{mut}). In line with our assumption that PI3K pathway activity impedes axonogenesis, SC scores were significantly lower (p=0.01) for TP53^{wt}/PTEN-PIK3CA^{mut} HNSCC as compared to all other groups (Fig. 3.20A). However, this difference was not evident in the presence of somatic *TP53* mutations, indicating that the impact of PI3K pathway activity on peripheral neurons in the TME is context-dependent and dominated by the *TP53* status. A similar context dependency was also evident for neurotrophic factors, such as NGF (Fig. 3.20B).

To further substantiate this assumption, we assessed the expression of miR-34a, which was recently reported as a p53-regulated target during neuron reprogramming in HNSCC [25]. MiR-34a exhibited a significantly lower expression in SC^{high} as compared to other tumors for TCGA-HNSC ($p<0.01$, Fig. 3.20C), and a significant difference in miR-34a related to the SC score was confirmed in other solid tumors from TCGA, such as LUSC, ESCA, CESC and PAAD (data not shown). Concerning the context-dependent role of PI3K pathway activity, highest miR-34a transcript levels were detected for TP53^{wt}/PTEN-PIK3CA^{mut} HNSCC, while its expression was significantly lower in the presence of somatic *TP53* mutations (Fig. 3.20D). A similar mode of regulation was also evident for TGF-β signaling with a significant difference between TP53^{wt}/PTEN-PIK3CA ^{wt} and TP53^{mut}/PTEN-PIK3CA ^{mut} tumors (Fig. 3.20E). Next, the SC score was computed based on RNA-seq data from 4NQO-induced tongue tumors of genetically modified mice carrying a gain-of-function (GOF) allele for *Pik3ca* alone or in combination with a *Tp53* mutation [177]. Again, significantly higher SC scores were detected for tongue tumors from Tp53^{mut} mice independent of the *Pik3ca* genotype as compared to wildtype (WT) controls or Tp53^{wt}/Pik3caGOF counterparts (Fig. 3.20F). Tongue tumors also confirmed significantly higher *Ngf* expression in the presence of *Tp53* mutations as compared to WT controls and Tp53^{wt}/Pik3ca^{GOF} mice (Fig. 3.20F).

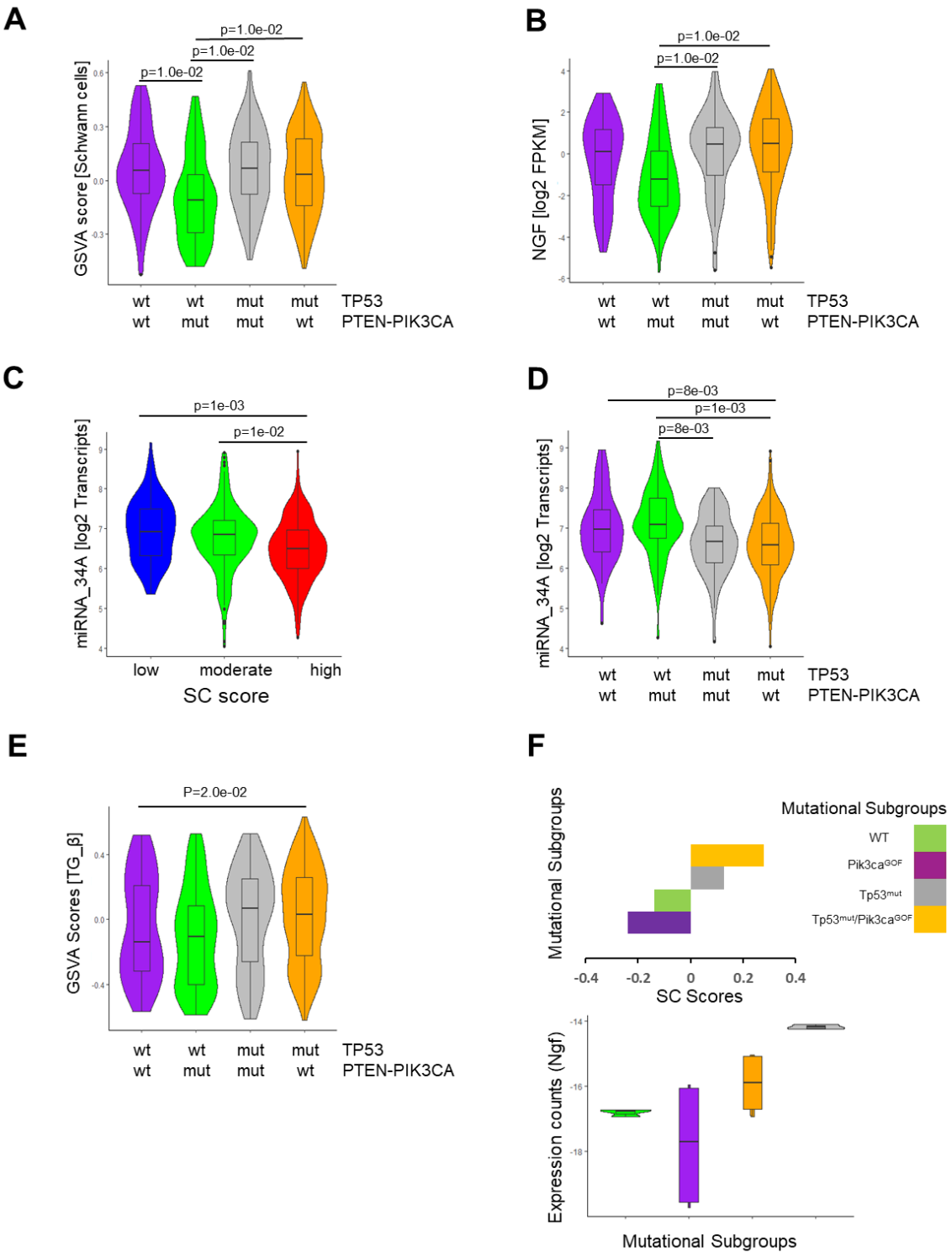

Figure 3.20: Impact of PI3K pathway activity, neurotrophic factors, and miRNA on the abundance of SCs in the context of somatic TP53 mutations in TCGA-HNSC, and tongue tumors from mice. *(**A**) Violin plots present differences among indicated mutational subgroups of TCGA-HNSC ($TP53^{wt}$/$PTEN\text{-}PIK3CA^{wt}$), ($TP53^{mut}$/$PTEN\text{-}PIK3CA^{wt}$), ($TP53^{wt}$/$PTEN\text{-}PIK3CA^{mut}$), ($TP53^{mut}$/$PTEN\text{-}PIK3CA^{mut}$) for the SC score, (**B**) NGF*

*expression values, (**D**) miR-34a expression values, (**E**) or GSVA scores for TGF-β signaling. **(C)** Violin plot shows statistically significant differences in mir-34a expression values for tumors with low, moderate, or high SC scores in TCGA-HNSC. **(F)** Bar plot presents SC scores (upper), or Violin Plot for Ngf expression values (lower) for 4NQO-induced tongue tumors from mice with indicated genotypes (wildtype (WT) controls, $Tp53^{mut}$, $Tp53^{mut}/Pik3ca^{GOF}$ or $Tp53^{mut}/Pik3ca^{GOF}$).*

3.2.6. The Immunosuppressive Phenotype in SC^{high} Tumors

Reduced levels of TILs as determined by xCell data correlation with SC score (Table S16) and accelerated TGF-β signaling (Fig. 3.19) suggested an immunosuppressive TME in SC^{high} HNSCC, which was further supported by deconvolution of RNA-seq data from TCGA-HNSC utilizing CibersortX and Kassandra tools (Fig. 3.21A-B). The former results were validated in different tumor entities: TCGA-CESC (Fig. 3.21C), and TCGA-BRCA (data not shown).

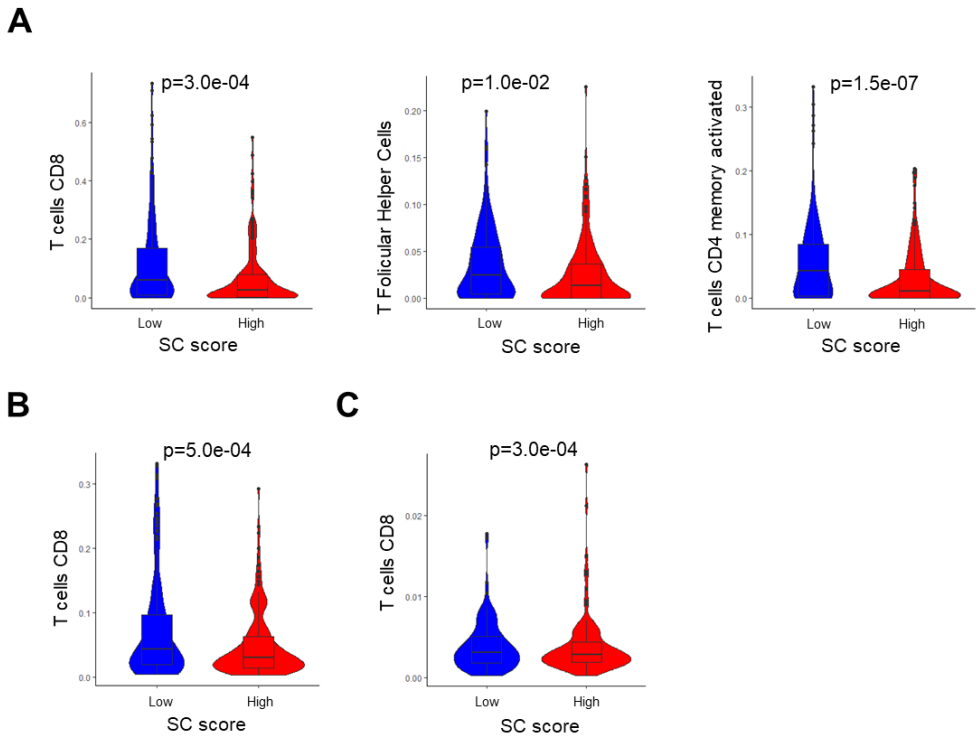

***Figure. 3.21: The enrichment of TILs* between SC score groups (low vs high) in *TCGA- (HNSC, CESC, BRCA) using three deconvolution algorithms (xCell and Cibersortx and Kassandra). (A)** Violin plots for T cell CD8, T follicular helper cells, T cells CD4 memory activated from CibersortX data, n=22 in TCGA-HNSC based on SC score (high vs low). The statistical significance was measured by a two-sided t-test. **(B)** Violin plots for T cell CD8 in Kassandra data tool, n=22 in TCGA-HNSC based on SC score (high vs low). **(C)** Violin plots for T cell CD8 from Kassandra data tool, n=22 in TCGA-CESC based on SC score (high vs low).*

3.2.7. Identification of Vulnerabilities by In-Silico Drug Screening and Oncopredict Scores

In order to identify potential vulnerabilities for subgroups of SC^{high} or SC^{low} HNSCC, we used OncoPredict scores [159] to impute sensitivity to all compounds with IC50 in the GDSC project (Table S21). This approach revealed potential vulnerabilities of SC^{high} HNSCC for EGFR inhibitors (e.g., CANERTINIB, AST-1306), MEK inhibitors (e.g., REFAMETINIB), and inhibitors of PI3K and mTOR (e.g., GSK1059615, TORIN-2, and WYE-125132), while SC^{low} tumors were particularly sensitive against drugs targeting the cell cycle or topoisomerases (e.g., CAMPTOTHECIN, IRINOTECAN, TENIPOSIDE, and TOPOTECAN) (Fig 3.22). Subsequently, we confirmed a higher cell cycle progression pathway activity in the SC^{low} (Fig. 3.19A-B). These results indicate certain cell cycle topoisomerase inhibitors could be beneficial for the patient of SC^{low}.

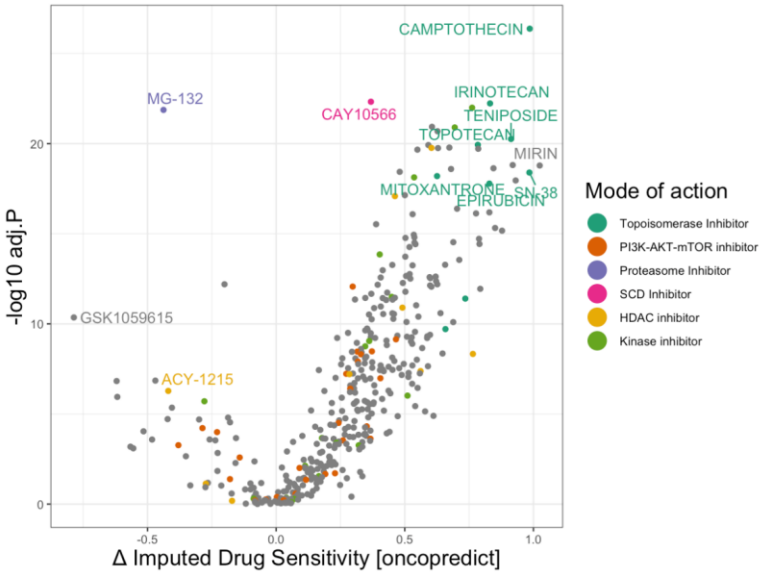

Figure 3.22: Volcano plot depicts differences between SC score (high vs low) in Oncopredict scores for TCGA-HNSC*. based on the CCLE RNA-seq and the drug response IC50 of compound GDSC1-2 drug screening project. Δ negative-imputed drug sensitivity score (oncopredict) scores indicate a*

highersensitivity and positive -scores a higher resistance of TCGA-HNSCC tumors to compouds of GDSC1-2. Statistical difference was measured by the Wilcoxon rank test.

4. Discussion

4.1. The Modulation of TME and Plasticity: A New Avenue for Cancer Research

In their benchmark review article of 2011, Hanahan and Weinberg introduced the hallmarks of cancer [3]. These hallmarks constitute an organizing principle for rationalizing the complexities of neoplastic disease [3]. Hallmarks of cancer are the mechanisms underlying the multistep process of tumorigenesis that can be distilled into a logical framework involving the acquisition of functional capabilities, which are collectively envisaged to be necessary for malignancy. These capabilities, embodied both in transformed cancer cells as well as in the heterotypic accessory cells that together constitute the TME, are conveyed by certain abnormal characteristics of the cancerous phenotype [145]. However, these hallmark traits, on their own, fail to address the complexities of cancer pathogenesis [145], which raises an attractive question of whether there are hidden factors and modulators that regulate the pathogenesis and aggressiveness of tumors?

In this context, metastasis is the primary cause of cancer morbidity and mortality, and the process involves a complex interplay between intrinsic tumor cell properties as well as mutual interactions between cancer cells and multiple components of the TME [178]. New evidence suggests that novel characteristics are required for invasive neoplastic cells to establish macroscopic secondary masses such as invasion and motility, plasticity, modulation of TME, and colonization [178]. Its already well established that EMT during cancer promotes disease progression and enhances the metastatic phenotype by bestowing upon previously benign carcinoma cell traits such as migration, invasion, resistance to anoikis, chemoresistance, and tumor-initiating potential [179]. A crucial characteristic of all metastases is their ability to restructure the local tissue by recruitment of new cells into the local microenvironment, eliciting mobilization of immune/inflammatory cells, manipulating the structure of

other tissues, altering metabolism of surrounding stroma, negating anti-tumor actions of the immune system, restructuring the behavior of other cancer cells, altering the extracellular matrix, or sharing normal behaviors of other cells to accomplish one or more steps of the metastatic cascade [178]. In the context of plasticity, cancer cell plasticity is a fundamental process in the generation of tumor heterogeneity [76]. Various tumor cell-intrinsic and extrinsic factors have been demonstrated to be involved in regulating lineage plasticity [45]. The determination of tumor composition at any time is purely a snapshot because selective pressures modify the composition and cellular behavior. Tumor cells communicate with each other as well as with normal stroma. Neoplastic cells can alter the growth rate of other cells and induce plasticity [180, 181]. In addition to the former hallmarks of metastasis the colonization of secondary tissues requires the same elements as the growth of the primary tumor such as nutrition and oxygen [182-184]. Importantly, the molecular intrinsic, and cellular extrinsic mechanisms that orchestrate the modulation of cancer cell plasticity of TME are still elusive and need to be addressed generously.

Therefore, in this study, I conducted integrative analysis of multi-omics data to highlight the most relevant alterations associated with cancer cells' plasticity depending on two different modes of action: Initially the intrinsic modulation of cancer cells' plasticity by unraveling the inverse regulation of SOX2- and SOX9-related gene networks in HNSCC and other tumor entities. Secondly, cancer cell-extrinsic mechanisms and modulators of plasticity and the role of the peripheral nervous system as an emerging new pathological component of the TME.

In conclusion, the main novelties of this study are (i) The established risk model which identifies patients with primary HNSCC, but also other cancers at a higher risk for treatment failure, who might benefit from a therapy targeting SOX2/SOX9-related gene regulatory and signaling networks, and (ii) the

establishment of an SC-related gene set as an accurate surrogate for the presence of peripheral nerves within HNSCC and across solid tumor entities. Moreover, unraveling the potential vulnerabilities of SC-related HNSCC subgroups emphasizing the need for a better characterization of these subgroups.

4.2. The Cancer Cell-Intrinsic Mechanisms and Modulators of Plasticity

Tumors represent a complex ecosystem of cells residing in genetically and phenotypically diverse states, and therapy-induced cellular plasticity has been postulated as a crucial adaptive response in therapy resistance and metastasis of cancers, including HNSCC. Recently, longitudinal single-cell RNA sequencing of patient-derived primary cells highlighted variable SOX2 and SOX9 expression patterns in drug-induced infidelity in the stem cell hierarchy of oral SCC [106]. However, the impact of SOX2/SOX9-related genetic programs in primary HNSCC and their association with risk factors or clinical features are still limited. Data of this study demonstrate a $SOX2^{high}/SOX9^{low}$ phenotype for HPV16-positive OPSCC, which is in line with recent reports on a positive association between SOX2 expression and HPV16-positive HNSCC [185, 186]. Moreover, an increased nuclear SOX2 staining in cervical carcinoma as compared to normal tissue was evident in several studies [187, 188]. In both HNSCC and cervical carcinoma, high SOX2 expression serves as a prognostic marker for improved clinical outcome [161, 185-187]. Though the molecular principle of elevated SOX2 expression in the pathogenesis of HPV16-driven carcinogenesis remains elusive, SOX2 upregulation by the viral E7 oncoprotein was demonstrated in vitro and in vivo [189]. In contrast, SOX9 expression progressively decreases during cervical carcinoma pathogenesis, and SOX9 silencing in HeLa cells promoted cell growth in culture and tumor formation in mice [190]. These data suggest a negative association among SOX9 and virus-related carcinogenesis, which is further supported by diminished SOX9 expression in a mouse model of HPV16-induced skin tumorigenesis [191]. As loss of SOX2 and a concomitant gain of SOX9 was recently established for oral SCC as an important mode of tumor evolution under the selection pressure of cisplatin [106], it is tempting to speculate that impaired

therapy-induced cellular plasticity contributes, at least in part, to improved survival of HPV16-positive OPSCC patients.

To fulfill their complex functions during tissue development, differentiation, and maintenance, SOX2 and SOX9 proteins are subjects of numerous post-translational modifications and interact with various partner proteins [97, 98]. Though a molecular subtype with low SOX2 and high SOX9 transcript levels was associated with unfavorable survival in the TCGA-HNSC cohort [106], the versatile regulation of both proteins might limit adequate assessment of their activity solely based on their transcript levels. Hence, in this study, a gene set was identified reflecting variable SOX2 and SOX9 transcript levels in HNSCC and established a risk model with a reliable prognostic value for TCGA-HNSC and independent HNSCC cohorts. An early and more accurate risk assessment is an urgent medical need for appropriate and more effective treatment of cancer patients with HNSCC and other tumor types. It will enable the stratification of either low-risk patients, who will benefit from less-intensive treatment to reduce therapy-related morbidity, or high-risk patients for treatment escalation including new options of targeted therapy to improve clinical outcome. So far, only patients with HPV16-positive OPSCC have been enrolled in clinical trials to test the concept of treatment de-escalation, and reliable risk models for HPV16-negative HNSCC are eagerly awaited [192]. Though the prognostic risk model based on transcript levels of the newly established 15-gene set requires validation in a larger prospective cohort, it has the potential to close this gap. This assumption is supported by an extensive subgroup analysis, which confirmed the prognostic value of the risk model for almost all conditions tested, with best performance for subgroups of HPV-negative HNSCC, at laryngeal or oropharyngeal subsites, with a smoking history, no histopathological evidence for angiolymphatic or perineural invasion, which are treated with radiotherapy.

Integrative analysis of multi-omics data elucidated differences in the mutational landscape among risk groups as underlying principles of inverse SOX2 and SOX9 regulation and potential drivers of cellular plasticity. As an example, a difference was identified in the frequency of truncating *NSD1* mutations, which have been attributed to a better prognosis in laryngeal SCC and a widespread global DNA hypomethylation phenotype [168-170]. Moreover, *NSD1* gene silencing in HNSCC cell lines resulted in a higher sensitivity to cisplatin [170], indicating that DNA methylation plays a critical role in the modulation of the SOX2 versus SOX9 balance. In support of this assumption, this study elucidated significantly lower DNA methylation and higher transcript levels for SOX2 in HNSCC with truncating *NSD1* mutation. Hence, disruptive *NSD1* mutations represent another molecular trait in addition to HPV16 with favorable prognosis, which might be due to limited adaptive therapy-induced cellular plasticity. This study also unraveled significant differences in the expression of several oncogenic gene sets among risk groups and indicates prominent activation of KRAS signaling in the presence of a $SOX2^{low}/SOX9^{high}$ phenotype. KRAS transmits signals from activated growth factor receptors, such as EGFR, which might explain this finding despite the lack of oncogenic KRAS mutations in most HNSCC [32]. The impact of KRAS signaling on cetuximab efficacy for HNSCC has been postulated, and patients with a germline KRAS variant have poor progression-free survival when treated with cisplatin [193, 194]. So far, possible links between KRAS and SOX2 or SOX9 in HNSCC have not been addressed but are well-established for other cancers. KRAS induces SOX9 expression and activity, which is required for the development of KRAS-mediated pancreatic ductal adenocarcinoma in mouse models [195-197]. Elevated SOX9 levels were also detected in human lung adenocarcinoma, particularly those with *KRAS* mutations, and experimental data provide compelling evidence for SOX9 upregulation by NOTCH signaling in lung cancer cells [198]. In contrast, KRAS-driven progression of lung adenocarcinoma in mice is supported by limited SOX2 expression, while SOX2 overexpression inhibits KRAS-activated lung adenocarcinoma [199, 200]. These findings raise the attractive question, of whether targeting of KRAS or NOTCH signaling in HNSCC has the

potential to limit therapy-induced cellular plasticity related to variable SOX2 and SOX9 expression to reduce treatment adaptation and resistance [200]. Strikingly, our in-silico drug screening analysis revealed a lower efficacy for numerous compounds targeting EGFR signaling for selected cancer cell lines of the CCLE from head and neck, esophagus, lung, pancreas, breast, and brain cancers with a higher risk score as compared to those with a lower risk score. Assessment of SOX2 and SOX9 expression patterns or the risk score based on the newly established 15-gene set could enable early selection of patients with HNSCC, but also other tumor types, who will benefit from EGFR targeting therapy or are at high risk for treatment failure despite the absence of activating somatic mutations in RAS oncogenes or downstream signaling pathways (Fig. 4.1).

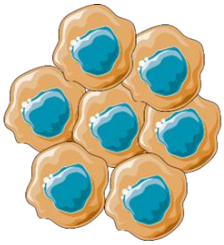

Status	$SOX2^{high}/SOX9^{low}$	$SOX2^{low}/SOX9^{high}$
Cancer cells	Epithelial	Mesenchymal
HPV16	Common	Rare
NSD1	Truncating mutations	Wildtype
SOX2 methylation	Low	High
KRAS signaling	Low	High
Prognosis (RT)	Favorable	Unfavorable
EGFRi	Sensitive	Resistance

Figure 4.1: Schematic illustration represents a summary of intrinsic modulators of cancer cell plasticity: *Assessment of SOX2 and SOX9 expression patterns defined by two main groups of ($SOX2^{high}/SOX9^{low}$ vs $SOX2^{low}/SOX9^{high}$) with different molecular and biological characteristics and features in TCGA-HNSC tumors. Abbreviations:(RT= Radiotherapy, EGFRi= EGFR inhibitors).*

4.3. The Cancer Cell-Extrinsic Mechanisms and Modulators of Plasticity

High density and functionality of peripheral nerves in the TME have been associated with poor prognosis in several cancers, such as head and neck [201], pancreatic [202], prostate [110], gastric [203], colorectal [204], and hematological cancers [14, 205].To date, only limited information on molecular processes and communication between cancer cells and nerves are available.

In the present study, a SC-related 43-gene set was established as an accurate surrogate for the presence of peripheral nerves in a TME. Based on the SC score patients of TCGA-HNSC were classified into three groups (SC^{low}, $SC^{moderate}$, SC^{high}). The positive correlation was also confirmed with gene expression data from four independent HNSCC cohorts and other solid tumors from TCGA with similar risk factors and histopathological characteristics (LUSC, CESC, and ESCA) or with well-established cancer-neuron-interaction in the TME (LUAD, BRCA, PAAD, PRAD) [174, 175].

It is well known from previous studies that *TP53* is the most commonly mutated gene in HNSCC and forms multiple aspects of tumor formation, including modulation of the TME [206, 207]. In a landmark study from 2020, it is well described that p53 loss of function serves as an important regulator of cancer–nerve crosstalk, thereby promoting tumor development and malignant progression [206] [207]. Furthermore, p53-deficient tumors communicate with neurons through a mechanism based on miR-34a that facilitates neuronal responses to environmental cues and determines the fate of cancer-associated neurons.

MiR-34a is one of the most characterized tumor suppressor miRNAs, which is lost or expressed at reduced levels in a variety of tumors. Moreover, the re-introduction of miR-34a mimics was found to inhibit cancer cell growth both in vitro and in vivo [208]. MiR-34a was also identified in another study focusing on tumor suppressor miRNAs with a critical function in EMT and metastasis [209].

In oral cancer patients, studies exhibited that miR-34a may have some significance in alleviating cancer-related pain based on the inhibition of nerve infiltration; however, the difference in physiological characteristics and other features between different types of cancers should be considered. For example, the autonomic nerve plays a crucial role in TME of prostate cancer, pancreatic cancer, and breast cancer, among others, but its role is less well-established in other cancers [210]. In pancreatic cancer, referred pains are a novel predictive marker for neural invasion and the *TP53* mutation plays an important role in the neural invasion of cancer cells [211].

In line with these findings, this study confirmed a higher frequency of somatic *TP53* mutations in SC^{high} while P53 pathway activity was higher in SC^{low} tumors.

Furthermore, the expression of miR-34a, which was reported as a p53-regulated target during neuron reprogramming in HNSCC [25] was analyzed in this study. The mir-34a exhibited a significantly lower expression in SC^{high} as compared to other tumors for TCGA-HNSC.

Interestingly a significant difference in miR-34a related to the SC score was confirmed in other solid tumors from TCGA, such as LUSC, ESCA, CESC, and PAAD raising an attractive question of whether the miR-34a as a tumor suppressor can be used in combination with currently established treatment regimens. However, the difference in nerve fibers and their physiological characteristics between different types of cancers should be considered.

The main finding of this study is a different pattern of PI3K pathway activity as a potentially new mechanism of regulation for axonogenesis and neuron density in the TME. The analysis of gene regulatory networks and oncogenic pathway activities revealed significantly higher GSVA scores for PI3K-AKT-MTOR and MTORC1 signaling in SC^{low} tumors, which may illustrate the decline of peripheral nerves within HPV16-positive tumors. Furthermore, the higher frequency of somatic mutations in *PTEN* combined with *PIK3CA* copy number gain at chromosome 3q26 for SC^{low} compared to SC^{high} suggested an

inverse association between PI3K pathway activity in cancer cells and peripheral nerve abundance in the TME potentially due to impaired tumor-related neurogenesis.

In line with the assumption that PI3K pathway activity impedes axonogenesis, the subgroup analysis based on *TP53, PIK3CA, and PTEN* mutations in tumors of the TCGA-HNSC cohort revealed that SC score were significantly lower for $TP53^{wt}$/PTEN-$PIK3CA^{mut}$ HNSCC as compared to all other groups. However, this difference was not evident in the presence of somatic *TP53* mutations, indicating that the impact of PI3K pathway activity on the TME abundance of peripheral neurons is context-dependent and dominated by the TP53 status. Further evidence strengthens the argument that PI3K pathway activity is context-dependent the higher SC scores in tumors from the induced tongue tumors of genetically modified mice with significantly higher SC scores for tumors from $Tp53^{mut}$ and $Tp53^{wt}$/$Pik3ca^{GOF}$ mice as compared to WT controls or $Pik3ca^{GOF}$ counterparts.

Based on seminal studies the PI3K signaling pathway is a well-known regulator of axon regeneration In the context of the TME recent research has demonstrated that cancer cells express neurotrophic markers such as NGF, BDNF, and GDNF and release axon guidance molecules such as Ephrin B1 to promote axonogenesis [142]. These molecules usually activate different receptors, among them the tyrosine-receptor kinases (Trks) TrkA, TrkB, and TrkC, and the p75 neurotrophin receptor [212]. Expression of NGF stimulates tumor cell proliferation and survival through the constitutive activation of the PI3K-AKT [213]. These receptors are also expressed on nerves, and the p75 neurotrophin receptor was reported to act as a chemoattractant for cancer cells [214]. The PI3k pathway activity has been well described in the context of HPV-16-induced tumorigenesis [215]. All of the major components of this pathway have been found to be frequently amplified or mutated in these types of cancers [215]. In OPSCC the activation of the PI3K signaling pathway by somatic mutation and/or copy-number

alterations of PIK3CA is a key feature of HPV-16 positive and seems to occur early in carcinogenesis [21, 216]. The HPV oncoproteins E6 and E7 alter and regulate PI3K/AKT pathway. PI3K/AKT is particularly important due to its relation to the initiation of malignancy, cell proliferation, metastasis, and also drug resistance [217].

Another highlight of this study is that a higher SC score was related to well-established oncogenic processes and pathways, such as TGF-β signaling. Studies demonstrated that local paracrine signaling from nerves to the tumor or to stromal cells in the TME regulates cancer growth and invasion, while tumor-derived factors remodel peripheral nerves, promoting further nerve ingrowth into the TME [218, 219].

On the other side, nerve-derived factors such as neurotransmitters and neuropeptides can modulate immune cell trafficking and function. Consequently, altered immune function can influence anti-cancer immunity and tumor growth-promoting inflammation [218]. Further studies in melanoma demonstrated that nociceptor sensory nerves promote $CD8^+$ T cell exhaustion in TME of melanoma through the release of neuropeptides, which enables tumor progression by impairing anti-tumor immunity [220].

In the context of immunosuppression its well-known from the literature that TGF-β signaling suppresses the function of adaptive and innate immune cells [221-224]. Previous studies demonstrated signaling pathways between primary sensory neurons, SC, and immune cells are highly correlated, and cytokines and chemokines are central components in this complex network. SCs, infiltrating macrophages, neutrophil granulocytes, and mast cells release cytokines with an anti-inflammatory or regulatory function such as transforming growth factor-β1 (TGF-β1) [225]. Furthermore, it is well-established that TGF-β triggers the EMT [94].

Interestingly, presented data indicate an immunosuppressive phenotype for SC^{high} tumors, based on the reduced levels of TILs as determined by xCell, Cibersortx, and Kassandra. On the other side, the higher GSVA scores of TGF-β signaling and EMT indicate the potential role of TGF-β in the induction of an immunosuppressive TME and also as a modulator of cancer cell invasion and motility in the same HNSCCs. In contrast, SC^{low} tumors demonstrated an immune-active TME by the enrichment of immune T cells and showed a highly significant enrichment of HPV16-positive OPSCC which was almost absent in the SC^{high} group. OPSCCs originate at anatomical sites with lymphoid tissue, in particular tonsils and base of the tongue, which could also explain a higher density of different immune cells in the TME. However, it is also worth speculating that the presence and activity of specific immune cell subsets have a negative impact on peripheral nerve density by inhibition of axonogenesis in an immune-active TME. These findings highlight promising therapeutic targets in the context of cancer-neuron-immune crosstalk and further investigation in co-culture models using cancer cells, SC and immune cells will be important as a proof-of-concept for future translation into clinical application.

Another finding of this study is the potential vulnerabilities for subgroups of SC^{high} or SC^{low} HNSCC as a solid basis for further testing in adequate pre-clinical models and long-term translation into clinical trials. Importantly, the computed Oncopredict scores predicted the sensitivity of SC^{low} tumors towards drugs targeting the cell cycle topoisomerases (e.g., CAMPTOTHECIN, IRINOTECAN, TENIPOSIDE, and TOPOTECAN).

Inhibitors of the DNA topoisomerase 1 (TOP1) and 2 (TOP2A and TOP2B) have shown considerable potential as therapeutic agents against cancers, including head and neck cancers [226-228]. However, their adverse pharmacokinetic profiles and off-target toxicities have hindered their clinical application. Both obstacles can be mitigated by targeting their delivery via tumor-specific antibody formulations. The

strategically chosen antibody must specifically and selectively target an antigen expressed on tumor cells; by using different tumor-targeting antibodies, the spectrum of tumor types is broadened [229]. TOP2A/B inhibitors such as doxorubicin and etoposide are medications commonly used to treat breast, lung, and testicular cancer, as well as lymphomas, sarcomas, and other neoplasms, even though they present dose-limiting toxicity and side effects [230]. A large number of small molecules have been identified as inhibitors of TOP1 or TOP2A/B. Many of them have been tested in clinical trials, but only a few have resulted in clinical success [230].

FDA-approved camptothecins (TOPOTECAN, IRINOTECAN, IRINOTECAN liposome) have been used in the treatment of metastatic cervical and ovarian carcinoma and pancreatic adenocarcinoma, or metastatic colon cancer in combination with 5-Fluorouracil and Cisplatin [231]. In a phase I trial study, IRINOTECAN (Y01610) demonstrated manageable toxicity and promising anti-tumor activity in patients with advanced esophageal carcinoma [232]. In addition, a phase III trial study found that the combination of irinotecan with S-1 was similarly tolerable, but significantly prolonged PFS compared to S-1 monotherapy as a second- or third-line treatment in patients with recurrent or metastatic ESCC [233]. In HNSCC a phase I/II prospective trial was applied with triple combination therapy using cisplatin, tegafur-uracil, and irinotecan which was tolerated and effective for selected patients, indicating that individualized choice of treatment could influence prognosis and quality of life in recurrent/metastatic HNSCC patients [234]. However, studies showed that CAMPTOTHECIN induces PD-L1 and immunomodulatory cytokines in colon cancer. These findings highlight the need to examine, in preclinical models and clinical situations, the potential benefits of combining DNA topoisomerase inhibitors with immune-checkpoint inhibitors [235].

Previous evidence exhibited that PI3K-AKT pathway activity mediates survival signals and is often related to treatment failure [236]. Moreover, aberrations of PI3K pathway have important clinical implications in the treatment of HNSCC. They frequently constitute ”gain of function” mutations that trigger oncogenesis, and PI3K mutations can also lead to the emergence of drug resistance after treatment with EGFR inhibitors [237]. About 66% of HNSCC harbor genomic alterations in one of the major components of PI3K pathway [238]. Targeting *PIK3CA* alteration in human squamous cell xenografts has demonstrated susceptibility to treatment in vitro and in vivo, leading a path for its clinical implication. Inhibition of PI3K by competitive blockage of ATP binding site led to decreased phosphorylation of AKT in several studies [239-241]. Preclinical data also suggested that additional molecular change should interact with *PIK3CA* alteration for tumorigenesis. Furthermore, cell lines engineered to harbor *PIK3CA* mutations in the ‘hotspots’ responded more favorably to PI3K/mTOR dual inhibition than PI3K inhibition only, indicating that tumor survival is not strictly dependent on the activated PI3K [242]. In a similar sense, PI3K inhibition demonstrated a markedly synergistic effect when combined with EGFR or MEK inhibition [243]. So, Compensatory hyperactivation of *PIK3CA* is one of the major mechanisms of treatment resistance [244].

Based on the oncopredict data analysis the list of top-ranked candidate compounds included EGFR inhibitors (e.g., CANERTINIB, AST-1306), MEK inhibitors (e.g., REFAMETINIB), and inhibitors of PI3K and mTOR (e.g., GSK1059615, TORIN-2, and WYE-125132).

In line with the GSVA computed scores, oncogenic pathways activity analysis showed low PI3K-AKT signaling in HNSCCs with high SC score, the inhibition of PI3K signaling in cancer cells might induce axonogenesis and peripheral nerve density in the TME, which could accelerate an immune suppressive phenotype and cancer cell dissemination. So, the PI3K inhibitors might not be the best option for treating HNSCCs with low SC score. Importantly, this analysis also predicted resistance of SC^{high} tumors

towards drugs targeting the cell cycle topoisomerases (e.g., CAMPTOTHECIN, IRINOTECAN, TENIPOSIDE, and TOPOTECAN).

Recent studies have shown Myc has been recently used as a target for new chemotherapeutics [245-247]. Since its primary mechanism is to induce cancer survival genes [248], dual inhibition of Myc and TOP2 can be beneficial. In addition, TOP2 has been demonstrated to be essential in efforts to relax DNA and expose the Myc promoter region for transcription [248]. Thus, the combination of Myc–TOP2 inhibition can help treat tumors.

The oncogenic pathway analysis revealed a higher GSVA score for SC^{low} HNSCC in pathways associated with cell cycle progression, including MYC or E2F target genes, and G2M checkpoint supporting the assumption that patients with a low SC score might benefit from treatment with topoisomerase inhibitors. These findings highlight promising therapeutic targets. Further investigation in the context of preclinical models will be important to translate this feasibility to clinical application.

Together, the assessment of the SC score as a surrogate marker for the presence of peripheral nerves in the TME enables to unravel novel biological insights and to identify characteristic molecular features as well as vulnerabilities of different subgroups of HNSCC and other tumor entities, which might pave the way for new therapeutic concepts for a more efficient and less toxic treatment of HNSCC patients (Fig.4.2).

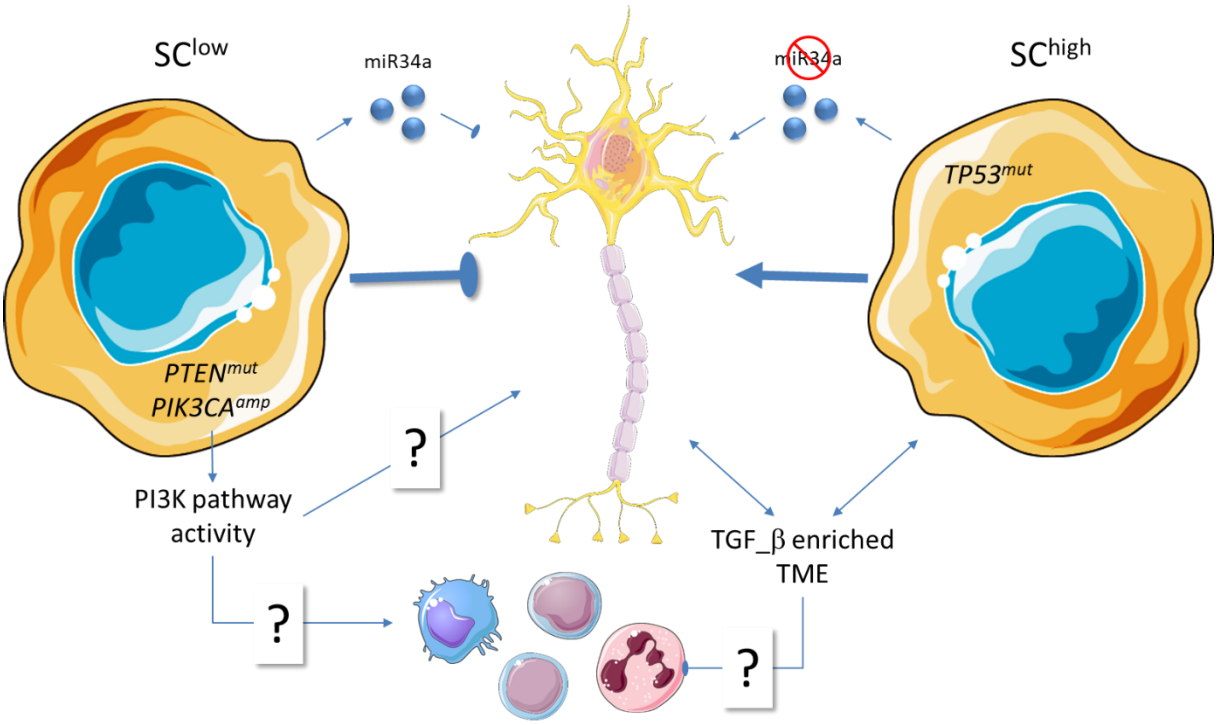

Figure 4.2: Schematic illustration represents a summary of extrinsic modulators of cancer cell plasticity in TME: *Assessment of Schwann cells as surrogate marker of the peripheral nerve in TME defined by two main groups of (SC^{high} and SC^{low}) with different molecular and biological characteristics and features representing the cancer nerve crosstalk in TCGA-HNSC tumors. Based on the presented graph open questions are raised in order to unravel the crucial factors and modulators in cancer nerve crosstalk: What are the molecular mechanisms behind the PI3k pathway activity that impedes neurogenesis and How does the pathway activity induce an active immune phenotype in SC^{low} HNSCCs? How does the TGF_β signaling induce an immunosuppressive TME in SC^{high}? Prospectively, how to achieve clinical treatment by cutting off nerves in solid tumors? How to target nerve-tumor communication to prevent tumor progression? What is the major biomolecule in the TME mediating axonogenesis, neurogenesis, and neural reprogramming process? Whether clinical neurologic drugs can be a way to treat tumors?*

4.4. Common Features of Cancer Cell Plasticity in the Intrinsic and Extrinsic Mode of Regulation

In this section, I aimed to discuss potential associations between both modes of cancer cell plasticity regulation and raise an interesting question of whether intrinsic regulation of cancer cell plasticity by

inverse SOX2 and SOX9 expression and extrinsic regulation by peripheral neurons are functionally connected.

Based on the clinical and histopathological features across HNSCCs with distinct SOX2/SOX9 expression subgroups demonstrated highly significant enrichment of perineural invasion $SOX2^{low}/SOX9^{high}$ compared to $SOX2^{high}/SOX9^{low}$ suggesting an exciting concept of SOX2/SOX9 as a modulator of cancer nerve crosstalk by altering the neurotrophic factors or miRNAs released by cancer cell to reprogram the nerve and drive neurogenesis and axonogenesis.

The data analysis of clinical and histopathological features across HNSCCs with distinct SC score demonstrated highly significant enrichment SOX2 expression and HPV16-positive OPSCC for the SC^{low} group which was almost absent in the SC^{high} group. These findings suggest further investigation in the context of preclinical models such as co-culture models between cancer cells and Schwann cells to mimic the cancer nerve crosstalk and also follow the plasticity regulation of the SOX2-SOX9 targets.

A common gene early growth response protein 2 (EGR2) was identified in the established risk model based on SOX2/SOX9 expression and the Schwann cells signatures. Studies showed that Schwann cell myelination depends on Krox-20/Egr2 and other promyelin transcription factors that are activated by axonal signals and control the generation of myelin-forming cells. The myelination is induced by neuroglin (NRG1) and SOX10 [249] Myelin-forming cells remain remarkably plastic and can revert to the immature phenotype, a process that is seen in injured nerves and demyelinating neuropathies [250]. The most characteristic compound of the myelin sheath positively affected by EGR2 is the peripheral myelin protein 22 (BMP22) [251], in addition to NRG1 and SOX10 are identified in this study as gene sets in the Schwann cells signature.

Worth noting that GAP43 is a neuron-specific, membrane-associated phosphoprotein whose expression is dramatically elevated during neuronal development and regeneration [252, 253],

and it serves as an intrinsic presynaptic determinant for neurite outgrowth and plasticity [254]. Neurotrophins (e.g., NGF), which are involved in both axon outgrowth and neuroblast migration, act in part through induction of Gap43 expression [255]. The IHC-staining of tumor tissues demonstrated high positive staining of anti-GAP43 antibodies in tumors with high SC scores. Moreover, NGF in this study was highly expressed in HNSCCs with high SC scores.

Further investigation in that context might unravel the potential role of GAP43, NGF, and EGR2 or its regulators between cancer cells and nerve fibers and might be identified as modulators of cancer cell plasticity.

5. Summary

In summary, I conducted an integrative analysis of multi-omics data to highlight the most relevant alterations associated with cancer cells' plasticity depending on two different modes of action:

5.1. The intrinsic modulation of cancer cells' plasticity in TME by unraveling the inverse regulation of SOX2- and SOX9-related gene networks in HNSCC and other tumor entities.

Firstly, differentially expressed genes (DEG) related to SOX2 and SOX9 transcription were identified in TCGA-HNSC, which enables the clustering of patients into groups with distinct clinical features and survival. Secondly, a prognostic risk model was established by LASSO Cox regression based on expression patterns of DEGs in TCGA-HNSC (training cohort) and was confirmed in independent HNSCC validation cohorts as well as other cancer cohorts from TCGA. Moreover, differences in the mutational landscape among risk groups of TCGA-HNSC demonstrated enrichment of truncating NSD1 mutations for the low-risk group and elucidated DNA methylation as a modulator of SOX2 expression. Additionally, GSVA revealed differences in several oncogenic pathways among risk groups, including upregulation of gene sets related to oncogenic KRAS signaling for the high-risk group. Finally, in silico drug screen analysis revealed numerous compounds targeting EGFR signaling with significantly lower efficacy for cancer cell lines with a higher risk phenotype, but also indicated potential vulnerabilities.

5.2. Cancer cell-extrinsic mechanisms and modulators of plasticity and the role of neuroglial activation as an emerging new component of TME that modulates cancer cell plasticity.

A SC-related 43-gene set was elucidated as an accurate surrogate for the presence of peripheral nerves across solid tumor entities. This model is characterized by higher oncogenic pathway activities such as TGF-β signaling in SC^{high} with an immunosuppressive phenotype and higher PI3K-AKT-MTOR pathway and cell cycle pathway activity in SC^{low} with an immune active phenotype and more sensitivity to

topoisomerase agents as potential treatment vulnerabilities. Finally, the impact of PI3K pathway activity on TME abundance of peripheral neurons is context-dependent and dominated by the *TP53* status.

6. References

1. Upadhyay, A., *Cancer: An unknown territory; rethinking before going ahead.* Genes Dis, 2021. **8**(5): p. 655-661.
2. Cooper, G.M., *The cell : a molecular approach / Geoffrey M. Cooper*. 2nd ed. 2000, Washington, D.C Sunderland, Mass: ASM Press Sinauer Associates. xxiv, 689 p. : ill. CD-ROM.
3. Hanahan, D. and R.A. Weinberg, *Hallmarks of cancer: the next generation.* Cell, 2011. **144**(5): p. 646-74.
4. Johnson, D.E., et al., *Head and neck squamous cell carcinoma.* Nat Rev Dis Primers, 2020. **6**(1): p. 92.
5. Jethwa, A.R. and S.S. Khariwala, *Tobacco-related carcinogenesis in head and neck cancer.* Cancer Metastasis Rev, 2017. **36**(3): p. 411-423.
6. Hashibe, M., et al., *Interaction between tobacco and alcohol use and the risk of head and neck cancer: pooled analysis in the International Head and Neck Cancer Epidemiology Consortium.* Cancer Epidemiol Biomarkers Prev, 2009. **18**(2): p. 541-50.
7. Kawakita, D. and K. Matsuo, *Alcohol and head and neck cancer.* Cancer Metastasis Rev, 2017. **36**(3): p. 425-434.
8. Denny, C.H., et al., *Consumption of Alcohol Beverages and Binge Drinking Among Pregnant Women Aged 18-44 Years - United States, 2015-2017.* MMWR Morb Mortal Wkly Rep, 2019. **68**(16): p. 365-368.
9. Seitz, H.K. and F. Stickel, *Molecular mechanisms of alcohol-mediated carcinogenesis.* Nat Rev Cancer, 2007. **7**(8): p. 599-612.
10. Garro, A.J., et al., *The effects of chronic ethanol consumption on carcinogen metabolism and on O6-methylguanine transferase-mediated repair of alkylated DNA.* Alcohol Clin Exp Res, 1986. **10**(6 Suppl): p. 73S-77S.
11. Matsuda, T., et al., *Specific tandem GG to TT base substitutions induced by acetaldehyde are due to intra-strand crosslinks between adjacent guanine bases.* Nucleic Acids Res, 1998. **26**(7): p. 1769-74.
12. Wang, M., et al., *Identification of DNA adducts of acetaldehyde.* Chem Res Toxicol, 2000. **13**(11): p. 1149-57.
13. Theruvathu, J.A., et al., *Polyamines stimulate the formation of mutagenic 1,N2-propanodeoxyguanosine adducts from acetaldehyde.* Nucleic Acids Res, 2005. **33**(11): p. 3513-20.
14. Demir, I.E., et al., *Clinically Actionable Strategies for Studying Neural Influences in Cancer.* Cancer Cell, 2020. **38**(1): p. 11-14.
15. Homann, N., et al., *High acetaldehyde levels in saliva after ethanol consumption: methodological aspects and pathogenetic implications.* Carcinogenesis, 1997. **18**(9): p. 1739-43.
16. Homann, N., et al., *Increased salivary acetaldehyde levels in heavy drinkers and smokers: a microbiological approach to oral cavity cancer.* Carcinogenesis, 2000. **21**(4): p. 663-8.
17. Khariwala, S.S., D. Hatsukami, and S.S. Hecht, *Tobacco carcinogen metabolites and DNA adducts as biomarkers in head and neck cancer: potential screening tools and prognostic indicators.* Head Neck, 2012. **34**(3): p. 441-7.
18. Wittekindt, C., et al., *HPV - A different view on Head and Neck Cancer.* Laryngorhinootologie, 2018. **97**(S 01): p. S48-S113.
19. Woodman, C.B., S.I. Collins, and L.S. Young, *The natural history of cervical HPV infection: unresolved issues.* Nat Rev Cancer, 2007. **7**(1): p. 11-22.
20. Sabatini, M.E. and S. Chiocca, *Human papillomavirus as a driver of head and neck cancers.* Br J Cancer, 2020. **122**(3): p. 306-314.

21. Lechner, M., et al., *HPV-associated oropharyngeal cancer: epidemiology, molecular biology and clinical management.* Nat Rev Clin Oncol, 2022. **19**(5): p. 306-327.
22. Leemans, C.R., P.J.F. Snijders, and R.H. Brakenhoff, *The molecular landscape of head and neck cancer.* Nat Rev Cancer, 2018. **18**(5): p. 269-282.
23. Roberts, S., et al., *Modelling human papillomavirus biology in oropharyngeal keratinocytes.* Philos Trans R Soc Lond B Biol Sci, 2019. **374**(1773): p. 20180289.
24. Parfenov, M., et al., *Characterization of HPV and host genome interactions in primary head and neck cancers.* Proc Natl Acad Sci U S A, 2014. **111**(43): p. 15544-9.
25. Amit, M., et al., *Loss of p53 drives neuron reprogramming in head and neck cancer.* Nature, 2020. **578**(7795): p. 449-454.
26. Hayes, D.N., C. Van Waes, and T.Y. Seiwert, *Genetic Landscape of Human Papillomavirus-Associated Head and Neck Cancer and Comparison to Tobacco-Related Tumors.* J Clin Oncol, 2015. **33**(29): p. 3227-34.
27. Cancer Genome Atlas, N., *Comprehensive genomic characterization of head and neck squamous cell carcinomas.* Nature, 2015. **517**(7536): p. 576-82.
28. Smeets, S.J., et al., *Genome-wide DNA copy number alterations in head and neck squamous cell carcinomas with or without oncogene-expressing human papillomavirus.* Oncogene, 2006. **25**(17): p. 2558-64.
29. Watson, I.R., et al., *Emerging patterns of somatic mutations in cancer.* Nat Rev Genet, 2013. **14**(10): p. 703-18.
30. Lechner, M., et al., *Targeted next-generation sequencing of head and neck squamous cell carcinoma identifies novel genetic alterations in HPV+ and HPV- tumors.* Genome Med, 2013. **5**(5): p. 49.
31. Liu, J., et al., *An Integrated TCGA Pan-Cancer Clinical Data Resource to Drive High-Quality Survival Outcome Analytics.* Cell, 2018. **173**(2): p. 400-416 e11.
32. Sanchez-Vega, F., et al., *Oncogenic Signaling Pathways in The Cancer Genome Atlas.* Cell, 2018. **173**(2): p. 321-337 e10.
33. Huang, C., et al., *Proteogenomic insights into the biology and treatment of HPV-negative head and neck squamous cell carcinoma.* Cancer Cell, 2021. **39**(3): p. 361-379 e16.
34. Reed, A.L., et al., *High frequency of p16 (CDKN2/MTS-1/INK4A) inactivation in head and neck squamous cell carcinoma.* Cancer Res, 1996. **56**(16): p. 3630-3.
35. Minarovits, J., et al., *Epigenetic Dysregulation in Virus-Associated Neoplasms.* Adv Exp Med Biol, 2016. **879**: p. 71-90.
36. Kostareli, E., et al., *HPV-related methylation signature predicts survival in oropharyngeal squamous cell carcinomas.* J Clin Invest, 2013. **123**(6): p. 2488-501.
37. Kitamura, N., et al., *Current Trends and Future Prospects of Molecular Targeted Therapy in Head and Neck Squamous Cell Carcinoma.* Int J Mol Sci, 2020. **22**(1).
38. Pfister, D.G., et al., *Head and neck cancers, Version 2.2014. Clinical practice guidelines in oncology.* J Natl Compr Canc Netw, 2014. **12**(10): p. 1454-87.
39. Chow, L.Q.M., *Head and Neck Cancer.* N Engl J Med, 2020. **382**(1): p. 60-72.
40. Puram, S.V. and J.W. Rocco, *Molecular Aspects of Head and Neck Cancer Therapy.* Hematol Oncol Clin North Am, 2015. **29**(6): p. 971-92.
41. Gath, H.J. and R.H. Brakenhoff, *Minimal residual disease in head and neck cancer.* Cancer Metastasis Rev, 1999. **18**(1): p. 109-26.
42. Haimovitz-Friedman, A., R.N. Kolesnick, and Z. Fuks, *Modulation of the Apoptotic Response: Potential for Improving the Outcome in Clinical Radiotherapy.* Semin Radiat Oncol, 1996. **6**(4): p. 273-283.

43. Forastiere, A.A., et al., *Use of Larynx-Preservation Strategies in the Treatment of Laryngeal Cancer: American Society of Clinical Oncology Clinical Practice Guideline Update.* J Clin Oncol, 2018. **36**(11): p. 1143-1169.
44. Forastiere, A.A., et al., *Concurrent chemotherapy and radiotherapy for organ preservation in advanced laryngeal cancer.* N Engl J Med, 2003. **349**(22): p. 2091-8.
45. Quintanal-Villalonga, A., et al., *Lineage plasticity in cancer: a shared pathway of therapeutic resistance.* Nat Rev Clin Oncol, 2020. **17**(6): p. 360-371.
46. Vermorken, J.B., et al., *Cisplatin, fluorouracil, and docetaxel in unresectable head and neck cancer.* N Engl J Med, 2007. **357**(17): p. 1695-704.
47. Hitt, R., et al., *Phase III study comparing cisplatin plus fluorouracil to paclitaxel, cisplatin, and fluorouracil induction chemotherapy followed by chemoradiotherapy in locally advanced head and neck cancer.* J Clin Oncol, 2005. **23**(34): p. 8636-45.
48. Gibson, M.K., et al., *Randomized phase III evaluation of cisplatin plus fluorouracil versus cisplatin plus paclitaxel in advanced head and neck cancer (E1395): an intergroup trial of the Eastern Cooperative Oncology Group.* J Clin Oncol, 2005. **23**(15): p. 3562-7.
49. Kanno, Y., et al., *Molecular Mechanisms of Chemotherapy Resistance in Head and Neck Cancers.* Front Oncol, 2021. **11**: p. 640392.
50. Cooper, J.S., et al., *Postoperative concurrent radiotherapy and chemotherapy for high-risk squamous-cell carcinoma of the head and neck.* N Engl J Med, 2004. **350**(19): p. 1937-44.
51. Bernier, J., et al., *Postoperative irradiation with or without concomitant chemotherapy for locally advanced head and neck cancer.* N Engl J Med, 2004. **350**(19): p. 1945-52.
52. Zhang, Y.J., et al., *Activation of c-Jun/JNK signaling predicts poor prognosis in nasopharyngeal carcinoma.* Int J Clin Exp Pathol, 2018. **11**(5): p. 2699-2706.
53. Zhang, N., et al., *5-Fluorouracil: mechanisms of resistance and reversal strategies.* Molecules, 2008. **13**(8): p. 1551-69.
54. Zunino, F., et al., *Molecular mechanisms of resistance to taxanes and therapeutic implications.* Drug Resist Updat, 1999. **2**(6): p. 351-357.
55. Orr, G.A., et al., *Mechanisms of Taxol resistance related to microtubules.* Oncogene, 2003. **22**(47): p. 7280-95.
56. Yusuf, R.Z., et al., *Paclitaxel resistance: molecular mechanisms and pharmacologic manipulation.* Curr Cancer Drug Targets, 2003. **3**(1): p. 1-19.
57. Jannetta, P.J., *Microsurgical management of trigeminal neuralgia.* Arch Neurol, 1985. **42**(8): p. 800.
58. Bonner, J.A., et al., *Radiotherapy plus cetuximab for squamous-cell carcinoma of the head and neck.* N Engl J Med, 2006. **354**(6): p. 567-78.
59. Vermorken, J.B., et al., *Platinum-based chemotherapy plus cetuximab in head and neck cancer.* N Engl J Med, 2008. **359**(11): p. 1116-27.
60. Moskowitz, H.S., et al., *Serum biomarker modulation following molecular targeting of epidermal growth factor and cyclooxygenase pathways: a pilot randomized trial in head and neck cancer.* Oral Oncol, 2012. **48**(11): p. 1136-45.
61. Kalyankrishna, S. and J.R. Grandis, *Epidermal growth factor receptor biology in head and neck cancer.* J Clin Oncol, 2006. **24**(17): p. 2666-72.
62. Kim, R., M. Emi, and K. Tanabe, *Cancer immunoediting from immune surveillance to immune escape.* Immunology, 2007. **121**(1): p. 1-14.
63. Ribas, A. and J.D. Wolchok, *Cancer immunotherapy using checkpoint blockade.* Science, 2018. **359**(6382): p. 1350-1355.
64. Wu, X., et al., *Application of PD-1 Blockade in Cancer Immunotherapy.* Comput Struct Biotechnol J, 2019. **17**: p. 661-674.

65. Argiris, A., et al., *Head and neck cancer.* Lancet, 2008. **371**(9625): p. 1695-709.
66. Hoffmann, T.K., et al., *Spontaneous apoptosis of circulating T lymphocytes in patients with head and neck cancer and its clinical importance.* Clin Cancer Res, 2002. **8**(8): p. 2553-62.
67. Topalian, S.L., et al., *Safety, activity, and immune correlates of anti-PD-1 antibody in cancer.* N Engl J Med, 2012. **366**(26): p. 2443-54.
68. Ferris, R.L., et al., *Nivolumab for Recurrent Squamous-Cell Carcinoma of the Head and Neck.* N Engl J Med, 2016. **375**(19): p. 1856-1867.
69. Fakhry, C., et al., *Human papillomavirus and overall survival after progression of oropharyngeal squamous cell carcinoma.* J Clin Oncol, 2014. **32**(30): p. 3365-73.
70. Lee, A.W., et al., *Retrospective analysis of patients with nasopharyngeal carcinoma treated during 1976-1985: survival after local recurrence.* Int J Radiat Oncol Biol Phys, 1993. **26**(5): p. 773-82.
71. Burtness, B., et al., *Pembrolizumab alone or with chemotherapy versus cetuximab with chemotherapy for recurrent or metastatic squamous cell carcinoma of the head and neck (KEYNOTE-048): a randomised, open-label, phase 3 study.* Lancet, 2019. **394**(10212): p. 1915-1928.
72. Blach, J., et al., *Failure of Immunotherapy-The Molecular and Immunological Origin of Immunotherapy Resistance in Lung Cancer.* Int J Mol Sci, 2021. **22**(16).
73. Bonaventura, P., et al., *Cold Tumors: A Therapeutic Challenge for Immunotherapy.* Front Immunol, 2019. **10**: p. 168.
74. Hamm, C.A., et al., *Immune profiling reveals the diverse nature of the immune response in NSCLC and reveals signaling pathways that may influence the anti-tumor immune response.* Exp Mol Pathol, 2019. **109**: p. 1-15.
75. Thankamony, A.P., et al., *Lineage Plasticity in Cancer: The Tale of a Skin-Walker.* Cancers (Basel), 2021. **13**(14).
76. Marusyk, A., V. Almendro, and K. Polyak, *Intra-tumour heterogeneity: a looking glass for cancer?* Nat Rev Cancer, 2012. **12**(5): p. 323-34.
77. Ghanei, Z., et al., *Isolation and characterization of breast cancer stem cell-like phenotype by Oct4 promoter-mediated activity.* J Cell Physiol, 2020. **235**(11): p. 7840-7848.
78. Koo, B.S., et al., *Oct4 is a critical regulator of stemness in head and neck squamous carcinoma cells.* Oncogene, 2015. **34**(18): p. 2317-24.
79. Liu, H.L., et al., *Oct4 Regulates the Transition of Cancer Stem-Like Cells to Tumor Endothelial-Like Cells in Human Liver Cancer.* Front Cell Dev Biol, 2020. **8**: p. 563316.
80. Christin, J.R., et al., *Stem Cell Determinant SOX9 Promotes Lineage Plasticity and Progression in Basal-like Breast Cancer.* Cell Rep, 2020. **31**(10): p. 107742.
81. Pisco, A.O. and S. Huang, *Non-genetic cancer cell plasticity and therapy-induced stemness in tumour relapse: 'What does not kill me strengthens me'.* Br J Cancer, 2015. **112**(11): p. 1725-32.
82. Shenoy, S., *Cell plasticity in cancer: A complex interplay of genetic, epigenetic mechanisms and tumor micro-environment.* Surg Oncol, 2020. **34**: p. 154-162.
83. Tiwari, R., N. Manzar, and B. Ateeq, *Dynamics of Cellular Plasticity in Prostate Cancer Progression.* Front Mol Biosci, 2020. **7**: p. 130.
84. Poltavets, V., et al., *The Role of the Extracellular Matrix and Its Molecular and Cellular Regulators in Cancer Cell Plasticity.* Front Oncol, 2018. **8**: p. 431.
85. Colotta, F., et al., *Cancer-related inflammation, the seventh hallmark of cancer: links to genetic instability.* Carcinogenesis, 2009. **30**(7): p. 1073-81.
86. Baram, T., et al., *Inflammation-Driven Breast Tumor Cell Plasticity: Stemness/EMT, Therapy Resistance and Dormancy.* Front Oncol, 2020. **10**: p. 614468.

87. Lu, H., et al., *A breast cancer stem cell niche supported by juxtacrine signalling from monocytes and macrophages.* Nat Cell Biol, 2014. **16**(11): p. 1105-17.
88. Yang, J., et al., *Guidelines and definitions for research on epithelial-mesenchymal transition.* Nat Rev Mol Cell Biol, 2020. **21**(6): p. 341-352.
89. Li, X., et al., *Disseminated Melanoma Cells Transdifferentiate into Endothelial Cells in Intravascular Niches at Metastatic Sites.* Cell Rep, 2020. **31**(11): p. 107765.
90. Hay, E.D., *An overview of epithelio-mesenchymal transformation.* Acta Anat (Basel), 1995. **154**(1): p. 8-20.
91. Mikheev, V.F., *[Role of genetic factors in the formation of trace reactions in man].* Zh Vyssh Nerv Deiat Im I P Pavlova, 1979. **29**(3): p. 510-7.
92. Nieto, M.A., *Epithelial plasticity: a common theme in embryonic and cancer cells.* Science, 2013. **342**(6159): p. 1234850.
93. Jia, D., et al., *Quantifying Cancer Epithelial-Mesenchymal Plasticity and its Association with Stemness and Immune Response.* J Clin Med, 2019. **8**(5).
94. Gonzalez, D.M. and D. Medici, *Signaling mechanisms of the epithelial-mesenchymal transition.* Sci Signal, 2014. **7**(344): p. re8.
95. Schepers, G.E., R.D. Teasdale, and P. Koopman, *Twenty pairs of sox: extent, homology, and nomenclature of the mouse and human sox transcription factor gene families.* Dev Cell, 2002. **3**(2): p. 167-70.
96. Kamachi, Y. and H. Kondoh, *Sox proteins: regulators of cell fate specification and differentiation.* Development, 2013. **140**(20): p. 4129-44.
97. Sarkar, A. and K. Hochedlinger, *The sox family of transcription factors: versatile regulators of stem and progenitor cell fate.* Cell Stem Cell, 2013. **12**(1): p. 15-30.
98. Grimm, D., et al., *The role of SOX family members in solid tumours and metastasis.* Semin Cancer Biol, 2020. **67**(Pt 1): p. 122-153.
99. Seo, E., et al., *Distinct functions of Sox2 control self-renewal and differentiation in the osteoblast lineage.* Mol Cell Biol, 2011. **31**(22): p. 4593-608.
100. Boyer, L.A., et al., *Core transcriptional regulatory circuitry in human embryonic stem cells.* Cell, 2005. **122**(6): p. 947-56.
101. Liu, K., et al., *The multiple roles for Sox2 in stem cell maintenance and tumorigenesis.* Cell Signal, 2013. **25**(5): p. 1264-71.
102. Wang, X., et al., *SOX2 enhances the migration and invasion of ovarian cancer cells via Src kinase.* PLoS One, 2014. **9**(6): p. e99594.
103. Wilbertz, T., et al., *SOX2 gene amplification and protein overexpression are associated with better outcome in squamous cell lung cancer.* Mod Pathol, 2011. **24**(7): p. 944-53.
104. Gatecel, C., et al., *[Effect of isoflurane and halothane on hepatic arterial and portal venous blood circulation in man].* Ann Fr Anesth Reanim, 1989. **8 Suppl**: p. R139.
105. Mu, P., et al., *SOX2 promotes lineage plasticity and antiandrogen resistance in TP53- and RB1-deficient prostate cancer.* Science, 2017. **355**(6320): p. 84-88.
106. Sharma, A., et al., *Longitudinal single-cell RNA sequencing of patient-derived primary cells reveals drug-induced infidelity in stem cell hierarchy.* Nat Commun, 2018. **9**(1): p. 4931.
107. Kuo, M.H., et al., *Cross-talk between SOX2 and TGFbeta Signaling Regulates EGFR-TKI Tolerance and Lung Cancer Dissemination.* Cancer Res, 2020. **80**(20): p. 4426-4438.
108. Lin, S.C., et al., *Epigenetic Switch between SOX2 and SOX9 Regulates Cancer Cell Plasticity.* Cancer Res, 2016. **76**(23): p. 7036-7048.
109. Jin, M.Z. and W.L. Jin, *The updated landscape of tumor microenvironment and drug repurposing.* Signal Transduct Target Ther, 2020. **5**(1): p. 166.

110. Magnon, C., et al., *Autonomic nerve development contributes to prostate cancer progression.* Science, 2013. **341**(6142): p. 1236361.
111. Xiao, Y. and D. Yu, *Tumor microenvironment as a therapeutic target in cancer.* Pharmacol Ther, 2021. **221**: p. 107753.
112. Qiu, G.Z., et al., *Reprogramming of the Tumor in the Hypoxic Niche: The Emerging Concept and Associated Therapeutic Strategies.* Trends Pharmacol Sci, 2017. **38**(8): p. 669-686.
113. Mao, X.Y., et al., *Live or let die: Neuroprotective and anti-cancer effects of nutraceutical antioxidants.* Pharmacol Ther, 2018. **183**: p. 137-151.
114. Vaupel, P., F. Kallinowski, and P. Okunieff, *Blood flow, oxygen and nutrient supply, and metabolic microenvironment of human tumors: a review.* Cancer Res, 1989. **49**(23): p. 6449-65.
115. Nagelkerke, A., et al., *The mechanical microenvironment in cancer: How physics affects tumours.* Semin Cancer Biol, 2015. **35**: p. 62-70.
116. Panciera, T., et al., *Mechanobiology of YAP and TAZ in physiology and disease.* Nat Rev Mol Cell Biol, 2017. **18**(12): p. 758-770.
117. Junttila, M.R. and F.J. de Sauvage, *Influence of tumour micro-environment heterogeneity on therapeutic response.* Nature, 2013. **501**(7467): p. 346-54.
118. Monje, M., et al., *Roadmap for the Emerging Field of Cancer Neuroscience.* Cell, 2020. **181**(2): p. 219-222.
119. Chen, S.H., et al., *Perineural invasion of cancer: a complex crosstalk between cells and molecules in the perineural niche.* Am J Cancer Res, 2019. **9**(1): p. 1-21.
120. Gysler, S.M. and R. Drapkin, *Tumor innervation: peripheral nerves take control of the tumor microenvironment.* J Clin Invest, 2021. **131**(11).
121. Carter, R.L., et al., *Perineural spread by squamous carcinomas of the head and neck: a morphological study using antiaxonal and antimyelin monoclonal antibodies.* J Clin Pathol, 1983. **36**(3): p. 269-75.
122. van Wyk, H.C., et al., *The role of perineural invasion in predicting survival in patients with primary operable colorectal cancer: A systematic review.* Crit Rev Oncol Hematol, 2017. **112**: p. 11-20.
123. Amit, M., S. Na'ara, and Z. Gil, *Mechanisms of cancer dissemination along nerves.* Nat Rev Cancer, 2016. **16**(6): p. 399-408.
124. Bakst, R.L., et al., *Perineural Invasion and Perineural Tumor Spread in Head and Neck Cancer.* Int J Radiat Oncol Biol Phys, 2019. **103**(5): p. 1109-1124.
125. Schmitd, L.B., C.S. Scanlon, and N.J. D'Silva, *Perineural Invasion in Head and Neck Cancer.* J Dent Res, 2018. **97**(7): p. 742-750.
126. Kurtz, K.A., et al., *Perineural and vascular invasion in oral cavity squamous carcinoma: increased incidence on re-review of slides and by using immunohistochemical enhancement.* Arch Pathol Lab Med, 2005. **129**(3): p. 354-9.
127. Miknyoczki, S.J., et al., *Neurotrophins and Trk receptors in human pancreatic ductal adenocarcinoma: expression patterns and effects on in vitro invasive behavior.* Int J Cancer, 1999. **81**(3): p. 417-27.
128. Faulkner, S., et al., *Tumor Neurobiology and the War of Nerves in Cancer.* Cancer Discov, 2019. **9**(6): p. 702-710.
129. Deborde, S. and R.J. Wong, *How Schwann cells facilitate cancer progression in nerves.* Cell Mol Life Sci, 2017. **74**(24): p. 4405-4420.
130. Zahalka, A.H. and P.S. Frenette, *Nerves in cancer.* Nat Rev Cancer, 2020. **20**(3): p. 143-157.
131. Wang, W., et al., *Nerves in the Tumor Microenvironment: Origin and Effects.* Front Cell Dev Biol, 2020. **8**: p. 601738.

132. Jobling, P., et al., *Nerve-Cancer Cell Cross-talk: A Novel Promoter of Tumor Progression.* Cancer Res, 2015. **75**(9): p. 1777-81.
133. Dantzer, R., *Neuroimmune Interactions: From the Brain to the Immune System and Vice Versa.* Physiol Rev, 2018. **98**(1): p. 477-504.
134. Antonica, A., et al., *Vagal control of lymphocyte release from rat thymus.* J Auton Nerv Syst, 1994. **48**(3): p. 187-97.
135. Nissen, M.D., E.K. Sloan, and S.R. Mattarollo, *beta-Adrenergic Signaling Impairs Antitumor CD8(+) T-cell Responses to B-cell Lymphoma Immunotherapy.* Cancer Immunol Res, 2018. **6**(1): p. 98-109.
136. Chen, H., et al., *beta2-AR activation induces chemoresistance by modulating p53 acetylation through upregulating Sirt1 in cervical cancer cells.* Cancer Sci, 2017. **108**(7): p. 1310-1317.
137. Hanahan, D. and M. Monje, *Cancer hallmarks intersect with neuroscience in the tumor microenvironment.* Cancer Cell, 2023. **41**(3): p. 573-580.
138. Prazeres, P., et al., *Ablation of sensory nerves favours melanoma progression.* J Cell Mol Med, 2020. **24**(17): p. 9574-9589.
139. Shao, J.X., et al., *Autonomic nervous infiltration positively correlates with pathological risk grading and poor prognosis in patients with lung adenocarcinoma.* Thorac Cancer, 2016. **7**(5): p. 588-598.
140. Cervantes-Villagrana, R.D., et al., *Tumor-induced neurogenesis and immune evasion as targets of innovative anti-cancer therapies.* Signal Transduct Target Ther, 2020. **5**(1): p. 99.
141. Li, X., et al., *Targeting tumor innervation: premises, promises, and challenges.* Cell Death Discov, 2022. **8**(1): p. 131.
142. Silverman, D.A., et al., *Cancer-Associated Neurogenesis and Nerve-Cancer Cross-talk.* Cancer Res, 2021. **81**(6): p. 1431-1440.
143. Palm, D. and F. Entschladen, *Neoneurogenesis and the neuro-neoplastic synapse.* Prog Exp Tumor Res, 2007. **39**: p. 91-98.
144. Ayala, G.E., et al., *Cancer-related axonogenesis and neurogenesis in prostate cancer.* Clin Cancer Res, 2008. **14**(23): p. 7593-603.
145. Hanahan, D., *Hallmarks of Cancer: New Dimensions.* Cancer Discov, 2022. **12**(1): p. 31-46.
146. Dworkin, R.H., et al., *Advances in neuropathic pain: diagnosis, mechanisms, and treatment recommendations.* Arch Neurol, 2003. **60**(11): p. 1524-34.
147. Demir, I.E., et al., *Investigation of Schwann cells at neoplastic cell sites before the onset of cancer invasion.* J Natl Cancer Inst, 2014. **106**(8).
148. Bockman, D.E., M. Buchler, and H.G. Beger, *Interaction of pancreatic ductal carcinoma with nerves leads to nerve damage.* Gastroenterology, 1994. **107**(1): p. 219-30.
149. Cao, S., et al., *Divergent viral presentation among human tumors and adjacent normal tissues.* Sci Rep, 2016. **6**: p. 28294.
150. Yu, G., et al., *clusterProfiler: an R package for comparing biological themes among gene clusters.* OMICS, 2012. **16**(5): p. 284-7.
151. Gu, Z., R. Eils, and M. Schlesner, *Complex heatmaps reveal patterns and correlations in multidimensional genomic data.* Bioinformatics, 2016. **32**(18): p. 2847-9.
152. Larsen, S.J., et al., *CoNVaQ: a web tool for copy number variation-based association studies.* BMC Genomics, 2018. **19**(1): p. 369.
153. Robinson, M.D., D.J. McCarthy, and G.K. Smyth, *edgeR: a Bioconductor package for differential expression analysis of digital gene expression data.* Bioinformatics, 2010. **26**(1): p. 139-40.
154. Subramanian, A., et al., *Gene set enrichment analysis: a knowledge-based approach for interpreting genome-wide expression profiles.* Proc Natl Acad Sci U S A, 2005. **102**(43): p. 15545-50.

155. Hanzelmann, S., R. Castelo, and J. Guinney, *GSVA: gene set variation analysis for microarray and RNA-seq data.* BMC Bioinformatics, 2013. **14**: p. 7.
156. Thorvaldsdottir, H., J.T. Robinson, and J.P. Mesirov, *Integrative Genomics Viewer (IGV): high-performance genomics data visualization and exploration.* Brief Bioinform, 2013. **14**(2): p. 178-92.
157. Ritchie, M.E., et al., *limma powers differential expression analyses for RNA-sequencing and microarray studies.* Nucleic Acids Res, 2015. **43**(7): p. e47.
158. Bankhead, P., et al., *QuPath: Open source software for digital pathology image analysis.* Sci Rep, 2017. **7**(1): p. 16878.
159. Maeser, D., R.F. Gruener, and R.S. Huang, *oncoPredict: an R package for predicting in vivo or cancer patient drug response and biomarkers from cell line screening data.* Brief Bioinform, 2021. **22**(6).
160. Hahsler, M., K. Hornik, and C. Buchta, *Getting Things in Order: An Introduction to the R Package seriation.* Journal of Statistical Software, 2008. **25**(3): p. 1 - 34.
161. Bayo, P., et al., *Loss of SOX2 expression induces cell motility via vimentin up-regulation and is an unfavorable risk factor for survival of head and neck squamous cell carcinoma.* Mol Oncol, 2015. **9**(8): p. 1704-19.
162. Holzinger, D., et al., *Viral RNA patterns and high viral load reliably define oropharynx carcinomas with active HPV16 involvement.* Cancer Res, 2012. **72**(19): p. 4993-5003.
163. Thierauf, J., et al., *Low SOX2 expression marks a distinct subset of adenoid cystic carcinoma of the head and neck and is associated with an advanced tumor stage.* PLoS One, 2018. **13**(3): p. e0194989.
164. Lawrence, M.S., et al., *Mutational heterogeneity in cancer and the search for new cancer-associated genes.* Nature, 2013. **499**(7457): p. 214-218.
165. Liberzon, A., et al., *Molecular signatures database (MSigDB) 3.0.* Bioinformatics, 2011. **27**(12): p. 1739-40.
166. Franzen, O., L.M. Gan, and J.L.M. Bjorkegren, *PanglaoDB: a web server for exploration of mouse and human single-cell RNA sequencing data.* Database (Oxford), 2019. **2019**.
167. Rouillard, A.D., et al., *The harmonizome: a collection of processed datasets gathered to serve and mine knowledge about genes and proteins.* Database (Oxford), 2016. **2016**.
168. Peri, S., et al., *NSD1- and NSD2-damaging mutations define a subset of laryngeal tumors with favorable prognosis.* Nat Commun, 2017. **8**(1): p. 1772.
169. Brennan, K., et al., *NSD1 inactivation defines an immune cold, DNA hypomethylated subtype in squamous cell carcinoma.* Sci Rep, 2017. **7**(1): p. 17064.
170. Bui, N., et al., *Disruption of NSD1 in Head and Neck Cancer Promotes Favorable Chemotherapeutic Responses Linked to Hypomethylation.* Mol Cancer Ther, 2018. **17**(7): p. 1585-1594.
171. Lepikhova, T., et al., *Drug-Sensitivity Screening and Genomic Characterization of 45 HPV-Negative Head and Neck Carcinoma Cell Lines for Novel Biomarkers of Drug Efficacy.* Mol Cancer Ther, 2018. **17**(9): p. 2060-2071.
172. Iorio, F., et al., *A Landscape of Pharmacogenomic Interactions in Cancer.* Cell, 2016. **166**(3): p. 740-754.
173. Corsello, S.M., et al., *Discovering the anti-cancer potential of non-oncology drugs by systematic viability profiling.* Nat Cancer, 2020. **1**(2): p. 235-248.
174. Hutchings, C., J.A. Phillips, and M.B.A. Djamgoz, *Nerve input to tumours: Pathophysiological consequences of a dynamic relationship.* Biochim Biophys Acta Rev Cancer, 2020. **1874**(2): p. 188411.

175. Hessmann, E., et al., *Microenvironmental Determinants of Pancreatic Cancer.* Physiol Rev, 2020. **100**(4): p. 1707-1751.
176. Aran, D., *Cell-Type Enrichment Analysis of Bulk Transcriptomes Using xCell.* Methods Mol Biol, 2020. **2120**: p. 263-276.
177. Garcia-Carracedo, D., et al., *PIK3CA and p53 Mutations Promote 4NQO-Initated Head and Neck Tumor Progression and Metastasis in Mice.* Mol Cancer Res, 2020. **18**(6): p. 822-834.
178. Welch, D.R. and D.R. Hurst, *Defining the Hallmarks of Metastasis.* Cancer Res, 2019. **79**(12): p. 3011-3027.
179. Chaffer, C.L., et al., *EMT, cell plasticity and metastasis.* Cancer Metastasis Rev, 2016. **35**(4): p. 645-654.
180. Kroesen, G., *[Damages to the cricoid cartilage in longterm intubation].* Prakt Anaesth, 1976. **11**(3): p. 174-5.
181. Rak, J.W. and R.S. Kerbel, *Growth advantage ("clonal dominance") of metastatically competent tumor cell variants expressed under selective two- or three-dimensional tissue culture conditions.* In Vitro Cell Dev Biol Anim, 1993. **29A**(9): p. 742-8.
182. Folkman, J., *Angiogenesis.* Annu Rev Med, 2006. **57**: p. 1-18.
183. Naumov, G.N., et al., *Tumor-vascular interactions and tumor dormancy.* APMIS, 2008. **116**(7-8): p. 569-85.
184. Kaplan, R.N., et al., *VEGFR1-positive haematopoietic bone marrow progenitors initiate the pre-metastatic niche.* Nature, 2005. **438**(7069): p. 820-7.
185. Baumeister, P., et al., *High Expression of EpCAM and Sox2 is a Positive Prognosticator of Clinical Outcome for Head and Neck Carcinoma.* Sci Rep, 2018. **8**(1): p. 14582.
186. Chung, J.H., et al., *SOX2 activation predicts prognosis in patients with head and neck squamous cell carcinoma.* Sci Rep, 2018. **8**(1): p. 1677.
187. Kim, B.W., et al., *Clinical significance of OCT4 and SOX2 protein expression in cervical cancer.* BMC Cancer, 2015. **15**: p. 1015.
188. Ji, J. and P.S. Zheng, *Expression of Sox2 in human cervical carcinogenesis.* Hum Pathol, 2010. **41**(10): p. 1438-47.
189. Organista-Nava, J., et al., *The HPV16 E7 oncoprotein increases the expression of Oct3/4 and stemness-related genes and augments cell self-renewal.* Virology, 2016. **499**: p. 230-242.
190. Wang, H.Y., P. Lian, and P.S. Zheng, *SOX9, a potential tumor suppressor in cervical cancer, transactivates p21WAF1/CIP1 and suppresses cervical tumor growth.* Oncotarget, 2015. **6**(24): p. 20711-22.
191. da Silva-Diz, V., et al., *Progeny of Lgr5-expressing hair follicle stem cell contributes to papillomavirus-induced tumor development in epidermis.* Oncogene, 2013. **32**(32): p. 3732-43.
192. Mehanna, H., et al., *De-Escalation After DE-ESCALATE and RTOG 1016: A Head and Neck Cancer InterGroup Framework for Future De-Escalation Studies.* J Clin Oncol, 2020. **38**(22): p. 2552-2557.
193. Chung, C.H., et al., *A 3'-UTR KRAS-variant is associated with cisplatin resistance in patients with recurrent and/or metastatic head and neck squamous cell carcinoma.* Ann Oncol, 2014. **25**(11): p. 2230-2236.
194. Liu, K., et al., *Upregulation of secreted phosphoprotein 1 affects malignant progression, prognosis, and resistance to cetuximab via the KRAS/MEK pathway in head and neck cancer.* Mol Carcinog, 2020. **59**(10): p. 1147-1158.
195. Kopp, J.L., et al., *Identification of Sox9-dependent acinar-to-ductal reprogramming as the principal mechanism for initiation of pancreatic ductal adenocarcinoma.* Cancer Cell, 2012. **22**(6): p. 737-50.

196. Zhou, H., et al., *SOX9 activity is induced by oncogenic Kras to affect MDC1 and MCMs expression in pancreatic cancer.* Oncogene, 2018. **37**(7): p. 912-923.
197. Chen, N.M., et al., *NFATc1 Links EGFR Signaling to Induction of Sox9 Transcription and Acinar-Ductal Transdifferentiation in the Pancreas.* Gastroenterology, 2015. **148**(5): p. 1024-1034 e9.
198. Capaccione, K.M., et al., *Sox9 mediates Notch1-induced mesenchymal features in lung adenocarcinoma.* Oncotarget, 2014. **5**(11): p. 3636-50.
199. Xu, X., et al., *The cell of origin and subtype of K-Ras-induced lung tumors are modified by Notch and Sox2.* Genes Dev, 2014. **28**(17): p. 1929-39.
200. Sutherland, K.D., et al., *Multiple cells-of-origin of mutant K-Ras-induced mouse lung adenocarcinoma.* Proc Natl Acad Sci U S A, 2014. **111**(13): p. 4952-7.
201. Gil, Z., et al., *Nerve-sparing therapy with oncolytic herpes virus for cancers with neural invasion.* Clin Cancer Res, 2007. **13**(21): p. 6479-85.
202. Ceyhan, G.O., et al., *Pancreatic neuropathy and neuropathic pain--a comprehensive pathomorphological study of 546 cases.* Gastroenterology, 2009. **136**(1): p. 177-186 e1.
203. Zhao, C.M., et al., *Denervation suppresses gastric tumorigenesis.* Sci Transl Med, 2014. **6**(250): p. 250ra115.
204. Albo, D., et al., *Neurogenesis in colorectal cancer is a marker of aggressive tumor behavior and poor outcomes.* Cancer, 2011. **117**(21): p. 4834-45.
205. Hanoun, M., et al., *Acute myelogenous leukemia-induced sympathetic neuropathy promotes malignancy in an altered hematopoietic stem cell niche.* Cell Stem Cell, 2014. **15**(3): p. 365-375.
206. Ravi, R., et al., *Regulation of tumor angiogenesis by p53-induced degradation of hypoxia-inducible factor 1alpha.* Genes Dev, 2000. **14**(1): p. 34-44.
207. Schmid, J.O., et al., *Cancer cells cue the p53 response of cancer-associated fibroblasts to cisplatin.* Cancer Res, 2012. **72**(22): p. 5824-32.
208. Misso, G., et al., *Mir-34: a new weapon against cancer?* Mol Ther Nucleic Acids, 2014. **3**(9): p. e194.
209. Jiang, C., et al., *MicroRNA-34a inhibits cell invasion and epithelial-mesenchymal transition via targeting AXL/PI3K/AKT/Snail signaling in nasopharyngeal carcinoma.* Genes Genomics, 2020. **42**(8): p. 971-978.
210. Bray, F., et al., *Global cancer statistics 2018: GLOBOCAN estimates of incidence and mortality worldwide for 36 cancers in 185 countries.* CA Cancer J Clin, 2018. **68**(6): p. 394-424.
211. Wang, P.H., et al., *The relationship between multiple clinicopathological features and nerve invasion in pancreatic cancer.* Hepatobiliary Pancreat Dis Int, 2013. **12**(5): p. 546-51.
212. Kruttgen, A., I. Schneider, and J. Weis, *The dark side of the NGF family: neurotrophins in neoplasias.* Brain Pathol, 2006. **16**(4): p. 304-10.
213. Adriaenssens, E., et al., *Nerve growth factor is a potential therapeutic target in breast cancer.* Cancer Res, 2008. **68**(2): p. 346-51.
214. Wang, W., et al., *Patterns of expression and function of the p75(NGFR) protein in pancreatic cancer cells and tumours.* Eur J Surg Oncol, 2009. **35**(8): p. 826-32.
215. Zhang, L., et al., *The role of the PI3K/Akt/mTOR signalling pathway in human cancers induced by infection with human papillomaviruses.* Mol Cancer, 2015. **14**: p. 87.
216. Gillison, M.L., et al., *Human papillomavirus and the landscape of secondary genetic alterations in oral cancers.* Genome Res, 2019. **29**(1): p. 1-17.
217. Manzo-Merino, J., et al., *The role of signaling pathways in cervical cancer and molecular therapeutic targets.* Arch Med Res, 2014. **45**(7): p. 525-39.
218. Mancusi, R. and M. Monje, *The neuroscience of cancer.* Nature, 2023. **618**(7965): p. 467-479.

219. Bhattacharjee, R., et al., *Mechanistic role of HPV-associated early proteins in cervical cancer: Molecular pathways and targeted therapeutic strategies.* Crit Rev Oncol Hematol, 2022. **174**: p. 103675.
220. Balood, M., et al., *Nociceptor neurons affect cancer immunosurveillance.* Nature, 2022. **611**(7935): p. 405-412.
221. Batlle, E. and J. Massague, *Transforming Growth Factor-beta Signaling in Immunity and Cancer.* Immunity, 2019. **50**(4): p. 924-940.
222. Kehrl, J.H., et al., *Production of transforming growth factor beta by human T lymphocytes and its potential role in the regulation of T cell growth.* J Exp Med, 1986. **163**(5): p. 1037-50.
223. Yang, L., Y. Pang, and H.L. Moses, *TGF-beta and immune cells: an important regulatory axis in the tumor microenvironment and progression.* Trends Immunol, 2010. **31**(6): p. 220-7.
224. Tauriello, D.V.F., E. Sancho, and E. Batlle, *Overcoming TGFbeta-mediated immune evasion in cancer.* Nat Rev Cancer, 2022. **22**(1): p. 25-44.
225. Scholz, J. and C.J. Woolf, *The neuropathic pain triad: neurons, immune cells and glia.* Nat Neurosci, 2007. **10**(11): p. 1361-8.
226. Albertella, M.R., et al., *Hypoxia-selective targeting by the bioreductive prodrug AQ4N in patients with solid tumors: results of a phase I study.* Clin Cancer Res, 2008. **14**(4): p. 1096-104.
227. Aisner, J., et al., *Sequencing topotecan and etoposide plus cisplatin to overcome topoisomerase I and II resistance: a pharmacodynamically based Phase I trial.* Clin Cancer Res, 2003. **9**(7): p. 2504-9.
228. Robert, F., S.J. Soong, and R.H. Wheeler, *A phase II study of topotecan in patients with recurrent head and neck cancer. Identification of an active new agent.* Am J Clin Oncol, 1997. **20**(3): p. 298-302.
229. Han, S., et al., *The Potential of Topoisomerase Inhibitor-Based Antibody-Drug Conjugates.* Pharmaceutics, 2022. **14**(8).
230. Delgado, J.L., et al., *Topoisomerases as anticancer targets.* Biochem J, 2018. **475**(2): p. 373-398.
231. Thomas, A. and Y. Pommier, *Targeting Topoisomerase I in the Era of Precision Medicine.* Clin Cancer Res, 2019. **25**(22): p. 6581-6589.
232. Liu, Y., et al., *Phase I study of liposomal irinotecan (LY01610) in patients with advanced esophageal squamous cell carcinoma.* Cancer Chemother Pharmacol, 2021. **88**(3): p. 403-414.
233. Huang, J., et al., *Irinotecan plus S-1 versus S-1 in patients with previously treated recurrent or metastatic esophageal cancer (ESWN 01): a prospective randomized, multicenter, open-labeled phase 3 trial.* Cancer Commun (Lond), 2019. **39**(1): p. 16.
234. Chen, S.C., P.M. Chang, and M.H. Yang, *Cisplatin/Tegafur/Uracil/Irinotecan Triple Combination Therapy for Recurrent/Metastatic Head and Neck Squamous Cell Carcinoma: A Phase I/II Clinical Study.* Oncologist, 2016. **21**(5): p. 537-8.
235. Bedi, D., et al., *Camptothecin Induces PD-L1 and Immunomodulatory Cytokines in Colon Cancer Cells.* Medicines (Basel), 2019. **6**(2).
236. Horn, D., et al., *Targeting EGFR-PI3K-AKT-mTOR signaling enhances radiosensitivity in head and neck squamous cell carcinoma.* Expert Opin Ther Targets, 2015. **19**(6): p. 795-805.
237. Jung, K., H. Kang, and R. Mehra, *Targeting phosphoinositide 3-kinase (PI3K) in head and neck squamous cell carcinoma (HNSCC).* Cancers Head Neck, 2018. **3**: p. 3.
238. Vander Broek, R., et al., *The PI3K/Akt/mTOR axis in head and neck cancer: functions, aberrations, cross-talk, and therapies.* Oral Dis, 2015. **21**(7): p. 815-25.
239. Maira, S.M., et al., *Identification and characterization of NVP-BKM120, an orally available pan-class I PI3-kinase inhibitor.* Mol Cancer Ther, 2012. **11**(2): p. 317-28.

240. Fritsch, C., et al., *Characterization of the novel and specific PI3Kalpha inhibitor NVP-BYL719 and development of the patient stratification strategy for clinical trials.* Mol Cancer Ther, 2014. **13**(5): p. 1117-29.
241. Garlich, J.R., et al., *A vascular targeted pan phosphoinositide 3-kinase inhibitor prodrug, SF1126, with antitumor and antiangiogenic activity.* Cancer Res, 2008. **68**(1): p. 206-15.
242. Wirtz, E.D., et al., *Response of head and neck squamous cell carcinoma cells carrying PIK3CA mutations to selected targeted therapies.* JAMA Otolaryngol Head Neck Surg, 2015. **141**(6): p. 543-9.
243. Mazumdar, T., et al., *A comprehensive evaluation of biomarkers predictive of response to PI3K inhibitors and of resistance mechanisms in head and neck squamous cell carcinoma.* Mol Cancer Ther, 2014. **13**(11): p. 2738-50.
244. Sheng, Q., et al., *Abstract 4261: Targeting HER3 and PI3K in head and neck squamous cancer cells.* Cancer Research, 2013. **73**(8_Supplement): p. 4261-4261.
245. Matias-Barrios, V.M. and X. Dong, *The Implication of Topoisomerase II Inhibitors in Synthetic Lethality for Cancer Therapy.* Pharmaceuticals (Basel), 2023. **16**(1).
246. Bayliss, R., et al., *A moving target: structure and disorder in pursuit of Myc inhibitors.* Biochem Soc Trans, 2017. **45**(3): p. 709-717.
247. Carabet, L.A., et al., *Computer-aided drug discovery of Myc-Max inhibitors as potential therapeutics for prostate cancer.* Eur J Med Chem, 2018. **160**: p. 108-119.
248. Dang, C.V., *MYC on the path to cancer.* Cell, 2012. **149**(1): p. 22-35.
249. Arthur-Farraj, P.J., et al., *Changes in the Coding and Non-coding Transcriptome and DNA Methylome that Define the Schwann Cell Repair Phenotype after Nerve Injury.* Cell Rep, 2017. **20**(11): p. 2719-2734.
250. Parkinson, D.B., et al., *c-Jun is a negative regulator of myelination.* J Cell Biol, 2008. **181**(4): p. 625-37.
251. Jessen, K.R. and R. Mirsky, *Negative regulation of myelination: relevance for development, injury, and demyelinating disease.* Glia, 2008. **56**(14): p. 1552-1565.
252. Goslin, K., et al., *Development of neuronal polarity: GAP-43 distinguishes axonal from dendritic growth cones.* Nature, 1988. **336**(6200): p. 672-4.
253. Skene, J.H., et al., *A protein induced during nerve growth (GAP-43) is a major component of growth-cone membranes.* Science, 1986. **233**(4765): p. 783-6.
254. Aigner, L., et al., *Overexpression of the neural growth-associated protein GAP-43 induces nerve sprouting in the adult nervous system of transgenic mice.* Cell, 1995. **83**(2): p. 269-78.
255. Jung, E., et al., *Emerging intersections between neuroscience and glioma biology.* Nat Neurosci, 2019. **22**(12): p. 1951-1960.

7. Publications

I. **Khorani K,** Schwaerzler J, Burkart S, Kurth I, Holzinger D, Flechtenmacher C, Plinkert PK, Zaoui K, Hess J. Establishment of a Plasticity-Associated Risk Model Based on a SOX2- and SOX9-Related Gene Set in Head and Neck Squamous Cell Carcinoma. The manuscript was published Online First in Mol Cancer Res. 2021 Oct;19(10):1676-1687. doi: 10.1158/1541-7786.MCR-21-0066. Epub 2021 Jul 20. PMID: 34285085. Main parts of this publication are based on the results presented in chapter 3.1-3.14 of this dissertation.

II. Burkart S, Weusthof C, **Khorani K**, Steen S, Stögbauer F, Unger K, Hess J, Zitzelsberger H, Belka C, Kurth I, Hess J. A Novel Subgroup of UCHL1-Related Cancers Is Associated with Genomic Instability and Sensitivity to DNA-Damaging Treatment. Cancers (Basel). 2023 Mar 8;15(6):1655. doi: 10.3390/cancers15061655. PMID: 36980544; PMCID: PMC10099714.

III. Weusthof C, Burkart S, Semmelmayer K, Stögbauer F, Feng B, **Khorani K**, Bode S, Plinkert P, Plath K, Hess J. Establishment of a Machine Learning Model for the Risk Assessment of Perineural Invasion in Head and Neck Squamous Cell Carcinoma. Int J Mol Sci. 2023 May 18;24(10):8938. doi: 10.3390/ijms24108938. PMID: 37240283; PMCID: PMC10218829.

8. Supplements

Due to limitations of space, only a part of the information is displayed in Table S8. More

details, please check the supplemental tables of the online manuscript (DOI: 10.1158/1541-7786.MCR-21-0066).

Table S1: Crosstab analysis for subgroups based on SOX9 protein expression and clinical as well as histopathological features of the OPSCC cohort.

		$SOX9^{low}$		$SOX9^{high}$		
Category	**Feature**	**n**	**%**	**n**	**%**	**p value[a]**
Tobacco	current	61	74.4%	48	85.7%	1.15E-01
	former	8	9.8%	5	8.9%	
	never	13	15.9%	3	5.4%	
Alcohol	current	63	76.8%	47	83.9%	3.70E-01
	former	11	13.4%	7	12.5%	
	never	8	9.8%	2	3.6%	
HPV16	yes	27	34.2%	4	7.1%	***2.34E-04***
	no	52	65.8%	52	92.9%	
Age [years]	<57.4	43	51.8%	25	44.6%	4.07E-01
	>57.4	40	48.2%	31	55.4%	
Gender	female	21	25.3%	17	30.4%	5.12E-01
	male	62	74.7%	39	69.6%	
Tumor size	T1-2	43	51.8%	17	30.4%	***1.20E-02***
	T3-4	40	48.2%	39	69.6%	
Lymph nodes	N0	15	18.1%	14	25.0%	3.24E-01
	N1-3	68	81.9%	42	75.0%	
Pathological grading	G1-2	43	56.6%	24	55.8%	9.36E-01
	G3	33	43.4%	19	44.2%	

[a] *significant p values (<0.05) are indicated in italic and bold*

Table S2: Crosstab analysis for subgroups based on SOX2 and SOX9 protein expression and clinical as well as histopathological features of the OPSCC cohort.

		$SOX2^{low}SOX9^{low}$		$SOX2^{high}SOX9^{low}$		$SOX2^{low}SOX9^{high}$		$SOX2^{high}SOX9^{high}$		
Category	**Feature**	**n**	**%**	**n**	**%**	**n**	**%**	**n**	**%**	**p value[a]**
Tobacco	current	24	80.0%	34	70.8%	26	89.7%	21	84.0%	4.93E-01
	former	3	10.0%	5	10.4%	2	6.9%	2	8.0%	
	never	3	10.0%	9	18.8%	1	3.4%	2	8.0%	
Alcohol	current	25	83.3%	36	75.0%	25	86.2%	21	84.0%	6.69E-01
	former	4	13.3%	6	12.5%	3	10.3%	3	12.0%	
	never	1	3.3%	6	12.5%	1	3.4%	1	4.0%	
HPV16	yes	21	75.0%	20	42.6%	1	3.4%	3	12.0%	***1.00E-03***
	no	7	25.0%	27	57.4%	28	96.6%	22	88.0%	
Age [years]	<57.4	17	56.7%	22	44.9%	16	55.2%	7	28.0%	1.32E-01
	>57.4	13	43.3%	27	55.1%	13	44.8%	18	72.0%	
Gender	female	5	16.7%	15	30.6%	11	37.9%	6	24.0%	2.95E-01
	male	25	83.3%	34	69.4%	18	62.1%	19	76.0%	
Tumor size	T1-2	16	53.3%	26	53.1%	10	34.5%	6	24.0%	***5.00E-02***
	T3-4	14	46.7%	23	46.9%	19	65.5%	19	76.0%	
Lymph nodes	N0	6	20.0%	8	16.3%	9	31.0%	5	20.0%	4.87E-01
	N1-3	24	80.0%	41	83.7%	20	69.0%	20	80.0%	
Pathological grading	G1-2	14	51.9%	27	58.7%	13	54.2%	11	57.9%	9.43E-01
	G3	13	48.1%	19	41.3%	11	45.8%	8	42.1%	

[a] *significant p values (<0.05) are indicated in italic and bold*

Table S3: Crosstab analysis for subgroups based on SOX2 and SOX9 transcript levels and clinical as well as histopathological features of the TCGA-HNSC cohort.

		$SOX2^{low}SOX9^{low}$		$SOX2^{high}SOX9^{low}$		$SOX2^{low}SOX9^{high}$		$SOX2^{high}SOX9^{high}$		
Category	**Feature[a]**	**n**	**%**	**n**	**%**	**n**	**%**	**n**	**%**	**p value[b]**
Tobacco	no	29	22.7%	24	20.5%	34	28.8%	24	18.9%	0.274
	yes	99	77.3%	93	79.5%	84	71.2%	103	81.1%	
Alcohol	no	44	34.6%	37	31.4%	34	28.6%	42	33.6%	0.749
	yes	83	65.4%	81	68.6%	85	71.4%	83	66.4%	
HPV16	no	124	96.9%	85	73.3%	111	99.1%	104	86.0%	***8.84E-11***
	yes	4	3.1%	34	29.3%	1	0.9%	17	14.0%	
Age [years]	<61	55	42.6%	68	56.7%	61	50.8%	60	46.2%	0.139
	>=61	74	57.4%	52	43.3%	59	49.2%	70	53.8%	
Gender	female	38	29.2%	24	20.0%	41	34.2%	30	23.1%	0.058
	male	92	70.8%	96	80.0%	79	65.8%	100	76.9%	
Subsite	hypopharynx	4	3.1%	1	0.8%	2	1.7%	3	2.3%	***2.12E-17***
	larynx	12	9.2%	31	25.8%	17	14.2%	51	39.2%	
	oral cavity	106	81.5%	54	45.0%	97	80.8%	51	39.2%	
	oropharynx	8	6.2%	34	28.3%	4	3.3%	25	19.2%	
Tumor size	cT1-2	40	32.0%	47	40.2%	48	42.1%	41	31.8%	0.207
	cT3-4	85	68.0%	70	59.8%	66	57.9%	88	68.2%	
	pT1-2	45	38.5%	47	45.6%	49	45.0%	37	31.9%	0.124
	pT3-4	72	61.5%	56	54.4%	60	55.0%	79	68.1%	
Lymph nodes	cN0	65	52.4%	56	49.6%	56	50.0%	62	48.1%	0.92
	cN1-3	59	47.6%	57	50.4%	56	50.0%	67	51.9%	
	pN0	50	46.3%	37	40.2%	39	39.0%	45	42.1%	0.727
	pN1-3	58	53.7%	55	59.8%	61	61.0%	62	57.9%	
Pathological grading	G1-2	99	78.0%	83	74.1%	93	78.8%	85	68.5%	0.233
	G3-4	28	22.0%	29	25.9%	25	21.2%	39	31.5%	

[a] *c=clinical, p=pathological*

[b] *significant p values (<0.05) are indicated in italic and bold*

Table S4: DEGs related to SOX2 and SOX9 expression in the TCGA-HNSC cohort.

		SOX2 edgeR		SOX9 edgeR		SOX2 limma		SOX9 limma	
Gene Symbol	**Gene ID**	**log2FC**	**FDR**	**log2FC**	**FDR**	**log2FC**	**adj.P.Val**	**log2FC**	**adj.P.Val**
ADAMTS6	11174	-1.73	2.63E-04	1.36	1.58E-03	-1.19	1.78E-02	1.24	2.46E-02
ADTRP	84830	-3.43	1.79E-18	2.05	4.59E-06	-3.43	3.10E-10	2.14	8.29E-03
ALDH3A1	218	5.26	4.67E-22	-2.38	3.40E-03	5.81	6.48E-11	-2.79	4.36E-02
APCDD1L	164284	-2.90	1.34E-06	2.50	2.54E-05	-2.74	7.56E-04	2.09	3.85E-02
ARHGAP29	9411	-1.70	1.10E-06	1.28	1.12E-03	-1.42	1.08E-03	1.13	3.81E-02
ART3	419	-2.49	3.29E-04	2.89	1.03E-04	-2.95	6.06E-05	2.33	3.72E-02
C12orf56	115749	1.49	4.26E-04	-1.01	1.93E-02	1.88	1.27E-03	-1.12	3.68E-02
CACNA2D3	55799	2.46	5.59E-11	-1.21	2.24E-02	2.43	1.01E-07	-1.47	2.65E-02
CAMK2N1	55450	-2.18	4.76E-09	2.08	9.20E-08	-1.93	7.76E-05	1.74	8.16E-03
CCDC9B	388115	-1.21	2.39E-03	1.16	6.51E-03	-1.80	1.90E-04	1.39	2.54E-02
CEBPB	1051	-1.67	5.92E-11	1.01	2.25E-04	-1.44	7.36E-07	1.22	2.30E-04
CGB8	94115	-4.79	3.17E-08	3.41	7.77E-05	-2.96	1.66E-04	2.54	8.97E-03
COL27A1	85301	-1.19	5.79E-05	1.14	2.36E-03	-1.07	1.76E-03	1.24	1.76E-02
DCBLD1	285761	-1.65	1.35E-09	1.61	1.57E-06	-1.58	3.39E-06	1.42	6.74E-03
DUSP6	1848	-1.50	2.89E-06	1.53	1.52E-04	-1.22	5.55E-04	1.53	8.29E-03
EGR2	1959	1.33	1.02E-03	1.59	2.44E-03	1.53	1.41E-03	1.67	4.00E-02
EPHB2	2048	-2.09	4.39E-10	1.35	1.05E-03	-2.28	1.48E-06	1.69	2.71E-03
EVPLL	645027	3.12	5.23E-08	-3.21	7.09E-06	2.86	4.43E-04	-3.61	1.63E-04
EXPH5	23086	1.23	3.00E-05	-1.68	6.92E-07	1.48	2.63E-05	-1.59	4.10E-04
FGF1	2246	-1.08	1.17E-02	1.85	1.11E-05	-1.15	1.33E-02	1.69	1.20E-03
FHOD3	80206	-2.27	7.46E-07	1.54	8.45E-04	-1.90	2.55E-03	2.12	7.05E-04
FOXC2	2303	-2.61	2.51E-07	3.55	3.48E-13	-2.73	5.25E-05	3.15	4.10E-04
FOXL1	2300	-1.77	2.05E-04	2.70	3.04E-12	-2.17	1.93E-04	2.26	3.53E-04
FOXP2	93986	2.30	6.46E-06	-1.29	4.10E-02	2.90	1.22E-05	-1.86	5.00E-02
FZD7	8324	2.85	2.10E-15	1.41	6.89E-03	2.89	7.43E-08	1.70	2.54E-02
GFPT2	9945	-1.62	2.90E-05	1.19	2.83E-03	-1.34	3.52E-03	1.29	1.26E-02
HDAC9	9734	-1.16	1.52E-03	1.80	2.05E-05	-1.28	1.59E-03	1.33	4.92E-02
ICAM1	3383	-1.66	8.87E-08	1.56	7.90E-05	-1.45	1.04E-04	1.61	6.01E-03
ITGB6	3694	-2.37	4.90E-07	1.29	8.50E-03	-2.18	3.57E-03	1.88	2.13E-02
KCNJ11	3767	1.66	6.77E-04	-1.59	1.27E-02	2.00	4.27E-04	-2.09	8.67E-03
KIF12	113220	-3.23	1.21E-08	2.82	1.24E-05	-3.14	3.15E-05	2.42	1.62E-02
LGALS1	3956	-2.56	5.46E-14	1.10	2.94E-03	-2.11	1.38E-07	1.25	1.14E-02
MYCL	4610	1.86	2.95E-06	-1.46	2.58E-04	1.76	1.56E-03	-1.43	1.74E-02
NOX5	79400	-2.35	1.01E-08	2.31	4.64E-04	-2.86	3.24E-08	2.29	4.33E-02
PDZD2	23037	-1.55	3.89E-04	1.08	2.58E-02	-1.59	2.26E-03	1.39	3.70E-02
PHACTR3	116154	3.01	1.04E-05	-3.53	2.14E-06	2.35	2.32E-03	-1.93	4.38E-02
PLAU	5328	-1.33	6.60E-05	1.29	4.66E-03	-1.15	4.67E-03	1.36	4.85E-02
PLAUR	5329	-1.77	1.61E-09	1.61	2.19E-05	-1.48	6.56E-06	1.19	2.49E-02
PMEPA1	56937	-1.98	1.74E-07	1.76	2.14E-06	-1.80	3.90E-04	2.01	4.66E-04
PRDM8	56978	-1.03	3.21E-03	1.40	6.29E-04	-1.35	2.07E-04	1.08	1.96E-02
PTPRR	5801	-1.12	3.23E-02	1.61	3.71E-03	-1.66	2.93E-03	1.46	2.82E-02
RASD2	23551	-1.71	4.25E-05	2.20	5.53E-04	-1.20	1.50E-02	2.46	8.29E-03
RASL11A	387496	3.48	1.01E-19	-1.91	6.01E-05	2.89	1.46E-06	-1.22	4.47E-02
ROR1	4919	-1.31	2.39E-03	1.68	1.21E-03	-1.28	4.30E-03	1.70	2.14E-02
SEC14L2	23541	-2.43	1.22E-16	2.02	3.78E-07	-2.32	1.51E-08	1.97	1.28E-03
SERPINA11	256394	1.74	3.46E-02	3.86	1.37E-07	1.73	3.12E-02	3.96	1.47E-06
SERPINA3	12	-1.83	3.58E-03	2.97	8.00E-04	-2.19	9.93E-04	3.19	5.88E-03
SERPINE1	5054	-2.52	3.11E-09	1.33	6.88E-03	-2.01	2.81E-04	1.57	3.81E-02
SH3TC2	79628	-1.66	1.33E-03	1.49	7.73E-03	-2.27	4.38E-04	1.85	2.70E-02
SLC47A1	55244	2.84	3.99E-10	-1.86	1.07E-03	2.26	1.84E-04	-1.56	5.00E-02
SVOPL	136306	1.70	2.74E-03	1.50	2.91E-02	2.29	6.53E-04	1.84	3.51E-02
TGM6	343641	3.39	2.44E-05	-4.19	6.94E-05	2.17	7.47E-03	-2.52	4.35E-02
TINAGL1	64129	-2.09	7.39E-07	2.26	2.10E-09	-1.90	6.10E-04	2.67	1.22E-06
TNFRSF12A	51330	-2.11	1.47E-12	1.19	2.16E-03	-2.15	7.57E-08	1.43	1.39E-02
TPRG1	285386	1.91	1.91E-06	-1.96	1.22E-06	1.78	1.31E-03	-1.49	4.26E-02
TREX2	11219	-1.08	8.19E-03	-2.81	8.53E-07	-1.01	2.47E-02	-1.83	3.20E-02
UGT1A7	54577	8.19	2.01E-18	-4.95	3.03E-06	8.94	3.10E-10	-4.92	7.96E-04

Table S5: Crosstab analysis for clusters based on gene set (n=57) and clinical as well as histopathological features of the TCGA-HNSC cohort.

		Cluster A1		Cluster A2		Cluster B1		Cluster B2		
Category	**Feature[a]**	**n**	**%**	**n**	**%**	**n**	**%**	**n**	**%**	**p value[b]**
Age [years]	≤61	26	52.0%	78	48.8%	43	55.1%	97	46.0%	5.46E-01
	>61	24	48.0%	82	51.3%	35	44.9%	114	54.0%	
Gender	female	8	16.0%	38	23.8%	26	33.3%	61	28.9%	1.15E-01
	male	42	84.0%	122	76.3%	52	66.7%	150	71.1%	
Tobacco	no	14	28.6%	29	18.5%	20	26.0%	48	23.1%	3.80E-01
	yes	35	71.4%	128	81.5%	57	74.0%	158	76.0%	
Alcohol	no	12	24.0%	54	34.8%	27	35.1%	64	31.1%	4.85E-01
	yes	38	76.0%	101	65.2%	50	64.9%	142	68.9%	
HPV16	no	33	67.3%	124	81.0%	73	97.3%	193	97.0%	***4.70E-11***
	yes	16	32.7%	29	19.0%	2	2.7%	6	3.0%	
Subsite	Hypopharynx	0	0.0%	3	1.9%	0	0.0%	7	3.3%	***2.57E-14***
	Larynx	10	20.0%	59	36.9%	12	15.4%	30	14.2%	
	Oral cavity	20	40.0%	69	43.1%	62	79.5%	156	73.9%	
	Oropharynx	20	40.0%	29	18.1%	4	5.1%	18	8.5%	
Tumor size	cT1-2	26	52.0%	58	37.9%	25	32.1%	66	32.5%	6.10E-02
	cT3-4	24	48.0%	95	62.1%	53	67.9%	137	67.5%	
	pT1-2	18	48.6%	58	41.1%	24	33.8%	76	39.2%	4.91E-01
	pT3-4	19	51.4%	83	58.9%	47	66.2%	118	60.8%	
Lymph nodes	cN0	15	30.0%	88	58.3%	35	47.3%	100	49.5%	***6.21E-03***
	cN1-3	35	70.0%	63	41.7%	39	52.7%	102	50.5%	
	pN0	10	30.3%	57	44.5%	26	38.8%	77	43.3%	4.60E-01
	pN1-3	23	69.7%	71	55.5%	41	61.2%	101	56.7%	
Pathological grading	G1-2	19	40.4%	120	79.5%	68	89.5%	152	73.8%	***1.07E-08***
	G3-4	28	59.6%	31	20.5%	8	10.5%	54	26.2%	
Pathological margin	R0	36	90.0%	117	84.8%	65	89.0%	172	87.8%	7.33E-01
	R1	4	10.0%	21	15.2%	8	11.0%	24	12.2%	
Angiolymphatic invasion	no	17	60.7%	62	60.2%	41	67.2%	98	67.1%	6.49E-01
	yes	11	39.3%	41	39.8%	20	32.8%	48	32.9%	
Perineural invasion	no	20	71.4%	72	69.2%	27	43.5%	66	42.3%	***2.30E-05***
	yes	8	28.6%	32	30.8%	35	56.5%	90	57.7%	

[a] *c=clinical, p=pathological*

[b] *significant p values (<0.05) are indicated in italic and bold*

Table S6: Crosstab analysis for risk model groups and clinical as well as histopathological features of the TCGA-HNSC cohort

		High risk		Low risk		
Category	**Feature[a]**	**n**	**%**	**n**	**%**	**p value[b]**
Age [years]	≤61	142	52.4%	112	49.1%	0.47
	>61	129	47.6%	116	50.9%	
Gender	female	80	29.5%	53	23.2%	0.11
	male	191	70.5%	175	76.8%	
Tobacco	yes	206	78.3%	172	76.1%	0.56
	no	57	21.7%	54	23.9%	
Alcohol	yes	184	68.7%	147	66.8%	0.67
	no	84	31.3%	73	33.2%	
HPV16	yes	7	2.7%	46	21.1%	***2.10E-10***
	no	251	97.3%	172	78.9%	
Subsite	Hypopharynx	7	2.6%	3	1.3%	***5.00E-06***
	Larynx	53	19.6%	58	25.4%	
	Oral Cavity	190	70.1%	117	51.3%	
	Oropharynx	21	7.7%	50	21.9%	
Tumor size	cT1-2	95	36.1%	80	36.2%	0.99
	cT3-4	168	63.9%	141	63.8%	
	pT1-2	93	38.0%	84	42.4%	0.36
	pT3-4	152	62.0%	115	58.1%	
Lymph nodes	cN0	120	46.5%	118	53.9%	0.11
	cN1-3	138	53.5%	101	46.1%	
	pN0	77	34.8%	93	50.3%	***1.70E-03***
	pN1-3	144	65.2%	92	49.7%	
Pathological grading	G1-2	202	76.5%	157	72.7%	0.19
	G3-4	62	23.5%	59	27.3%	
Pathological margin	R0	218	85.5%	172	89.6%	0.20
	R1	37	14.5%	20	10.4%	
Angiolymphatic invasion	yes	79	40.7%	41	28.5%	***0.02***
	no	115	59.3%	103	71.5%	
Perineural invasion	yes	111	55.2%	54	37.2%	***4.35E-04***
	no	90	44.8%	95	65.5%	
Radiation	yes	145	63.9%	134	65.0%	0.80
	no	82	36.1%	72	35.0%	

[a] *c=clinical, p=pathological*

[b] *significant p values (<0.05) are indicated in italic and bold*

Table S7: (A) Univariate and multivariate Cox regression analysis for overall survival of the TCGA-HNSC cohort.

		Univariate	95% CI			Multivariate	95% CI		
Category	**Feature**[c]	**HR**	**lower**	**upper**	**p value**[b]	**HR**	**lower**	**upper**	**p value**[b]
Gender	Male[a]	1.396	1.021	1.910	***0.04***	1.198	0.748	1.919	0.45
	Female								
Age (years)	<61[a]	1.229	0.916	1.648	0.17				
	>61								
Tobacco	no[a]	1.029	0.723	1.465	0.87				
	yes								
Alcohol	no[a]	0.934	0.685	1.275	0.67				
	yes								
HPV16	no[a]	0.333	0.164	0.677	***2.0E-03***	0.781	0.240	2.543	0.68
	yes								
Tumor size	cT1-2[a]	1.204	0.878	1.650	0.25				
	cT3-4								
	pT1-2[a]	1.811	1.290	2.550	***6.2E-04***	2.482	1.403	4.391	***1.8E-03***
	pT3-4								
Lymph node metastasis	cN0[a]	1.254	0.936	1.681	0.13				
	cN+								
	pN0[a]	2.082	1.453	2.984	***6.5E-05***	1.331	0.805	2.200	0.27
	pN+								
Pathological grading	G1-2[a]	0.984	0.705	1.374	0.92				
	G3-4								
Resection margin	R0[a]	1.768	1.208	2.586	***3.4E-03***	2.387	1.417	4.023	***1.1E-03***
	R1								
Angiolymphatic invasion	no[a]	1.724	1.200	2.476	***3.2E-03***	0.904	0.562	1.417	0.68
	yes								
Perineural invasion	no[a]	2.161	1.502	3.110	***3.3E-05***	1.669	1.047	2.661	***3.1E-02***
	yes								
Risk model	low[a]	2.730	1.971	3.781	***1.5E-09***	2.344	1.409	3.898	***1.0E-03***
	high								

[a] *reference*

[b] *significant p values (<0.05) are indicated in italic and bold*

[a] *c=clinical, p=pathological*

Table 7:(B) Univariate and multivariate Cox regression analysis for disease-specific survival of the TCGA-HNSC cohort.

		Univariate	95% CI			Multivariate	95% CI		
Category	**Feature[c]**	**HR**	**lower**	**upper**	**p value[b]**	**HR**	**lower**	**upper**	**p value[b]**
Gender	Male[a]	1.03	0.67	1.59	0.89				
	Female								
Age (years)	<61[a]	1.02	0.70	1.48	0.93				
	>61								
Tobacco	no[a]	1.05	0.67	1.65	0.84				
	yes								
Alcohol	no[a]	1.30	0.85	2.01	0.23				
	yes								
HPV16	no[a]	0.33	0.14	0.82	***1.7E-02***	0.781	0.185	3.302	0.74
	yes								
Tumor size	cT1-2[a]	1.46	0.95	2.23	0.08				
	cT3-4								
	pT1-2[a]	2.42	1.50	3.89	***2.8E-04***	4.535	1.922	10.698	***5.6E-04***
	pT3-4								
Lymph node metastasis	cN0[a]	1.28	0.88	1.87	0.20				
	cN+								
	pN0[a]	2.38	1.46	3.87	***5.1E-04***	1.165	0.658	2.065	0.60
	pN+								
Pathological grading	G1-2[a]	0.99	0.65	1.52	0.96				
	G3-4								
Resection margin	R0[a]	2.45	1.55	3.85	***1.1E-04***	2.571	1.453	4.552	***1.2E-03***
	R1								
Angiolymphatic invasion	no[a]	1.57	0.99	2.50	0.06				
	yes								
Perineural invasion	no[a]	2.26	1.43	3.57	***5.0E-04***	1.405	0.812	2.429	0.22
	yes								
Risk model	low[a]	2.95	1.93	4.51	***6.1E-07***	2.590	1.399	4.796	***2.5E-03***
	high								

[a] *reference*

[b] *significant p values (<0.05) are indicated in italic and bold*

[a] *c=clinical, p=pathological*

Table S8: GSVA for low versus high risk groups for TCGA-HNSC based on MSigDB (h - hallmarks and c6 - oncogenic signature).

Gene set(Top 20 based on the lowest adj.p-value)	p value	adj. p value	mean high	mean low
KRAS.DF.V1_UP	1.18E-21	2.77E-19	0.05	-0.17
MEL18_DN.V1_UP	3.07E-21	3.61E-19	0.09	-0.19
BCAT.100_UP.V1_UP	1.27E-20	9.96E-19	0.08	-0.14
BCAT_GDS748_UP	9.70E-20	5.70E-18	0.08	-0.14
BMI1_DN_MEL18_DN.V1_UP	1.53E-19	7.20E-18	0.08	-0.17
HALLMARK_EPITHELIAL_MESENCHYMAL_TRANSITION	1.07E-17	4.18E-16	0.09	-0.21
KRAS.300_UP.V1_UP	2.44E-17	8.18E-16	0.06	-0.14
KRAS.600_UP.V1_UP	4.21E-17	1.24E-15	0.05	-0.12
HALLMARK_HYPOXIA	4.00E-16	1.04E-14	0.03	-0.15
BMI1_DN.V1_UP	2.31E-15	5.42E-14	0.06	-0.16
ESC_V6.5_UP_LATE.V1_DN	1.29E-14	2.76E-13	0.01	-0.11
HALLMARK_COAGULATION	3.04E-14	5.96E-13	0.04	-0.14
LEF1_UP.V1_UP	4.70E-14	8.50E-13	0.04	-0.12
HALLMARK_KRAS_SIGNALING_UP	6.84E-14	1.15E-12	0.05	-0.14
PDGF_UP.V1_UP	8.49E-13	1.33E-11	0.02	-0.12
KRAS.LUNG.BREAST_UP.V1_UP	1.57E-12	2.31E-11	0.02	-0.13
HALLMARK_GLYCOLYSIS	3.59E-12	4.96E-11	0.03	-0.11
CYCLIN_D1_KE_.V1_UP	7.80E-12	1.02E-10	0.02	-0.10
HALLMARK_TNFA_SIGNALING_VIA_NFKB	1.08E-11	1.34E-10	0.05	-0.16
PKCA_DN.V1_DN	2.66E-11	3.13E-10	0.04	-0.08

Table S9: Univariate and multivariate Cox regression analysis for overall survival of the combined HNSCC validation cohort (GSE117973, GSE39368, GSE65858).

		Univariate	95% CI			Multivariate	95% CI		
Category	**Feature[c]**	**HR**	**lower**	**upper**	**p value**	**HR**	**lower**	**upper**	**p value**
Gender	Male[a]	1.142	0.759	1.712	5.00E-01				
	Female								
Age (years)	<61[a]	1.166	0.842	1.615	4.00E-01				
	>61								
Tobacco	no[a]	1.684	1.047	2.710	***3.00E-02***	1.95	1.1691	3.253	8.1E-02
	yes								
Alcohol	no[a]	1.248	0.882	1.765	2.00E-01				
	yes								
HPV16	no[a]	0.896	0.565	1.421	6.00E-01	0.8405	0.5193	1.3494	6.00E-01
	yes								
Tumor size	pT1-2[a]	2.81	1.899	4.157	***7.00E-08***	2.567	1.6975	3.881	***1.20E-05***
	pT3-4								
Lymph node metastasis	pN0[a]	1.727	1.172	2.546	***5.00E-03***	1.561	1.0322	2.359	***1.91E-02***
	pN+								
Risk model	low[a]	2.582	1.82	3.651	***3.00E-08***	3.091	2.1165	4.515	***2.0E-08***
	high								

[a] *reference, significant p values (<0.05) are indicated in italic and bold*

[b] *GSE41613 was excluded due to lack of HPV16-positive HNSCC*

[c] *p=pathological*

Table S10: (A) Univariate and multivariate Cox regression analysis for overall survival of the TCGA-PAAD cohort.

		Univariate	95% CI			Multivariate	95% CI		
Category	**Feature[c]**	**HR**	**lower**	**upper**	**p value[b]**	**HR**	**lower**	**upper**	**p value[b]**
Gender	Male[a] Female	0.797	0.497	1.279	3.00E-01				
Age (years)	<61[a] >61	1.482	0.837	2.623	2.00E-01				
Tobacco	no[a] yes	1.092	0.681	1.700	7.00E-01				
Alcohol	no[a] yes	1.110	0.654	1.884	7.00E-01				
Tumor size	pT1-2[a] pT3-4	2.075	1.069	4.029	***3.00E-02***	1.689	0.810	3.522	***1.63E-01***
Lymph node metastasis	pN0[a] pN+	2.140	1.259	3.654	***4.00E-03***	1.888	1.055	3.379	***3.23E-02***
Pathological grading	G1-2[a] G3-4	1.618	1.040	2.510	***3.00E-02***	1.299	0.814	2.073	2.72E-01
Resection margin	R0[a] R1	1.717	1.096	2.689	***2.00E-02***	1.586	0.999	2.518	***5.03E-02***
Risk model	low[a] high	2.046	1.286	3.257	***2.00E-03***	2.139	1.305	3.507	***2.00E-03***

[1] *reference*

[2] *significant p values (<0.05) are indicated in italic and bold*

[c] *p=pathological*

Table S10: (B) Univariate and multivariate Cox regression analysis for overall survival of the TCGA-LUAD cohort.

		Univariate	95% CI			Multivariate	95% CI		
Category	**Feature[c]**	**HR**	**lower**	**upper**	**p value[b]**	**HR**	**lower**	**upper**	**p value[b]**
Gender	Male[a] Female	1.037	0.766	1.403	0.80				
Age (years)	<61[a] >61	1.209	0.890	1.638	0.20				
Tobacco	no[a] yes	0.874	0.570	1.340	0.50				
Tumor size	pT1-2[a] cT3-4	2.314	1.561	3.431	***2.00E-05***	2.542	1.620	3.991	***5.0E-05***
Lymph node metastasis	pN0[a] pN+	2.082	1.453	2.984	***4.00E-10***	2.161	1.505	3.102	***3.0E-05***
Resection margin	R0[a] R1	4.241	2.313	7.774	***4.00E-07***	2.220	1.151	4.280	***1.7E-02***
Risk model	low[a] high	1.570	1.123	2.195	***5.0E-03***	1.610	1.074	2.413	***2.1E-02***

[a] *reference*

[b] *significant p values (<0.05) are indicated in italic and bold*

[c] *p=pathological*

Table S10: (C) Univariate and multivariate Cox regression analysis for overall survival of the TCGA-ESSC cohort.

		Univariate	95% CI			Multivariate	95% CI		
Category	**Feature[c]**	**HR**	**lower**	**upper**	**p value[b]**	**HR**	**lower**	**upper**	**p value[b]**
Gender	Male[a] Female	2.87	1.029	8.003	***4.00E-02***	1.373	0.4261	4.427	4.53E-01
Age (years)	<61[a] >61	1.148	0.68	1.9	6.00E-01				
Tobacco	no[a] yes	2.057	1.031	4.1	***4.00E-02***	1.764	0.7115	4.374	2.21E-01
Alcohol	no[a] yes	0.69	0.4	1.17	2.00E-01				
Tumor size	pT1-2[a] pT3-4	1.079	0.6198	1.878	9.00E-01				
Lymph node metastasis	pN1-2[a] pN3-4	3.093	1.634	5.855	***3.00E-04***	2.518	1.1529	5.497	***2.05E-02***
Pathological grading	G1-2[a] G3-4	1.621	0.9	2.91	1.00E-01				
Resection margin	R0[a] R1	2.602	1.237	5.476	**9.00E-03**	3.456	1.1294	10.577	***2.66E-02***
Perineural invasion	no[a] yes	2.303	1.502	7.551	2.00E-01				
Risk model	low[a] high	2.16	1.0346	4.508	***1.00E-02***	1.68	0.8178	3.453	1.58E-01

[a] *reference*

[b] *significant p values (<0.05) are indicated in italic and bold*

[c] *p=pathological*

Table S10: (D) Univariate and multivariate Cox regression analysis for overall survival of the TCGA-BRCA cohort.

		Univariate	95% CI			Multivariate	95% CI		
Category	**Feature[c]**	**HR**	**lower**	**upper**	**p value[b]**	**HR**	**lower**	**upper**	**p value[b]**
Age (years)	<61[a] >61	1.201	0.700	2.042	5.00E-01				
Tumor size	pT1-2[a] pT3-4	2.001	1.001	4.038	***5.00E-02***	2.482	1.403	4.391	***5.0E-02***
Lymph node metastasis	pN0[a] pN+	2.082	1.453	2.984	***2.00E-02***	1.331	0.805	2.200	2.00E-01
Estrogen Receptor metastasis	ESR-[a] ESR+	0.680	0.400	1.140	*1.00E-01*	1.331	0.805	2.200	2.00E-01
Risk model	low[a] high	2.463	1.128	5.378	***2.00E-02***	2.344	1.409	3.898	1.6E-01

[a] *reference*

[b] *significant p values (<0.05) are indicated in italic and bold*

[c] *p=pathological*

Table S11: Summary of drugs with significant differences in DSS among HNSCC cell lines with high vs. low risk scores.

Drug Name	PubChem	Spearman´s rho	p-value[a]	Target/Mode of action	Target Pathway
Galiellalactone	3698011	-0.47	***1.02E-03***	STAT3	JAK-STAT signaling
Pipobroman	4842	-0.33	***2.54E-02***	Alkylation	
SB-743921	49867937	-0.33	***2.93E-02***	Kinesin spindle protein (KSP) inhibitor	
Entinostat	4261	-0.28	6.05E-02	HDAC1, HDAC3	Chromatin histone acetylation
Omacetaxine	65305	-0.28	6.19E-02	Protein synthesis inhibitor	
Trametinib	11707110	-0.27	7.68E-02	MEK inhibhitor	MAPK/ERK signaling
TAK-733	24963252	-0.27	7.86E-02	MEK inhibhitor	MAPK/ERK signaling
PF-04708671	51371303	-0.25	9.69E-02	Kinase inhibitor	RSK p70 subfamily
Carboplatin	426756	0.25	9.76E-02	DNA crosslinking	
Uracil mustard	6194	0.26	8.69E-02	Alkylation	
NVP-RAF265	11656518	0.32	***3.42E-02***	BRAF	RAS-RAF signaling
Tamatinib	11213558	0.33	***2.91E-02***	Non-receptor kinase inhibitor	SYK family
Topotecan	60700	0.33	***2.78E-02***	DNA topoisomerase type I inhibitor	DNA replication
Vismodegib	24776445	0.37	***1.28E-02***	SMO	Hedgehog pathway and ABC transporter inhibitor
Lestaurtinib	126565	0.41	***5.72E-03***	FLT3, JAK2, NTRK1, NTRK2, NTRK3	Other, kinases

[a] *significant p-values are indicated in italic and bold*

Table S12: Summary of drugs with significant differences in IC50 values (GDSC1-2) among CCLE cell lines (head and neck, lung, esophagus, pancreas, breast, CNS) with high vs. low risk scores.

Drug Name	Drug ID	Spearman´s rho	p-value	Target[a]	Target Pathway[a]	PubChem
RIBOCICLIB	1632	-0.31	4.73E-02	CDK4, CDK6	Cell cycle	44631912
KIN001-135	91	-0.29	8.11E-03	IKK	Other, kinases	11626927
THZ-2-49	344	-0.19	1.28E-03	CDK9	Cell cycle	
(5Z)-7-OXOZEAENOL	1242	-0.16	7.35E-03	TAK1	Other, kinases	9863776
AXITINIB	1021	-0.13	1.49E-02	PDGFR, KIT, VEGFR	RTK signaling	6450551
PIPERLONGUMINE	1243	-0.13	2.54E-02	Induces reactive oxygen species	Other	637858
CHIR-99021	154	-0.12	4.07E-02	GSK3A, GSK3B	WNT signaling	9956119
FORETINIB	308	-0.12	4.28E-02	MET, KDR, TIE2, VEGFR3/FLT4, R	RTK signaling	42642645
AST-1306	381	0.12	4.89E-02	EGFR, ERBB4	RTK signaling	24739943
PELITINIB	282	0.12	3.88E-02	EGFR	EGFR signaling	6445562
IPA-3	176	0.13	3.79E-02	PAK1	Cytoskeleton	521106
CI-1033, CANERTINIB	362	0.13	3.33E-02	EGFR, ERBB2, ERBB4	RTK signaling	156414
PILARALISIB, XL-147	372	0.13	2.78E-02	PI3K	PI3K/MTOR signali	56599306
DACOMITINIB, PF-00299804	363	0.13	2.58E-02	EGFR, ERBB2, ERBB4	RTK signaling	11511120
GSK591, EPZ015866, GSK3203591	2110	0.13	4.05E-02	PMRT5	Chromatin histone	117072552
MIM1	446	0.14	2.34E-02	MCL1	Apoptosis regulati	16241412
ALPELISIB	1560	0.14	2.98E-02	PI3Kalpha	PI3K/MTOR signali	56649450
PRT062607	1631	0.14	3.75E-02	SYK	Other, kinases	44462758
UMI-77, UMI 77	1939	0.14	3.29E-02	MCL1	Apoptosis regulati	992586
A-83-01	477	0.14	1.80E-02	TGFB	Other	16218924
AZD5582	1617	0.16	2.09E-02	XIAP, cIAP	Apoptosis regulati	49847690
AGI-6780	562	0.16	8.32E-03	IDH2 R140Q mutant	Metabolism	71299339
AZD8931	1549	0.16	1.26E-02	EGFR, ERBB2, ERBB3	EGFR signaling	11488320
ERLOTINIB	1168	0.16	1.48E-02	EGFR	EGFR signaling	176870
FTY-720, FINGOLIMOD HYDROCHLORIDE; GIL	546	0.17	5.67E-03	S1P	Other	107969
CUDC-101	273	0.17	5.07E-03	HDAC1-10, EGFR, ERBB2	Other	24756910
METAP2 INHIBITOR, A832234	410	0.17	4.69E-03	MetAP2	Other	53413272
CPI-613	415	0.17	4.43E-03	Metabo, Mitochondria	Other	24770514
GEFITINIB	1010	0.17	8.41E-05	EGFR	EGFR signaling	123631
RU-SKI-43	576	0.18	3.41E-03	Shh	Other	46006640
LAPATINIB	1558	0.18	4.35E-03	EGFR, ERBB2	RTK signaling	208908
AFATINIB	1032	0.19	8.78E-06	ERBB2, EGFR	EGFR signaling	10184653
IBRUTINIB	1799	0.19	3.81E-03	BTK	Other, kinases	24821094
AZD3759	1915	0.20	2.62E-03	EGFR	EGFR signaling	78209992
KOBE2602	563	0.24	4.49E-05	RAS effector	RTK signaling	3827738
OSIMERTINIB	1919	0.27	4.13E-05	EGFR	EGFR signaling	71496458

[a] *according to Genomics of Drug Sensitivity in Cancer (https://www.cancerrxgene.org/)*

Table S13: Summary of drugs with significant differences in viability values (PRISM) among CCLE cell lines (head and neck, lung, esophagus, pancreas, breast, CNS) with high vs. low risk scores.

Drug Name	Drug ID	Spearman´s rho[a]	p-value	Target/Mode of Action	Mode of Action	PubChem
oxotremorine-m	BRD-K01942991-005-08-2	-0.265566818	2.51E-05	CHRM1, CHRM2, CHRM3, CHRM4	acetylcholine receptor agonist	4629
IOX2	BRD-K98251413-001-04-0	-0.251801776	5.39E-05	EGLN1, KDM2A, KDM5C	hypoxia inducible factor inhibitor	54685215
RS-100329	BRD-K08640512-003-02-3	-0.251446428	6.56E-05	ADRA1A, ADRA1D	adrenergic receptor antagonist	3567002
azilsartan-medoxomil	BRD-K25723200-001-02-7	-0.248385644	9.24E-05	AGTR1, AGTR2	angiotensin receptor antagonist	135409642
chlorpyrifos	BRD-K08303368-001-10-0	-0.239192768	2.31E-04	ACHE	acetylcholinesterase inhibitor	2730
amiloride	BRD-K97181089-003-24-7	-0.235932218	1.58E-04	AOC1, ASIC1, ASIC2, ASIC3, PKD2, PKD2L1, PLAU, SCNN1A, SCNN1B, SCNN1D, , SCNN1G, SLC9A1, TRPC7, TRPV2	sodium channel blocker	16231
alacepril	BRD-K51784806-001-01-6	-0.232995882	2.50E-04	ACE	angiotensin converting enzyme inhibi	71992
clofoctol	BRD-K02900412-001-11-3	-0.229773805	2.65E-04		protein synthesis inhibitor	2799
SN-6	BRD-A14316475-001-02-3	-0.22712005	3.04E-04		sodium/calcium exchange inhibitor	
lercanidipine	BRD-A18992208-003-02-7	-0.22449302	4.00E-04	CACNA2D1, CACNG1	calcium channel blocker	65866
nateglinide	BRD-K44353683-001-08-3	-0.218210806	6.15E-04	ABCC8, KCNJ10, KCNJ11, PPARG	insulin secretagogue	5311309
diflunisal	BRD-K22031190-001-23-6	-0.216793357	5.72E-04	PTGS1, PTGS2	prostanoid receptor antagonist	3059
AG-1024	BRD-K08310154-001-03-8	-0.213304314	7.22E-04	IGF1R	insulin growth factor receptor inhibitc	2044
estriol	BRD-K17016787-001-16-7	-0.212258244	7.49E-04	ESR1, ESR2	estrogen receptor agonist	5756
CHIR-99021	BRD-K16189898-003-03-3	-0.209216437	8.32E-04	CDK1, GSK3A, GSK3B, MAPK1	glycogen synthase kinase inhibitor	9956119
telmesteine	BRD-A05523972-001-01-5	-0.208137858	9.52E-04		mucolytic agent	65946
aceclofenac	BRD-K68538666-001-12-3	-0.207961215	9.61E-04	PTGS2	prostanoid receptor antagonist	71771
muscimol	BRD-K60441002-001-04-8	-0.205460013	1.19E-03	GABRA1, GABRA2, GABRA3, GABRA4, GABRA5 , GABRA6, GABRR1, GABRR2, GABRR3	benzodiazepine receptor agonist	4266
CHIR-98014	BRD-K42973005-001-04-0	-0.205427543	1.11E-03	GSK3A, GSK3B	glycogen synthase kinase inhibitor	53396311
SGI-1027	BRD-K61228301-001-01-2	0.202955796	1.25E-03	DNMT1, DNMT3A, DNMT3B	DNA methyltransferase inhibitor	24858111
buclizine	BRD-A91444184-300-01-9	0.206333443	1.16E-03	CHRM1, HRH1	histamine receptor antagonist	6729
dronedarone	BRD-K05524748-003-04-4	0.206795647	1.33E-03	ADRA1A, ADRA1B, ADRA1D, ADRA2A, ADRA2B, ADRA2C, ADRB1, CACNA1C, CACNA1D, CACNA1F, CACNA1S, CACNB1, CACNB2 , CACNB3, CACNB4, KCNA5, KCNH2, KCNK2, SCN1A	adrenergic receptor antagonist	208898
BIBU-1361	BRD-K49294207-300-03-8	0.206840529	1.15E-03	EGFR	EGFR inhibitor	17756796
icotinib	BRD-K31698212-001-02-9	0.208709583	8.57E-04	EGFR	EGFR inhibitor	22024915
nexturastat-a	BRD-K70402238-001-02-8	0.209633846	8.52E-04	HDAC1, HDAC6	HDAC inhibitor	71462653
talmapimod	BRD-K17555800-003-01-5	0.210492584	8.30E-04	MAPK11, MAPK14	p38 MAPK inhibitor	9871074
canertinib	BRD-K50168500-001-07-9	0.214380262	6.61E-04	AKT1, EGFR, ERBB2, ERBB4	EGFR inhibitor	156414
spironolactone	BRD-K90027355-001-13-3	0.215426331	8.87E-04	AR, CACNA1A, CACNA1B, CACNA1C, CACNA1D, CACNA1H, CACNA1I, CACNA1S, CACNA2D1, CACNA2D2, CACNA2D3, CACNB1, CACNB2, CACNB3, CACNB4	mineralocorticoid receptor antagonis	5833
AST-1306	BRD-K26838195-075-04-9	0.215648605	5.83E-04	EGFR, ERBB2	EGFR inhibitor	24739943
poziotinib	BRD-K50010139-001-02-3	0.2179508	5.93E-04	EGFR, ERBB2, ERBB4	EGFR inhibitor	25127713
pelitinib	BRD-K08799216-001-05-3	0.22140749	5.66E-04	EGFR	EGFR inhibitor	6445562
BIBX-1382	BRD-K70914287-300-02-8	0.222035041	4.17E-04	EGFR, ERBB2	EGFR inhibitor	6918508
ibrutinib	BRD-K70301465-001-02-6	0.229591916	2.68E-04	BLK, BMX, BTK	Bruton's tyrosine kinase (BTK) inhibito	24821094
gefitinib	BRD-K64052750-001-17-5	0.232442635	2.30E-04	EGFR	EGFR inhibitor	123631
ACY-1215	BRD-K82928847-001-04-7	0.236039139	2.07E-04	HDAC1, HDAC2, HDAC3, HDAC6, HDAC8	HDAC inhibitor	53340666
SRC-kinase-inhibitor-I	BRD-K50495309-001-02-0	0.244708784	9.39E-05	CSK, LCK, RIPK2	src inhibitor	1474853
pyroxamide	BRD-K11663430-001-02-3	0.245230127	9.07E-05	HDAC1	HDAC inhibitor	4996
osimertinib	BRD-K42805893-001-04-9	0.247882552	7.08E-05	EGFR	EGFR inhibitor	71496458
U-18666A	BRD-K22025381-003-01-9	0.252433314	5.53E-05		oxidosqualene cyclase inhibitor	9954082
AEE788	BRD-K40718343-001-02-6	0.254141898	4.57E-05	EGFR, ERBB2, ERBB4, FGFR2, FGFR3, KDR	EGFR inhibitor, VEGFR inhibitor	10297043
AZD8931	BRD-K98572433-001-02-9	0.257774492	3.93E-05	EGFR, ERBB2, ERBB3	EGFR inhibitor	11488320
PD-153035	BRD-K26603252-003-04-9	0.261659831	3.72E-05	EGFR, KDR	EGFR inhibitor	4705
ARRY-334543	BRD-K46386702-001-02-1	0.266585129	2.08E-05	ERBB2	EGFR inhibitor	42642648
tyrphostin-AG-1478	BRD-K68336408-001-10-9	0.268098717	1.94E-05	EGFR, MAPK14	EGFR inhibitor	2051
GW-583340	BRD-K79930101-300-03-7	0.268877436	1.63E-05	EGFR, ERBB2	EGFR inhibitor	5329480
PD-168393	BRD-K17702546-001-03-2	0.2737306	1.13E-05	EGFR, ERBB2, SRC	EGFR inhibitor	4708
AV-412	BRD-K23190681-001-01-1	0.277366498	9.67E-06	EGFR, ERBB2	protein tyrosine kinase inhibitor	11700696
neratinib	BRD-K85606544-001-09-1	0.295976493	3.41E-06	EGFR, ERBB2, KDR	EGFR inhibitor	9915743
OSI-420	BRD-K73309154-003-02-8	0.351818399	1.18E-08	EGFR	EGFR inhibitor	10317566

[a] *cut-off: -0.2>Spearman´s rho>0.2 and p<0.05*

Table S14: SC-related 43-gene sets with standardized empirical p values.

Genes	Detailed Gene name	-log10 p-value
PMP22	peripheral myelin protein 22	2.81656
MPZ	myelin protein zero	2.54736
NRG1	neuregulin 1	2.42235
MAG	myelin associated glycoprotein	2.42176
NGFR	nerve growth factor receptor	2.33684
NF1	neurofibromin 1	2.29585
NGF	nerve growth factor (beta polypeptide)	2.28323
NF2	neurofibromin 2 (merlin)	2.26797
PRX	periaxin	2.22408
MBP	myelin basic protein	2.16073
SOX10	SRY (sex determining region Y)-box 10	1.9964
GJB1	gap junction protein, beta 1, 32kDa	1.99162
CNTF	ciliary neurotrophic factor	1.86462
BDNF	brain-derived neurotrophic factor	1.81839
GALC	galactosylceramidase	1.80412
GDNF	glial cell derived neurotrophic factor	1.79904
EGR2	early growth response 2	1.79397
ERBB3	erb-b2 receptor tyrosine kinase 3	1.77128
GFAP	glial fibrillary acidic protein	1.75974
NTF3	neurotrophin 3	1.72733
DAG1	dystroglycan 1 (dystrophin-associated glycoprotein 1)	1.66507
CNTNAP1	contactin associated protein 1	1.66207
MTMR2	myotubularin related protein 2	1.64557
ENO2	enolase 2 (gamma, neuronal)	1.63506
B3GAT1	beta-1,3-glucuronyltransferase 1	1.63406
POU3F1	POU class 3 homeobox 1	1.61559
NFASC	neurofascin	1.5893
FN1	fibronectin 1	1.54391
LAMA2	laminin, alpha 2	1.48411
ERBB2	erb-b2 receptor tyrosine kinase 2	1.47475
LAMB2	laminin, beta 2 (laminin S)	1.4575
CADM4	cell adhesion molecule 4	1.42414
ERBB4	erb-b2 receptor tyrosine kinase 4	1.41169
GAP43	growth associated protein 43	1.41169
GLDN	gliomedin	1.40616
CNP	2',3'-cyclic nucleotide 3' phosphodiesterase	1.39559
MAL	mal, T-cell differentiation protein	1.38688
DRP2	dystrophin related protein 2	1.38139
FGF2	fibroblast growth factor 2 (basic)	1.3554
GAN	gigaxonin	1.32958
NES	nestin	1.32055
NRCAM	neuronal cell adhesion molecule	1.3201
NCAM1	neural cell adhesion molecule 1	1.31108

Table S15: Spearman's correlation matrix for GSVA scores based on RNA-seq data from TCGA-HNSC (n=500).

Gene sets	Gene set (n)	SC-score
HARMONIZOME_SCHWANN_CELLS (SC-related 43-gene set)	43	1
PANGLAO_DB_SCHWANN_CELLS	19	0.66112476
GO_SYMPATHETIC_NERVOUS_SYSTEM_DEVELOPMENT	21	0.62827177
REACTOME_EGR2_AND_SOX10_MEDIATED_INITIATION_OF_SCHWANN_CELL_MYELINATION	29	0.60311872
GO_MYELIN_SHEATH	43	0.55565367
GO_AXONOGENESIS_INVOLVED_IN_INNERVATION	6	0.48016447
GO_PERIPHERAL_NERVOUS_SYSTEM_AXON_REGENERATION	10	0.44812478
MYELINATING_SCHWANN_CELLS (MOUSE)	430	0.44499418
CURATED_TRANSCRIPTS_NOT_IDENTIFIED_PREVIUOSLY_AS_SCHWANN_CELLS (MOUSE)	99	0.42765589
NON_MYELINATING_SCHWANN_CELLS (MOUSE)	535	0.41947732
GO_RESPONSE_TO_NERVE_GROWTH_FACTOR	52	0.36634677
GO_SYMPATHETIC_GANGLION_DEVELOPMENT	9	0.36525755
GO_SCHWANN_CELL_MIGRATION	5	0.31797388
GO_PERIPHERAL_NERVOUS_SYSTEM_NEURON_DIFFERENTIATION	12	0.21466499
NEGATIVE_REGULATION_OF_SCHWANN_CELL_PROLIFERATION	6	0.0483725
GO_PERIPHERAL_NERVOUS_SYSTEM_MYELIN_MAINTENANCE	9	-0.0217303

Table S16: Spearman's correlation matrix for GSVA scores of the SC-related 43-gene set and xCell cell population(Top5 positive-negative) based on RNA-seq data from TCGA-HNSC (n=500).

xCell matrrix	SC-score	Astrocytes	Neurons
SC-score	1	0.567658798	0.289282
Astrocytes	0.567659	1	0.301562
Chondrocytes	0.450066	0.654120268	0.348103
Mesangial.cells	0.317449	0.461368199	0.021335
Fibroblasts	0.313226	0.520162175	0.213045
Pericytes	0.299175	0.346295327	0.186732
CD4+.memory.T-cells	-0.27301	-0.190284834	-0.26625
Th1.cells	-0.27997	-0.203026153	-0.13716
CD8+.Tcm	-0.29878	-0.133087957	-0.36218
CD8+.naive.T-cells	-0.30321	-0.162004993	0.061117
pro.B-cells	-0.3598	-0.370960348	-0.21797

Top 5 positive-negative correlated cells

Table S17: Crosstab analysis based on the subgroups of SC score in TCGA-HNSC (n=500).

		SC^{high}		$SC^{moderate}$		SC^{low}		
Category	**Feature**	**n**	**%**	**n**	**%**	**n**	**%**	**p value**
Age [years]	≤61	80	47.9%	78	47.0%	86	51.8%	6.40E-01
	>61	87	52.1%	88	53.0%	80	48.2%	
Gender	female	52	31.1%	43	25.9%	38	22.9%	2.00E-01
	male	115	68.9%	123	74.1%	128	77.1%	
Tobacco	yes	129	97.0%	123	96.9%	126	98.4%	8.50E-01
	no	4	3.0%	4	3.1%	2	1.6%	
Alcohol	yes	111	96.5%	104	97.2%	116	97.5%	6.00E-01
	no	4	3.5%	3	2.8%	4	3.4%	
HPV16	yes	3	1.9%	16	10.2%	34	21.1%	***2.33E-06***
	no	155	98.1%	141	89.8%	127	78.9%	
Subsite	Hypopharynx	2	1.2%	3	1.8%	5	3.0%	***7.39E-05***
	Larynx	33	19.8%	48	28.9%	30	18.1%	
	Oral Cavity	121	72.5%	94	56.6%	92	55.4%	
	Oropharynx	11	6.6%	21	12.7%	39	23.5%	
Tumor size	cT1-2	62	37.6%	62	39.0%	51	31.9%	3.00E-01
	cT3-4	103	62.4%	97	61.0%	109	68.1%	
	pT1-2	63	40.6%	61	42.4%	52	36.1%	2.00E-01
	pT3-4	92	59.4%	83	57.6%	92	63.9%	
Lymph nodes metastasis	cN0	85	52.1%	84	54.2%	69	43.4%	1.00E-01
	cN1-3	78	47.9%	71	45.8%	90	56.6%	
	pN0	61	43.0%	59	42.4%	50	37.0%	5.90E-02
	pN1-3	81	57.0%	70	50.4%	85	63.0%	
Pathological grading	G1-2	129	79.1%	120	75.0%	110	70.1%	2.00E-01
	G3-4	34	20.9%	40	25.0%	47	29.9%	
Resection margin	R0	16	10.5%	20	13.6%	21	14.3%	6.80E-01
	R1	137	89.5%	127	86.4%	126	85.7%	
Angiolymphatic invasion	yes	48	38.1%	34	30.9%	38	37.3%	5.50E-02
	no	78	61.9%	76	69.1%	64	62.7%	
Perineural invasion	yes	78	60.0%	43	39.1%	44	40.0%	***2.50E-04***
	no	52	40.0%	67	60.9%	66	60.0%	

[a] *c=clinical, p=pathological*

[b] *significant p values (<0.05) are indicated in italic and bold*

Table S18: Somatic mutation frequency of MutSig genes for TCGA-HNSC (n=500).

Gene Symbol	SC^{low}	$SC^{moderate}$	SC^{high}	p-value [1]
PTEN	10.24%	6.63%	1.20%	***0.002226***
TP53	65.06%	71.08%	80.24%	***0.007892***
REG1A	3.01%	6.02%	0.60%	***0.01901***
OR2M5	2.41%	8.43%	3.59%	***0.02484***
NOTCH1	13.86%	22.89%	25.15%	***0.02662***
RSRC1	19.88%	16.87%	9.58%	***0.02788***
AGTR1	20.48%	17.47%	10.18%	***0.03103***
NSD1	12.65%	17.47%	8.38%	***0.04608***
EP300	12.05%	4.82%	7.19%	***0.04696***
SPATA16	25.90%	24.10%	15.57%	0.052
REG1B	3.61%	3.01%	0.00%	0.05509
NPFFR2	6.02%	5.42%	1.20%	0.0573
LIN28B	2.41%	4.22%	0.60%	0.09811
FAT1	24.70%	34.94%	28.74%	0.1194
OR2M2	4.22%	4.82%	1.20%	0.1485
C6	9.64%	12.05%	5.99%	0.1568
B2M	2.41%	3.61%	0.60%	0.1686
PDE10A	7.23%	3.01%	4.19%	0.1797
GATA2	6.02%	6.02%	2.40%	0.2023
SMAD4	9.04%	4.22%	8.98%	0.21
TGFBR2	4.22%	7.23%	8.98%	0.2182
RARG	2.41%	4.22%	1.20%	0.22
MEF2C	4.82%	1.81%	2.40%	0.2341
HBG2	3.01%	1.81%	0.60%	0.2544
RAC1	6.63%	3.01%	4.19%	0.2772
ZNF716	4.82%	8.43%	8.98%	0.2897
PIK3CA	39.16%	33.73%	31.14%	0.2924
KHDRBS2	1.81%	4.22%	4.79%	0.3017
EYA1	5.42%	9.64%	6.59%	0.3084
LCP1	3.61%	5.42%	2.40%	0.348
ZNF99	2.41%	5.42%	4.79%	0.3537
ALKAL1	3.01%	3.61%	5.99%	0.3594
KRT17	1.20%	1.20%	2.99%	0.3664
RHOA	4.22%	2.41%	1.80%	0.3807
HLA-B	4.82%	6.02%	2.99%	0.4141
CUL3	3.61%	6.02%	6.59%	0.4449
OR6C65	3.01%	2.41%	4.79%	0.4603
CD1E	4.82%	3.61%	2.40%	0.4949
NRF1	1.81%	1.20%	2.99%	0.4951
OR5L1	2.41%	4.22%	4.79%	0.4961
HRAS	8.43%	6.02%	5.39%	0.4993
ZNF676	5.42%	4.22%	2.99%	0.5
MAPK1	2.41%	3.61%	4.79%	0.5073
FBXW7	7.23%	9.64%	6.59%	0.5502
NEDD8	1.81%	1.81%	0.60%	0.5562
ULK2	0.00%	2.41%	1.80%	0.5562
NXPH1	3.61%	1.81%	2.40%	0.5735
OR5D13	3.61%	6.02%	4.79%	0.5907
ZNF750	6.02%	3.61%	4.79%	0.5907
AK5	1.81%	3.01%	3.59%	0.6028
HLA-A	4.22%	6.02%	6.59%	0.6179
RASA1	4.82%	4.82%	2.99%	0.6318
EPHA2	5.42%	4.22%	6.59%	0.6333
DOK6	5.42%	7.83%	5.99%	0.6445
DPPA2	6.02%	8.43%	6.59%	0.6673
HIST1H3C	1.20%	2.41%	2.40%	0.6673
ITGA8	4.22%	6.02%	5.99%	0.7071
KEAP1	4.82%	6.63%	3.59%	0.7071
TRIM43	1.20%	2.41%	1.80%	0.7116
POM121L12	10.24%	9.64%	7.78%	0.7215
FCRL4	5.42%	3.61%	4.79%	0.7279
EPDR1	1.81%	3.01%	2.99%	0.7318
OR8J3	4.22%	4.22%	2.99%	0.7971
NFE2L2	9.04%	10.84%	10.78%	0.8
P2RY11	1.81%	0.00%	2.99%	0.9
HIST1H2BG	2.41%	2.41%	1.80%	0.9076
KIR3DL2	1.81%	2.41%	2.40%	0.913
PSG8	3.01%	3.01%	2.40%	0.9254
NEK5	3.61%	4.22%	3.59%	0.9447
POTEG	3.61%	4.22%	4.19%	0.9511
PRB2	4.82%	5.42%	4.79%	0.9566
CASP8	13.25%	13.25%	13.17%	0.9997
CDKN2A	49.40%	53.61%	58.68%	0.9997
OR4K5	3.01%	3.01%	2.99%	0.9999

[1] *Chi-square-test, significant values are indicated as bold and italic*

Table S19: Association of the SC score with Hallmark gene sets from MSigDB for TCGA-HNSC (n=333).

Gene set ID	log2FC [1]	adj. p-value
HALLMARK_EPITHELIAL_MESENCHYMAL_TRANSITION	0.512031961	1.60E-40
HALLMARK_MYOGENESIS	0.456724996	2.71E-53
HALLMARK_ANGIOGENESIS	0.404117732	3.08E-32
HALLMARK_HEDGEHOG_SIGNALING	0.382604352	6.15E-53
HALLMARK_UV_RESPONSE_DN	0.351304836	4.11E-39
HALLMARK_KRAS_SIGNALING_UP	0.305417418	4.25E-35
HALLMARK_COAGULATION	0.273146183	4.01E-28
HALLMARK_APICAL_JUNCTION	0.259053771	3.08E-32
HALLMARK_KRAS_SIGNALING_DN	0.223984994	3.48E-25
HALLMARK_ESTROGEN_RESPONSE_EARLY	0.206042335	1.32E-24
HALLMARK_APICAL_SURFACE	0.185841151	1.58E-19
HALLMARK_TGF_BETA_SIGNALING	0.18288065	6.71E-09
HALLMARK_NOTCH_SIGNALING	0.176299927	1.18E-13
HALLMARK_IL2_STAT5_SIGNALING	0.175628064	9.63E-14
HALLMARK_HYPOXIA	0.174129106	1.01E-12
HALLMARK_INFLAMMATORY_RESPONSE	0.168664349	2.21E-07
HALLMARK_WNT_BETA_CATENIN_SIGNALING	0.143135292	1.97E-11
HALLMARK_COMPLEMENT	0.127517555	2.23E-06
HALLMARK_IL6_JAK_STAT3_SIGNALING	0.117499814	3.21E-04
HALLMARK_PANCREAS_BETA_CELLS	0.106763234	2.60E-06
HALLMARK_ESTROGEN_RESPONSE_LATE	0.103730748	1.26E-08
HALLMARK_TNFA_SIGNALING_VIA_NFKB	0.102696799	1.70E-03
HALLMARK_ANDROGEN_RESPONSE	0.091002719	9.29E-05
HALLMARK_BILE_ACID_METABOLISM	0.07967943	1.52E-06
HALLMARK_XENOBIOTIC_METABOLISM	0.066065989	4.14E-05
HALLMARK_HEME_METABOLISM	0.052431143	2.99E-03
HALLMARK_APOPTOSIS	0.042553367	3.50E-02
HALLMARK_ALLOGRAFT_REJECTION	0.037068618	3.53E-01
HALLMARK_PROTEIN_SECRETION	0.00097978	9.80E-01
HALLMARK_CHOLESTEROL_HOMEOSTASIS	0.000522159	9.83E-01
HALLMARK_GLYCOLYSIS	-0.041117886	5.19E-02
HALLMARK_P53_PATHWAY	-0.057627257	5.62E-03
HALLMARK_INTERFERON_GAMMA_RESPONSE	-0.061227237	1.68E-01
HALLMARK_SPERMATOGENESIS	-0.061574418	3.29E-04
HALLMARK_MITOTIC_SPINDLE	-0.06394167	4.19E-02
HALLMARK_ADIPOGENESIS	-0.074032126	4.46E-04
HALLMARK_PI3K_AKT_MTOR_SIGNALING	-0.075386419	1.26E-03
HALLMARK_PEROXISOME	-0.081517313	2.81E-06
HALLMARK_UV_RESPONSE_UP	-0.08240058	3.35E-07
HALLMARK_FATTY_ACID_METABOLISM	-0.116106138	2.50E-09
HALLMARK_REACTIVE_OXYGEN_SPECIES_PATHWAY	-0.121370914	7.69E-06
HALLMARK_INTERFERON_ALPHA_RESPONSE	-0.151497486	4.09E-03
HALLMARK_MTORC1_SIGNALING	-0.17074056	8.64E-10
HALLMARK_UNFOLDED_PROTEIN_RESPONSE	-0.205204951	2.36E-13
HALLMARK_G2M_CHECKPOINT	-0.368066082	2.13E-22
HALLMARK_DNA_REPAIR	-0.386324026	3.91E-43
HALLMARK_OXIDATIVE_PHOSPHORYLATION	-0.391872183	2.55E-28
HALLMARK_MYC_TARGETS_V2	-0.432919223	3.51E-24
HALLMARK_E2F_TARGETS	-0.488592619	8.48E-32
HALLMARK_MYC_TARGETS_V1	-0.489307082	7.04E-37

[1] SC^{low} vs SC^{high}

Table S20: Spearman's correlation matrix for SC and PROGENy scores based on RNA-seq data from TCGA-HNSC (n=496).

PROGENy	SC score
SC score	1
TGF_ß	0.321409178
Estrogen	0.282957855
WNT	0.190647138
Androgen	0.143443781
Trail	0.126091338
TNFa	0.116487846
p53	0.077227827
EGFR	0.027353423
Hypoxia	0.005628618
MAPK	-0.031383779
VEGF	-0.044325805
PI3K	-0.048508886
NFkB	-0.08258224
JAK_STAT	-0.088602236

Table S21: In silico drug sensitivity screening of GDSC project for SC score (high vs low) in TCGA-HNSC, n=333 based on OncoPredict scores.

Drugs	mode of action	Mean Difference	Target	p.value
CAMPTOTHECIN	topoisomerase inhibitor	0.985707268	TOP1	4.21E-27
CAY10566	selective SCD1 inhibitor	0.368330644		4.76E-23
IRINOTECAN	topoisomerase inhibitor	0.831374075	TOP1, TOP1MT	5.9E-23
MK-1775	WEE1 kinase inhibitor	0.761666919	WEE1	1.02E-22
MG-132	proteasome inhibitor	-0.437839238	PSMB1	1.35E-22
T0901317	Anti-proliferation_LXR agonist	0.605779548		1.17E-21
SORAFENIB	FLT3 inhibitor, KIT inhibitor, PDGFR tyrosine kinase receptor inhibitor RAF inhibitor, RET tyrosine kinase inhibitor, VEGFR inhibitor	0.694202289	BRAF, DDR2, FGFR1, FLT1, FLT3, FLT4, KDR, KIT, PDGFRB, RAF1, RET	1.27E-21
OLAPARIB	PARP inhibitor	0.627382867	PARP1, PARP2	2.06E-21
TENIPOSIDE	topoisomerase inhibitor	0.912919677	TOP2A, TOP2B	5.55E-21
TOPOTECAN	topoisomerase inhibitor	0.78395068	TOP1, TOP1MT	1.17E-20
VX-702	p38 MAPK inhibitor	0.591708542	MAPK11, MAPK12, MAPK14	1.2E-20
CISPLATIN	DNA alkylating agent, DNA synthesis inhibitor	0.673236592	XIAP	1.66E-20
AR-42	HDAC inhibitor	0.603688163	HDAC1	1.73E-20
MN-64		0.629224516		1.77E-20
PEVONEDISTAT	nedd activating enzyme inhibitor	0.785435441	NAE1, UBA3	1.93E-20
CAY10603		0.549107748		2.17E-20
GEMCITABINE	ribonucleotide reductase inhibitor	0.919461228	CMPK1, RRM1, RRM2, TYMS	1.54E-19
MIRIN		1.024366592		1.64E-19
5-FLUOROURACIL	thymidylate synthase inhibitor	0.844684453	DPYD, TYMS	2.33E-19
PEMETREXED	dihydrofolate reductase inhibitor, thymidylate synthase inhibitor	0.679806587	ATIC, DHFR, GART, TYMS	2.56E-19

Top20 drugs based on the lowest P-value

Mean Difference SC^{low} *vs* SC^{high}

Acknowledgments

First of all, I would like to express my deep gratitude to my supervisor Prof. Dr. Jochen Hess for offering me the opportunity to perform my Ph.D. thesis after a successful Masters in the section of experimental and translational head and neck oncology in the departments of otolaryngology and head and neck surgery at the university hospital Heidelberg. I was always very enthusiastic about our scientific discussions. I always felt appreciated because of his creative scientific mindset, knowledge, and the encouraging and critical discussions that motivated me always to give 100%. Furthermore, I would like to thank my faculty supervisor Prof. Dr. Dr. George Stoecklin for his support in the last three years as a chair of the TAC meeting in addition to the TAC members Prof. Dr. Thomas Kunar, Dr. Marc Zapatka, and Dr. Jens Strelau for all scientific discussions we had that helped me to structure my projects to a successful Ph.D. thesis. Nevertheless, I would like to thank Prof. Dr. Peter Angel and Dr. Tim Waterboer for acting as members of the examination committee for the Ph.D. defense.

Also, I would like to express my deep gratitude to my lab team. I'm grateful for all kinds of support from the technicians and all other colleagues, who helped me to improve my skills which affect my projects positively.

Finally, I would like to thank my family, especially my wife for being such an amazing supporter, and my sisters who took care of my parents during my absence in my Master's and Ph.D.

Karam Khorani

08.07.2023, Heidelberg